Stony Brook University

Synapse Formation and Neuromuscular Transmission in a Zebrafish Choline Acetyltransferase Mutant

A Dissertation Presented

by

Meng Wang

to

The Graduate School

in Partial Fulfillment of the

Requirements

for the Degree of

Doctor of Philosophy

in

Neuroscience

Stony Brook University

December 2007

Stony Brook University

The Graduate School

Meng Wang

We, the dissertation committee for the above candidate for the

Doctor of Philosophy degree, hereby recommend

acceptance of this dissertation.

Paul Brehm, Ph.D., Dissertation Advisor
Professor, Department of Neurobiology and Behavior

Simon Halegoua, Ph.D., Chairperson of Defense
Professor and Interim Chair, Department of Neurobiology and Behavior

Gary Matthews, Ph.D., Professor
Department of Neurobiology and Behavior

Howard Sirotkin, Ph.D., Assistant Professor
Department of Neurobiology and Behavior

Laurinda Jaffe, Ph.D., Professor and Interim Chair
Department of Cell Biology
University of Connecticut Health Center

This dissertation is accepted by the Graduate School

Lawrence Martin
Dean of the Graduate School

Abstract of the Dissertation

Synapse Formation and Neuromuscular Transmission in a Zebrafish Choline Acetyltransferase Mutant

by

Meng Wang

Doctor of Philosophy

in

Neuroscience

Stony Brook University

2007

Upon touch stimulation, the zebrafish motility mutant *bajan* displays greatly diminished escape response with an incomplete initial bend and much weakened subsequent tail movements. The purpose of this dissertation has been to determine the molecular culprit for the defective motility phenotype and examine the functional consequences of the *bajan* mutation. Consistent with the behavior, both spontaneous miniature endplate current and evoked endplate current from fast skeletal muscle cells showed much smaller amplitude but normal current kinetics in *bajan* mutants, indicating aberrant neuromuscular transmission. Fluorescence imaging of the major pre- and post-synaptic markers in whole-mount zebrafish preparation did not reveal obvious morphological defects at the neuromuscular junction. The lack of immediate candidate genes prompted the employment of the positional cloning strategy.

Based on the result of bulk segregant analysis and sequencing, a mutation at a splice acceptor site was found in the zebrafish homolog of the gene encoding choline

acetyltransferase (ChAT), the enzyme responsible for acetylcholine biosynthesis. This mutation completely disrupted the normal pre-mRNA splicing pattern and created three transcripts, all of which encode much truncated ChAT proteins without proper enzymatic functions. Absence of fluorescence signal in anti-ChAT antibody staining in the mutant fish confirmed the RT-PCR results. Two pieces of additional evidence further supported the mutation in ChAT as underlying *bajan*'s motility phenotype: successful phenocopy by injecting morpholino in wild type embryos to block the same splice recognition site and achieving behavioral rescue by injecting wild type ChAT mRNA into mutant homozygotes.

In further examination of the functional consequences of ChAT mutation, fluorescence imaging of postsynaptic AchR clusters in dissociated skeletal muscle cells showed enlarged area of single AchR clusters, consistent with but less severe than what was seen in the ChAT knockout mice. This mild morphological alteration at the neuromuscular junction could be explained by the presence of residual acetylcholine, suggested by the similar effect of acetylcholinesterase inhibitor on the current kinetics in wild type and *bajan*. The decrease of mEPCs frequency and amplitude over time in mutant fish suggested that the source of residual acetylcholine is likely from the pre-fertilization deposit of maternal ChAT mRNA or protein.

TABLE OF CONTENTS

LIST OF FIGURES

CHAPTER 2

CHAPTER 3

CHAPTER 4

CHAPTER 5

LIST OF TABLES

ACKNOWLEDGMENTS

It has been a great privilege for me to do my graduate study in a special group where scientists in several labs share research resources and experiences from which I benefited immensely. My first and most earnest acknowledgments must go to my advisor, Dr. Paul Brehm, whom I greatly respect both academically and personally. A most caring mentor, he impressed me everyday during my graduate years for his enthusiasm in biological research and his great sense of humor. Without his continuous support and guidance, this dissertation could not have been written.

I would also like to express my gratitude for my dissertation committee chair, Dr. Simon Halegoua, and other members of my committee, Dr. Gary Matthews, Dr. Howard Sirotkin and Dr. Laurinda Jaffe, who generously provided their invaluable advice for this dissertation project.

The Brehm lab is a fun place to be. I will always cherish the happy days I shared with my friends in the lab. I want to give special thanks to Dr. Hua Wen, my good friend and permanent lunch partner, from whom I learned so much and with whom I shared numerous interesting discussions and endless laughter.

My gratitude also goes to my parents who offered unconditional love and support throughout my life, and my husband who, with his love, opened me to a whole new life experience.

In the end, I want to dedicate this thesis to my three-month-old son, Janik, who has become the sunshine in my life since his birth.

CHAPTER 1

INTRODUCTION

Zebrafish as a model system

During evolution, many of the basic biological processes are conserved across species. However, the advantages offered by certain individual species provide unique opportunities to tackle fundamental questions in biology. These simpler, idealized organisms are termed model systems.

Ideal model systems possess certain traits such as rapid development with short generation time, ready availability and tractability (Bolker, 1995). Many popular model organisms meet one or more of these criteria, but most fail to fulfill all of the features. For instance, Drosophila has been the most popular genetics model system largely due to the readily obtainable mutants and easily visualized polytene chromosomes (Bingham et al, 1981), but many crucial biological questions unique to the vertebrate animals simply cannot be addressed in an invertebrate organism. A case in point is the difference in neuromuscular transmission. In Drosophila the neurotransmitter is glutamate and the muscle receptors are glutamatergic. In another invertebrate model system, the roundworm c. elegans, neuromuscular transmission is a mixture of both excitatory and inhibitory drive. Even vertebrate preparations fail to exhibit the collective advantages offered by animal model systems. The vertebrate xenopus has been known for its amenability to

experimental manipulation, which yields a powerful heterologous expression system for *in vivo* functional studies of a large number of proteins (Keller et al, 1991), but genetic studies can be complicated by their pseudotetraploid genome (Warkman et al, 2007). In the case of the mouse, its mammalian nature and the unique employment of embryonic stem (ES) cells techniques for targeted gene modification have made it *the* model of studying gene function and development in mammals (Picciotto 1999). Despite all these assets, mouse is an expensive and slow developing model system to use, which greatly limits the application of *in vivo* genome-wide genetic approaches. Such limitations of the aforementioned model systems underscore the search for new organisms. Zebrafish, a tropical freshwater teleost native to southern Asia, has emerged as a preeminent vertebrate model system. Since chosen by Streisinger as a model system for developmental studies in the 1980's (Streisinger et al, 1981), the zebrafish has proved to be an excellent model system for the following reasons:

First, the zebrafish is an organism befitting for laboratory use due to its ready availability and easy breeding.

Although indigenous to Asia, zebrafish is a popular aquarium pet worldwide, making them readily available. This species is easy to maintain in a laboratory environment and the methods for its husbandry are well established (Westerfield, the zebrafish book). Also, adults reach only 3-4 cm in length, rendering them easy to keep in large numbers in a relatively small space. Once reaching sexual maturation at around 2.5 to 3 months, the adult fish reproduce robustly until they reach about 2 years of age (Streisinger et al, 1981). With a relatively short generation time for a vertebrate system,

mature female fish usually produce 200-300 eggs at weekly intervals (Streisinger et al, 1981), a number big enough for most experimental procedures including standard genetic analyses.

Second, the rapid external development of optically clear embryos makes zebrafish well suited for developmental studies.

The embryonic development of zebrafish is fast and synchronous in one clutch. The early developmental events evolve on an hourly basis with a full body plan established at around 12 hpf (hours post-fertilization), subdivisions in the brain apparent at 16.5 hpf, and a regular heart beat at 26 hpf (Kimmel et al, 1995). Such rapid progress facilitates the application of time-lapse imaging and use of landmarks in early developmental studies.

Moreover, the embryos develop entirely ex-utero starting from the fertilization, allowing *in vivo* analysis of embryogenesis and organogenesis at all stages of development. Completely transparent during the first 24 hours, the embryos are encompassed in clear chorions, allowing unprecedented non-invasive assessment of gross morphological changes as well as changes in the developing internal organs (Haffter et al, 1996; Driever et al, 1996). This high degree of transparency persists until 96 hpf (Briggs et al, 2002), and with the aid of optical techniques such as differential interference contrast, individual neurons could be visualized for patch clamping in an intact 48-72 hpf larval preparation (Ribera and Nusslein-Volhard, 1998, Wen and Brehm, 2005). When combined with the use of molecular markers such as green fluorescent protein (GFP) which can act as temporal and spatial clues to gene expression patterns, the embryonic

accessibility could potentially associate the mutated gene with a certain developmental pathway or assign it a specific cellular identity (Amsterdam et al, 1996, Higashijima et al, 1997, Long et al, 1997), providing insights for link between the gene and its functions.

Third, zebrafish displays excellent experimental tractability.

The zebrafish embryos are amenable to many embryological manipulations such as introduction of foreign RNA/DNAs (Ando et al, 2001) or antisense morpholino oligos by microinjection (Nasevicius et al, 2000), which enable either induction or knockdown of target gene expressions. The relatively large embryos (~1mm) are easy to inject and the immediate effect can be observed with the mere aid of a dissecting microscope. Using the microinjection technique, transgenic lines have been generated for cell lineage tracing and transgene expression (Stuart et al, 1990; Linney et al, 1999; Long et al, 1997).

Another unique quality of this system is the ease with which cells can be transplanted between mutant and wild type embryos, creating a mosaic pattern of the target gene expression (Mizuno et al, 1999). Mosaic analysis is useful in distinguishing between primary and secondary defects caused by the mutation (Grunwald, 1996). The malleability of zebrafish is also beneficial in embryotoxicity studies and chemical screenings, in which compounds added directly to the embryo water ensure a fast and even exposure and effects can be quickly assessed thanks to the rapid embryonic development (Peterson et al, 2000).

Fourth, intrinsic qualities and fast growing resources render zebrafish a powerful model for genetic studies.

Zebrafish is amenable to forward and reverse genetic strategies, both of which seek the link between genes and their functions by modifying gene expression at various levels, albeit through opposite approaches. Forward genetic analysis starts from random mutagenesis, continues with selections based on various phenotypes and ends in revelation of the molecular identity of the disrupted gene (Malicki et al, 2002). The phenotype-driven approach immediately links the mutated gene to its particular function. When multiple mutants display similar phenotype, the underlying molecular culprits could be associated with one specific process, thus putting more pieces of puzzles into the largely unfinished picture of intracellular signaling pathways (Grunwald 96).

Thanks to its ease of maintenance, high fecundity, external fertilization, rapid development and optical clarity (Kimmel et al, 1989), zebrafish has successfully introduced mutant screening into the vertebrate genetics (Driever et al, 1996, Haffter et al, 1996). Screenings from different labs have since discovered a large number of critical genes in various pathways, such as hemotopoiesis (Amatruda and Zon, 1999), embryonic development (Haffter et al, 1996) and locomotion (Granato et al, 1996), and systems such as visual system (Baier et al, 1996; Brockerhoff et al, 1995; Malicki et al, 1996), cardiovascular system (Warren et al, 1998; Fishman et al, 1997) and kidney (Drummond et al, 1998).

Reverse genetic approach, on the other hand, starts from genes of interest, identify their roles by deliberately interfering the target gene expression and search for subsequent effects, thereby assigning it to a given signaling pathway. In terms of the availability of powerful molecular genetic tools, zebrafish doesn't have the privilege of the mouse system, in which the application of embryonic stem (ES) cells for targeted genetic

modification allows extensive manipulation of the genome. However, morpholino knockdown has been successful in down regulating gene expression in early zebrafish embryos (Heasman et al, 2002). It has been shown to effectively and specifically replicates phenotypes of loss-of-function mutants (Nasevicius et al, 2000). The advantage of morpholino over knockout strategy lies in the possibility of downregulating expression of multiple genes at one time (Malicki et al, 2002). Moreover, the adaptation of TILLING (Targeting-Induced Local Lesions IN Genome) technique in zebrafish allows selective mutagenesis in the gene of interest (Wienholds et al, 2003).

Last, zebrafish is a good model system for human disease and clinical research.

Although many cellular processes could be extrapolated from invertebrate organisms, certain studies such as organogenesis and the functions of vertebrate genes require a vertebrate model with good tractability. Zebrafish allows these vertebrate-specific questions to be addressed with the powerful embryonic and genetic techniques obtained from invertebrate systems such as drosophila and C. elegans (Dooley 2000). These qualities, in addition to the highly conserved intracellular pathways and regulating mechanisms within the vertebrate system, make it an appropriate model for studies of human diseases. For example, many clinical syndromes such as long QT syndrome, bradycardia and congenital sideroblastic anemia, have found their counterparts in the zebrafish mutants (Arnaout et al, 2007; Baker et al, 1997; Brownlie et al, 1998).

Overall, zebrafish as a model system has yielded numerous important findings and with the ongoing advances of resources and techniques, it has yet more to offer.

Explore neuromuscular transmission using forward genetics and electrophysiology in zebrafish

Owing to its large size, easy accessibility and relative simplicity in connectivity, the synapse at neuromuscular junction (NMJ) is an extensively studied model for synaptic transmission and synapse development (Ruff 2003; Sanes and Lichtman, 1999, Goda and Davis, 2003). On the pre-synaptic side of the neuromuscular junction are active zones, specialized regions of the presynaptic neuronal plasmamembrane, where synaptic vesicles filled with the neurotransmitter acetylcholine (Ach) reside (Dreyer et al, 1973). Once triggered by the nerve impulses propagating down from the motoneuron soma, the clusters of synaptic vesicles fuse with the active zone membrane and Ach is released in a quantal manner (Katz and Miledi, 1966). Traveling through the synaptic cleft, Ach binds to the densely clustered acetylcholine receptors (AchRs) on the post-synaptic muscle cell membrane directly opposing the active zones (del Castillo and Katz, 1955; Salpeter et al, 1988), causing depolarization of the muscle cell (Fatt and Katz, 1953) and subsequently leads to muscle fiber contraction. Although the multiple steps of the transmission process have been under intense investigation, many of the mechanisms governing early synapse formation and regulation of the synaptic activity at the neuromuscular synapse are yet to be clarified.

Recently, zebrafish has emerged as a powerful model for studying synaptic transmission and synapse development at the NMJ (Ono et al, 2001, Flangan-Steet et al, 2005). Compared to the high lethality at birth in mouse mutants due to suffocation (Misgeld et al, 2002), the rapid external development of zebrafish embryos provides a

time window during which *in vivo* studies of the developing neuromuscular synapse can be carried out (Briggs et al, 2002). At 21 hpf, embryos already start to show functional responses such as the avoidance to touch (Saint-Amant and Drapeau, 1998); at around 30 hpf, embryos display escape response and swimming upon stimulation; between 48 and 72 hpf, the larvae have hatched and display spontaneous "burst swimming" pattern (Buss and Drapeau, 2001); after 5 days, the zebrafish are able to perform sustained swimming and search for food. The stereotypic time course of motor behavior development enables easy assessment of locomotory defects during early development.

Another bonus of studying NMJ in zebrafish lies in its amenability for physiology recordings. The small and electrically compact muscle cells facilitate effective voltage clamp and the accessibility to spinal cord neurons due to optical clarity of the embryos renders neuronal recording feasible (Nguyen et al, 1999; Wen and Brehm, 2005). Recently, based on the stereotypic innervation pattern of spinal motoneurons in each segment (Westerfield et al, 1986), a paired neuron-muscle recording scheme has been established and applied to testing the hypothesis of open channel block of AchRs (Wen and Brehm 2005), offering a unique preparation to study neuromuscular transmission and synaptic plasticity.

Moreover, unlike mammals, zebrafish motoneurons have rather simple and robust innervation patterns (Westerfield et al, 1986). In each segment of the spinal cord, there are 3 primary motoneurons with individual characteristics in morphology (Eisen 99). With almost no overlap in their target muscle regions, Rostral Primary motoneuron (RoP) innervates the ventro-medial regions, Middle Primary motoneuron (MiP) innervates the dorsal muscle and Caudal Primary motoneuron innervates the ventral-lateral region.

Therefore, at early embryonic stage, muscle cells are initially innervated by individual, identified axons (Westerfield et al, 1986, Flanagan-Steet et al, 2005). The structural simplicity, combined with the transparency of the embryos, enables live imaging of synaptogenesis at NMJ.

Forward genetics and locomotory mutant screening

Mutation studies are essential for determination of gene functions. Large-scale phenotypic screens can define genes as critical to developmental, physiological, or pathological processes. The first large-scale chemical mutagenesis and screenings searched mostly for dramatic morphological defects (Driever et al, 1996, Haffter et al, 1996). However, utilizing the robust escape response in zebrafish larva as screening criteria, Granato et al identified 166 motility mutants with various phenotypes (Granato et al, 1996). These mutants from the locomotion screen have successfully revealed critical functions of major players in various links of the neuromuscular transmission, such as AchR (Westerfield et al, 1990, Ono et al, 2001), RAPSYN (Ono et al, 2002), MUSK (Zhang et al, 2004), dystroglycan (Parsons et al, 2002), DHP receptor (Schredelseker et al, 2005, Ono et al, 2001), SERCA (Gleason et al, 2005). Mutant studies also facilitated the discovery of unanticipated roles in previously identified genes (Ono et al, 2004). However, so far almost all of the mutants identified had defects in postsynaptic genes. The mechanisms of much more complicated presynaptic release of the NMJ is still elusive.

Bajan was one of the locomotory mutants found in the Tubingen screen, with the characteristic of reduced locomotion (Granato et al, 1996). Initial imaging studies showed

no obvious defect at the NMJ, raising the possibility of a defect of the presynaptic origin. Following the previously successful examples in revealing the underlying mechanisms with a combination of physiology and imaging tools, I set out to determine the molecular and functional bases of the impaired locomotory function of *bajan*.

CHAPTER 2

CHARACTERIZATION OF *BAJAN* SYNAPSE MORPHOLOGY AND NEUROTRANSMISSION

Introduction

Escape responses of a wild type zebrafish larvae feature a fast stereotypic C-bend of the body away from a threatening stimulus followed by rapid alternating tail movements (Eaton and Didomenico, 1986). Starting from 30 hpf (hours post-fertilization), this escape response occurs with a short latency, high speed and clear directionality enabling the developing zebrafish to avoid predators (Eaton and Didomenico, 1986). Due to its simplicity and reproducibility, touch response testing was used to successfully identify 166 motility mutants in the first large-scale zebrafish genetic screen (Granato 96). These motility mutants were divided into 14 phenotypically distinct groups based on the qualitative response results and any associated morphological defects.

Over the years, however, due to the complexity of the escape response circuit, it is inevitable that motility mutants identified based on this criteria are in fact a large mixture with defects in sensory inputs (Svoboda et al, 2001), central nervous system circuits (Cui et al, 2005), neuronal development (Guo et al, 1999, Lorent et al, 2001), neuromuscular transmission (Ono et al, 2001, Schredelseker et al, 2005) and muscle contractility

(Gleason et al, 2005), etc. It also became clear that the original grouping based on motility phenotype could be misleading. For example, *sho* and *two* mutants both belong to group B4 with reduced locomotion. However, *sho* dysfunction results from a mutation in the gene encoding the glial glycine transporter, a protein responsible for regulating the level of the inhibitory neurotransmitter (Cui et al, 2005). On the other hand, the *two* phenotype results from a mutation in RAPSYN, a molecule involved in post-synaptic organization and AchR aggregation (Ono et al, 2002). Similarly, *acc* and *beo* mutants which are both in the subgroup C1 turned out to have mutations in the muscle specific ATPase (Gleason et al, 2005), and in the glycine receptor beta subunit 2 (Hirata et al, 2005), respectively. These uncertainties call for the more accurate assessments of function before undertaking laborious genetic approaches to pin down the mutation. Otherwise the mutation may ultimately fall outside the area of interest, which in our case is the motor pathway that includes neuromuscular transmission. Consequently, we established a set of experiments that includes three complementary methods to help uncovering the mutation.

First, high-speed movies of the rapid escape response provide quantitative information about potential defects in motility. Due to the extremely fast escape response it is impossible for analysis by either the naked eyes or standard video rate cameras. Therefore, I used a high-speed digital camera set to 1000 frames per second capture rate (Photron Fastcam PCI camera, San Diego CA) to record the movement. When needed, additional motion detection software Videoquant (Viewpoint LS, Montreal, Canada) was employed to analyze and quantify the response. Offline measurements of individual frames provided quantification of movements by plotting pixel displacement as a

function of time. Wild type response plots were then used as a standard to compare to the mutant responses, rendering detailed and quantitative behavioral analysis.

Second, electrophysiological recording was used to detect functional abnormalities at the neuromuscular junctions. For this purpose I recorded synaptic currents from the skeletal muscle using the whole cell recording technique. The muscle of zebrafish is small and uniquely suited for this type of analysis because of the high input resistance (Luna and Brehm, 2006). I recorded spontaneous endplate currents (mEPCs) from muscle and obtained evoked endplate currents (EPCs) using the paired recording of motoneuron and target muscle (Wen and Brehm, 2005). mEPCs represent the inward cation currents conducted by AchRs when activated by acetylcholine released spontaneously (without neuronal action potential) from the motor neuron presynaptic terminals. The frequency, amplitude and shape of the mEPCs can indicate potential abnormalities in presynaptic neurotransmitter release, postsynaptic receptor kinetics or neurotransmitter clearance. For example, *sop* and *red* (Ono et al, 2001) share the same paralytic phenotype, but *sop* lacks mEPCs while mEPCs are completely normal in *red* mutants. The identification of the culprit genes confirmed different underlying mechanisms as *sop* has a mutation in AchR delta subunit which prevents expression of AchRs (Ono et al, 2001), whereas *red* has a mutation in the muscle dihydropyridine receptor, downstream to synaptic transmission (Ono et al, 2001, Schredelseker et al, 2005). In another motility mutant twister, mEPCs with very slow decay kinetics implicated defective AchR function, a proposal that was later validated by the identification of a mutation in the pore-forming region in the α subunit of the muscle nAchRs (Lefebvre et al, 2004).

EPCs provide additional information to help identify the defective gene. Mutant fish that are defective in certain presynaptic functions, such as motoneuron excitability, neuronal calcium channel function, presynaptic proteins important for calcium-dependent vesicle release or calcium clearance in the presynaptic terminal would be expected to show abnormalities in EPCs but not in mEPCs. Our lab developed a paired neuron-muscle recording scheme involving simultaneous whole cell patch clamping on the caudal primary motoneuron (CaP) and one of its target fast muscle cells (Wen and Brehm, 2005). When the whole cell configurations on both neuron and muscle were achieved, action potentials can be elicited under current clamp mode by injecting currents into the soma and corresponding evoked responses were recorded from the muscle cell. The highly stereotypic innervation patterns in each myotome of zebrafish larvae enable us to successfully identify the primary motoneuron and its target muscle cells (Westerfield et al, 1986). Spontaneous and evoked responses provide complimentary information regarding neuromuscular transmission. Therefore, combining the results from muscle recordings and paired neuron-muscle recordings could reveal important cues as to which side of the synapse the mutation resides.

The third approach for identifying candidate mutations capitalizes on the transparency of the zebrafish larvae for the purpose of imaging either live or fixed whole-mount preparations. In this manner either pre- or post-synaptic labels can detect potential abnormalities in synapse formation and organization, helping to decipher the possible cause for motility defects (Ono et al, 2000; Ono et al, 2001). For example, zn-1/znp-1 antibodies were used to recognize primary and secondary motor neuron axons and detect aberrant nerve branching pattern (Trevarrow et al, 1990). Presynaptic neuronal terminals

have been visualized in detail using an antibody against synaptic vesicle protein 2, an abundant protein present on the synaptic vesicle membrane (Janz & Sudhof, 1999). On the postsynaptic side, two most frequently used synaptic markers are two representative snake toxins, α-bungarotoxin and fasciculin. α-bungarotoxin is a toxin from the banded krait that binds the α-subunit of AchRs specifically and irreversibly (Anderson MJ 74). Fasciculin II (FASII), isolated from green mamba toxin, binds to cholinesterase molecule and block the enzymatic activity (Karlsson et al, 1984). In wild type fish, when labeled with the fluorescence-conjugated α-bungarotoxin and FASII, AchR clusters and cholinesterase distribution show overlapping pattern on the muscle (Ibanez-Tallon et al, 2004). Several motility mutant lines were successfully identified on the basis of fluorescence labeling of these postsynaptic markers. A mutation in AchR δ subunit was identified based on the lack of bungarotoxin staining in sofa potato mutants (Ono et al, 2001) and the mutation in RAPSYN was revealed in the twitch once (two) mutant due to the abnormal distribution pattern found in bungarotoxin staining (Ono et al, 2002). Similarly, a mutation in acetylcholinesterase was found in ziehharmonica (zim) when the mutant showed an absence of AchE in FASII labeling (Behra et al, 2002; Downes et al, 2004).

Considering the previous success in identifying mutations with the aforementioned approaches, similar methods were used to in an attempt to unravel the mechanism underlying *bajan* (*baj*) mutant's motility phenotype. *Bajan* was originally identified in the first large-scale mutant screen conducted in Tubingen, Germany (Granato et al, 1996). It was grouped as one of the locomotory mutants based on its reduced mobility in the touch-response screening. Apart from the impaired motility,

bajan homozygotes do not display obvious morphological defects or other developmental abnormalities. They never develop a swimming bladder and are consequently generally viable only until around 120 hpf. Heterozygous *bajan* embryos, however, are indistinguishable from their wild type siblings. They survive till adulthood and reach sexual maturity at around 3 months, similar to the wild type fish.

In addition to their locomotory dysfunctions, many motility mutants displayed various defects in trunk muscle development and differentiation, in heart and otoliths development and in axon formation during early development (Granato et al, 1996). Based on the reduced motility and lack of obvious morphological defects in the muscle or other tissues, we postulated that the *bajan* mutation might reside in one of the links related to the neuromuscular transmission. Therefore, studying *baj* and uncovering the gene responsible for its phenotype could potentially provide additional information about the neuromuscular junction, or the upstream presynaptic mechanism that is yet to be further elucidated.

In this chapter, I describe the initial studies on *baj* using a combination of the behavioral, electrophysiological and imaging techniques to dissect the mutant's motility phenotype in order to help identify the mutation.

Methods

Fish strain

Brian's wild type strain was obtained from Brian's Aquarium on Long Island.

Mutant fish bajtf247 was generated in an ENU mutagenesis and motility screen conducted at the Max Planck Institute (Tubingen, Germany) (Granato 96).

Fish rearing

Zebrafish were kept in an on-site Marine Biotech system that is set to 27°C and a 13-hour light cycle. Wild type fish were kept at an average density of 5 fish per 2 L tank. Heterozygous *baj* mutants were kept in individual 1 liter tanks except for the weekly breeding time. Crosses were set up late in the afternoon to early evening in a breeding tank with males and females separated by a barrier. The barrier was removed the next morning to promote egg laying and fertilization. Eggs were collected in embryo water (40g/L instant ocean with 1ppm methylene blue) and sorted on the basis of health. The viable eggs were then counted and maintained in an incubator at 28°C.

Identification of homozygous and heterozygous baj fish

Potential adult heterozygous *baj* pairs were mated and all the offspring were examined at 48-72 hpf when the *baj* motility phenotype was most robust. It was sometimes necessary to manually dechorionate the unhatched *baj* homozygotes. Homozygous was sorted by gentle prodding on the larvae tails with a blunt-end tungsten needle and their responses were examined under a stereomicroscope (Stemi SV6, Zeiss). While wild type larvae quickly engaged in an escape response, homozygous *baj* displayed much diminished touch response and inability to swim out of the visual field. Larvae that showed mutant phenotype were then counted and compared to the expected Mendelian ratio. When approximately a quarter of the offspring showed the mutant

phenotype, the parents were identified as heterozygous *baj* fish. All heterozygous *baj* fish identified based on offspring's motility phenotype were later confirmed with genotyping (methods see Chapter 3).

Solutions for electrophysiology experiments

100% Hanks (in mM: 137.5 NaCl, 5.4 KCl, 1 MgSO4, 0.44 KH2PO4, 0.25 Na2HPO4, 4.2 NaHCO3, 1.3 CaCl2, 5 Na-HEPES)

Bath recording solution BRS (in mM): 134 NaCl, 2.9 KCl, 2.1 CaCl2, 1.2 MgCl2, 10 Glucose, 10 Na-HEPES, pH 7.4 and 293mOsm.

Neuronal pipette recording solution (in mM): 115 K-gluconate, 15 KCl, 2 MgCl2, 10 K-HEPES, 1 BAPTA, 4 Mg-ATP, pH 7.3 and 290 mOsm.

Muscle pipette recording solution (in mM): 120 KCl, 10 K-HEPES, 5 BAPTA, pH 7.4 and 290 mOsm.

Behavioral analysis

To assess the motility deficiency of *baj* mutant in the earliest movements of spontaneous coiling, before they can be identified on the basis of touch response deficiency, all the offspring of adult heterozygous *baj* pairs were examined at 24 hpf. After dechorionization, their movements were continuously monitored under a stereomicroscope (Stemi SV6, Zeiss) for 5 minutes. Embryos that display any spontaneous movements during this period of time were transferred into a separate petri dish. The rest of the embryos were raised until after 48 hpf for identification based on

touch response and genotyping. The number of homozygous *baj* and siblings were then counted and compared in both groups.

For high-speed imaging of the larval touch response, individual 48 hpf wildtype and mutant zebrafish larva was placed in 35mm petri dish containing 10% Hanks. Escape response were elicited by a gentle prod to the tip of the tail with a tungsten needle (0.004in O.D.; A-M systems Inc.). Images of the escape response (512 x 512 pixels) were captured at the rate of 1000 frames per second with the Photron Fastcam PCI camera (San Diego CA). The digital camera was mounted on top of a stereomicroscope (Stemi SV6, Zeiss). Recordings continued until the fish moved out of the visual field or stopped swimming. Individual frames of the high-speed movie were then examined offline for analysis of the mutant motility phenotype.

Electrophysiology

Fish preparation

Larval fish which aged between 52 hpf and 120 hpf were anethetized by placing them in 10% Hanks solution containing 0.08% tricaine methane sulphonate (MS222; Wester Chemicals Inc., Scottsdale AZ) for 2 minutes. Embryos were subsequently decapitated and transferred into a Sylgard (Dow-corning, Midland MI)-coated recording chamber filled with bath recording solution. The tail was pinned down laterally onto the Sylgard lining by inserting two tungsten pins through the notochord at approximately tail segments 5 and 14. The skin between two pins on the topside was then removed. Subsequent steps were performed on Axioskop FS upright microscope (Zeiss, Oberkochen, Germany) and viewed with 10X and 40X physiology achroplan objectives

(Zeiss). The superficial slow muscle layer on the ventral side was removed to give access to the deeper fast muscle cells.

Recordings of the spontaneous synaptic response (mEPCs)

For mEPC (miniature endplate current) recording, 1.5 μM tetrodotoxin (TTX) was present in the bath solution throughout the recording to block nerve action potentials and ensure that all currents recorded were spontaneous synaptic responses. Muscle recording pipettes were pulled from 1.5 mm O.D. Kwik-Fil borosilicate glass (World Precision Instruments Inc., Sarasota, FL) to a 2 to 3 μm outer diameter tip with a very short taper to minimize the pipette resistance. Typically, the muscle recording pipette measured 2 to 4 Mohm when filled with the muscle pipette solution. While positioning the recording pipette to approach the muscle surface, positive pressure was applied to keep the tip clean by gently blowing through a pipette tip. Once the giga-ohm seal was obtained, gentle suction was applied to rupture the cell membrane within the pipette tip and the whole-cell voltage clamp configuration was achieved at the holding potential of –50 mV. Spontaneous synaptic responses were recorded as muscle cells were held at –50mV to inactivate sodium channels and minimize contraction. All recordings were done at room temperature.

Data acquisition and analysis

An EPC 10/2 dual patch clamp amplifier (List Electronics, Darmstadt-Eberstad, Germany) was used for simultaneous current clamp recordings from neuron and voltage clamp recordings from muscle. The resultant analog signals were sampled at 50 KHz for

neuron and 50 to 100 KHz for muscle. The acquisition was controlled using Pulse software (HEKA Elektronik, Lambrecht, Germany). Traces were analyzed offline using either Minianalysis (Synaptosoft, Decatur, GA), Pulsefit (HEKA Elektronik, Lambrecht, Germany) or IGOR Pro (WaveMetrics, Lake Oswego, OR). The rise time of synaptic currents were determined on the basis of 10 to 90% of peak amplitude. The decay time constant was determined by fitting the current decay (90% to 10%) to a single exponential function. Individual embryos used in recordings were selected based on motility phenotype and later confirmed by genotyping to be mutant homozygotes (genotyping methods see chapter 3).

Statistical significance of differences between wild type and mutants was assessed by Student's t-test (two-tailed). Data were considered significant at $P<0.05$.

Fluorescence imaging of synaptic markers

To label AchRs, decapitated 52 to 76 hpf larvae were placed in 100% Hanks and the skin along one side of the tails were removed. This was followed by a 15-minute incubation in 0.1 μM α-bungarotoxin conjugated to either Alexa Fluor 647 or tetraethylrhodamine (Molecular Probes, Eugene OR). The larvae were then washed in toxin-free 100% Hanks for 2 hours with frequent changes of solution to remove non-specific binding of the toxin.

For staining of acetylcholinesterase, decapitated and skinned larvae were incubated for one hour in a 100% Hanks containing approximately 0.12 μM Fasciculin II (Alomone Labs) conjugated to Alexa Fluor 633 (Molecular Probes). To minimize the nonspecific labeling of fasciculin, I added 0.1% bovine serum albumin (Sigma-Aldrich).

Fish were then washed for 1.5 hours in toxin-free 100% Hanks. All *in vivo* toxin staining were done at room temperature and protected from light.

To label synaptic vesicles with FM1-43, decapitated and skinned 72 hpf larvae were incubated for 15 minutes in 100% Hanks containing 1 μM TTX (Alomone Labs, Israel). For FM1-43 dye loading, a three-step procedure was used: first, prefill the fish with 10 μM FM1-43 (Molecular Probes) and 1 μM TTX in 100% Hanks for 15 minutes; second, load with 10 μM FM1-43 in high potassium terminal loading solution (in mM: 97 NaCl, 45 KCl, 1 $MgSO_4$, 5 Na-HEPES, 5 $CaCl_2$) for 5 minutes; third, complete the loading with 10 μM FM1-43 and 1 μM TTX in 100% Hanks for 3 minutes. Subsequently, larvae were transferred to a low calcium solution (0.5 mM $CaCl_2$ in 100% Hanks with 1 μM TTX) followed by three washes for 1 minute, 4 minutes and 10 minutes. To remove the excessive FM1-43 dye from the extracellular space, larvae were treated with 1 mM ADVASEP-7 (CyDex) in the low calcium solution for 5 minutes. Finally, larvae underwent six 3 minutes washes in the low calcium solution prior to mounting and observation.

Staining for synaptic vesicle 2 (SV2) was carried out using whole-mount immunohistochemistry. Larvae were anesthetized on ice and fixed overnight at 4°C in 4% paraformaldehyde diluted in 1X phosphate buffered saline (PBS) (Gibco). Specimens were then rinsed briefly in PBS, decapitated to increase accessibility to the tissue, washed in distilled water to dissolve salts, permeabilized in acetone for 7 minutes at –20°C, rinsed again in distilled water, and transferred to blocking solution (PBS with 0.5% Triton X and 5% donkey serum) for 1 hour incubation at room temperature. Embryos were then incubated overnight at 4°C in primary antibody, mouse monoclonal anti-SV2

(Developmental Studies Hybridoma Bank, University of Iowa) 1:100 in blocking solution. The following day, specimens were washed extensively in PBST (PBS with 0.5% Triton X) for 2 hours and transferred to secondary antibody (goat anti-mouse antibody conjugated to CY5 from Jackson Labs) 1: 500 in PBST for overnight incubation at 4°C. Embryos were again washed extensively in PBST before imaging. For double staining of AchR, α-bungarotoxin (10^{-7} μM) was added into secondary antibody incubation for 15 minutes prior to PBST wash and mounting.

For imaging, the labeled embryos were mounted in 1% agarose, with the intact side (non-skinned) flush against the bottom of a glass coverslip. Fluorescent images were captured on a Zeiss 510 Meta confocal Axiovert 200 microscope using a C-Apochromat 40X water-immersion objective. For comparison purpose, images of wildtype specimens were captured first to establish optimization of image settings before applying them to mutant specimens.

Results

Baj homozygotes lack spontaneous early movement

Homozygous *bajan* lack spontaneous coiling between 23 and 30 hpf. Slow, spontaneous alternating tail contraction (coiling) is the earliest motion observed in the zebrafish embryos (Saint-Amant and Drapeau, 1998). In order to examine whether this early motor behavior is affected in the mutants, I compared the spontaneous coiling from dechorionated wild type and mutant embryos between 23 and 30 hpf. All of the wild type

embryos (n=89) displayed at least one spontaneous tail contractions during the 5-minute observation period. When the offspring of *baj* heterozygous parents were examined, approximately one fourth of the embryos exhibited no coiling movement. These embryos were raised until after 48 hpf when their touch responses can be assessed by high-speeding imaging. 100% of embryos that lack early coiling movement showed defective touch response at 48 hpf. Subsequently, all of them were further confirmed to be mutant homozygotes by genotyping.

Baj displays attenuated escape response

To further study the motility behavior of *baj*, high-speed movies of stimulus-evoked escape response from homozygous *baj* larvae were analyzed and compared to the wild type responses. Such comparison revealed a significant difference in the initial touch avoidance and subsequent swimming behavior. Upon a single touch on the tail, 48 hpf wild type larvae (Fig 1, top panel) responded with an initial C-bend which peaked at around 20ms after stimuli, a more variable second bend to the opposite side and several tail beats to swim off. This fast stereotypic response became robust and incredibly consistent in individual wild type embryos after 32-36 hpf (Saint-Amant and Drapeau, 1998). *Baj* homozygotes, however, showed diminished initial C-bend (Fig 1, bottom panel) and such greatly reduced amplitude in the subsequent tail contractions that they were barely visible. Although the latency between the stimulus and the onset of the response appeared to be normal, *baj* displayed a much weaker escape response and failed to swim away from the stimuli. In contrast, the escape responses of *baj* heterozygote were indistinguishable from those of wild type fish.

Preliminary electrophysiological recordings indicated decreased amplitude in the mEPCs from baj

Whole cell voltage clamp recording from fast skeletal muscle cell in 72 hpf wild type and *baj* fish was performed to quickly assess whether the neuromuscular transmission is defective at mutant NMJ. Consistent with the diminished touch response, the amplitudes of spontaneous synaptic responses (mEPCs) were much smaller than that of the wild type, as shown in the sample traces of mEPCs (Fig 2A) for one representative fast muscle cell from wild type and *baj*. The shape of mEPCs in wild type and *baj* are very similar in that they both exhibit a fast rising phase and a slower single exponential decay, except that *baj* has much smaller amplitude. The frequency distributions for the amplitude, rise time and decay time constant (Fig 2B, C, D) were also compared between wild type and *baj*. The frequency distribution plot from the representative cells showed the difference in current amplitude between wild type and *baj*. In the plot, the wild type events ranged between 0.4 and 1.2 nA while almost all events in *baj* fell below 0.4 nA (Fig 2B). The distribution of rise times and decay time constants from the two representative cells showed comparable patterns (Fig 2C, 2D).

Florescence imaging of synaptic markers showed normal distribution pattern at baj NMJ

In order to test whether the observed defective neuromuscular transmission is a direct result of aberrant patterning of postsynaptic organization, fluorescence-conjugated α-bungarotoxin (α-Btx) were used to label the post-synaptic AchRs. In 72 to 80 hpf wild type larva, α-bungarotoxin labeled AchRs showed organized clusters on the postsynaptic

muscle cell membrane, as shown in the two- to three-myotome region in the larval tail (Fig 3, top panel). The most intensive labeling occurred at the ends of each segments (or muscle cells), as well as some punctate locations in the middle of the segments, indicating the locations of neuromuscular junctions. Fasciculin II (FASII) staining of acetylcholinesterase (AchE) completely overlapped with the α-Btx staining of the AchRs, showing well-clustered postsynaptic sites (Fig 3, middle panel). In *baj* mutants of the same age, both AchRs and AchE showed normal distribution pattern that are indistinguishable from the wild type.

To examine the presynaptic motoneuron axon branching, I co-labeled two presynaptic markers with the postsynaptic AchR clusters, the presynaptic SV2 (Synaptic Vesicle 2) protein (Bajalieh et al, 1992; Janz and Sudhof, 1999) and FM 1-43, a styryl dye commonly used to mark presynaptic terminal (Liu and Tsien, 1995) or study vesicle recycling (Betz and Bewick, 1992). Results from both experiments showed that the distribution of the presynaptic motoneuron axons were indistinguishable between *baj* mutants and wild type fish (Fig 4 & 5). Also, the presynaptic terminal overlapped completely with the AchR clusters on the postsynaptic muscle cell membrane, indicating the proper contact between pre and postsynaptic sites during synapse formation (Sanes and Lichtman, 1999).

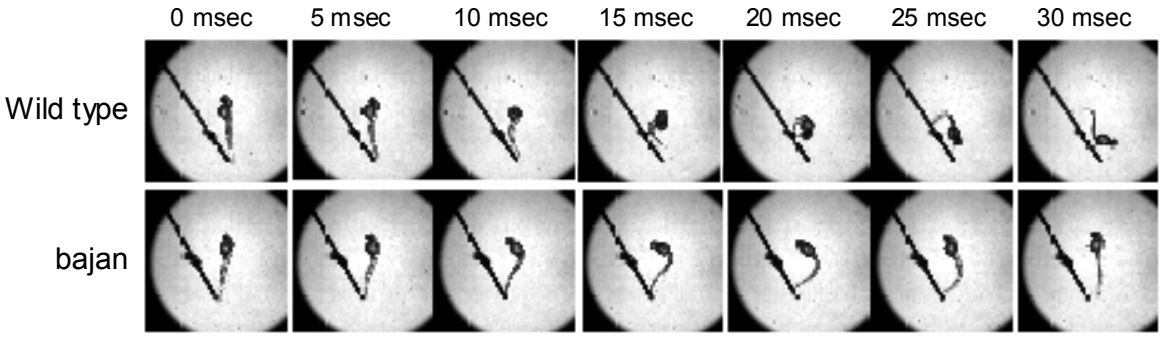

Figure 1. Touch-elicited escape responses in 48 hpf wild type and *baj* larvae

The escape responses of 48 hpf wild type (top) and homozygous *baj* (bottom) larvae were elicited by a gentle prod to the tip of the tail with a tungsten needle. Individual frames, captured at the rate of 1000 frames per second, were shown with 5 msec intervals. Note the diminished C-bend at 20 msec and the barely discernible subsequent tail movements in *baj* larva (bottom).

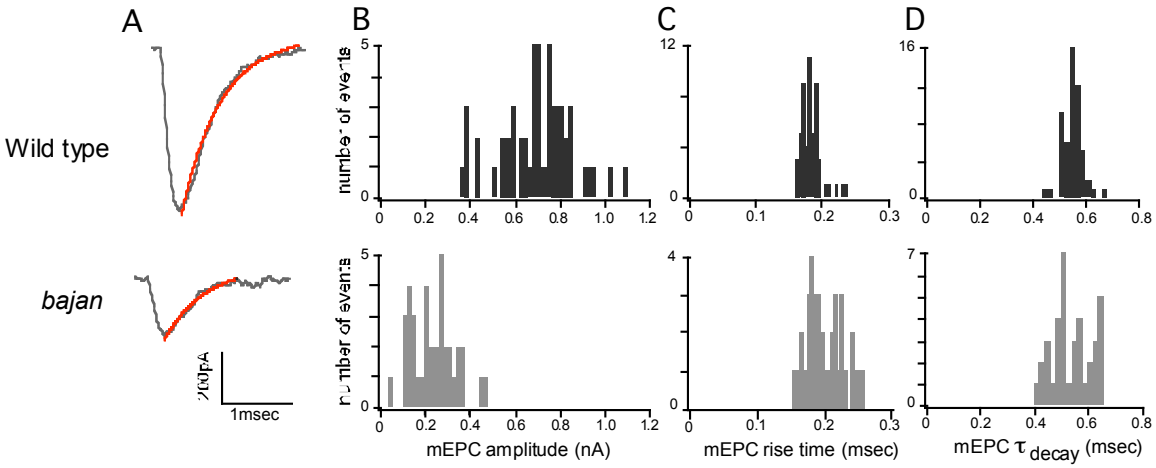

Figure 2. Preliminary whole-cell voltage clamp recordings of spontaneous synaptic responses

Data presented were obtained from a single recording in fast skeletal muscle in 72 hpf wild type and *baj* larvae. (A) Sample traces of individual mEPCs recorded at –50 mV membrane potential. The decay phase is fitted with single exponential function (red). (B) Frequency distributions of mEPC amplitude. (C) Frequency distributions of 10 to 90% rise time. (D) Frequency distributions of decay time constant (τ).

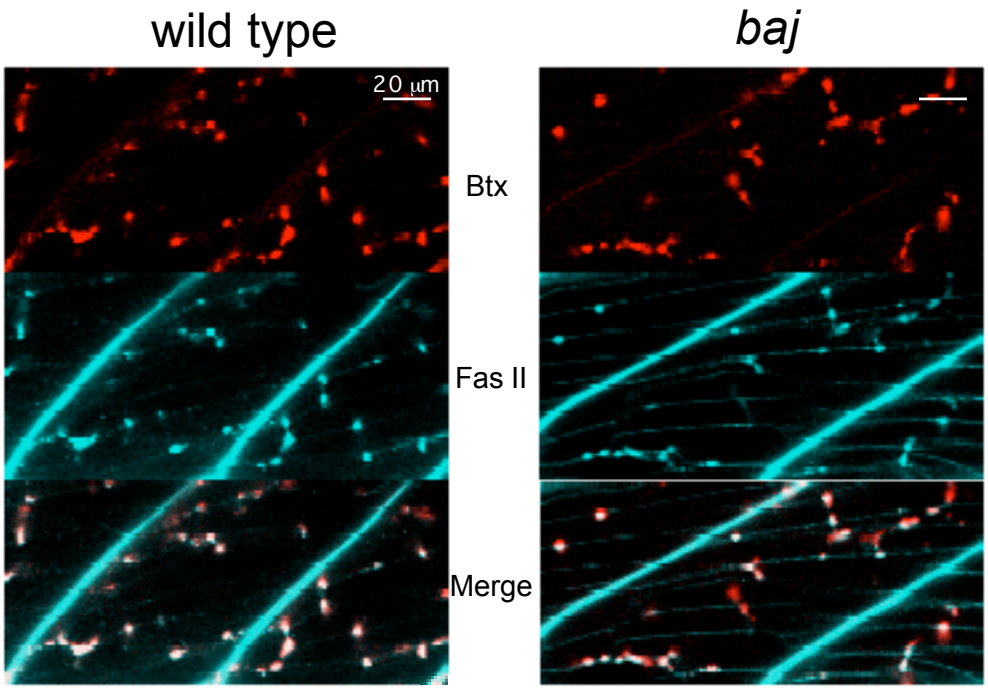

Figure 3. Double staining of postsynaptic AchRs clusters and acetylcholinesterase

Whole-mount staining of postsynaptic AchRs with tetramethylrhodamine-conjugated α-bungarotoxin (top) and acetylcholinesterase with Alexa Fluor 647-conjugated fasciculin II (middle) in 48 hpf wild type (left) and *baj* (right). Lateral view of two hemi-segments of the tail is shown.

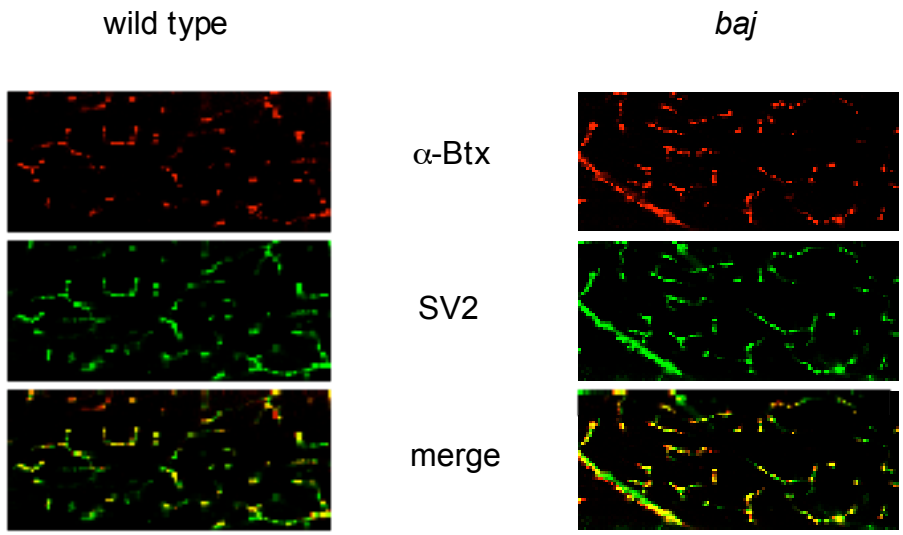

Figure 4. Double staining of AchR clusters and Synaptic Vesicle Protein 2 (SV2)

Whole mount staining of AchR with tetramethylrhodamine-conjugated α-bungarotoxin (top) and synaptic vesicle 2 protein (SV2) with mouse monoclonal antibody visualized with CY 5-conjugated goat anti-mouse secondary antibody (middle) in 72 hpf wild type (left) and *baj* (right).

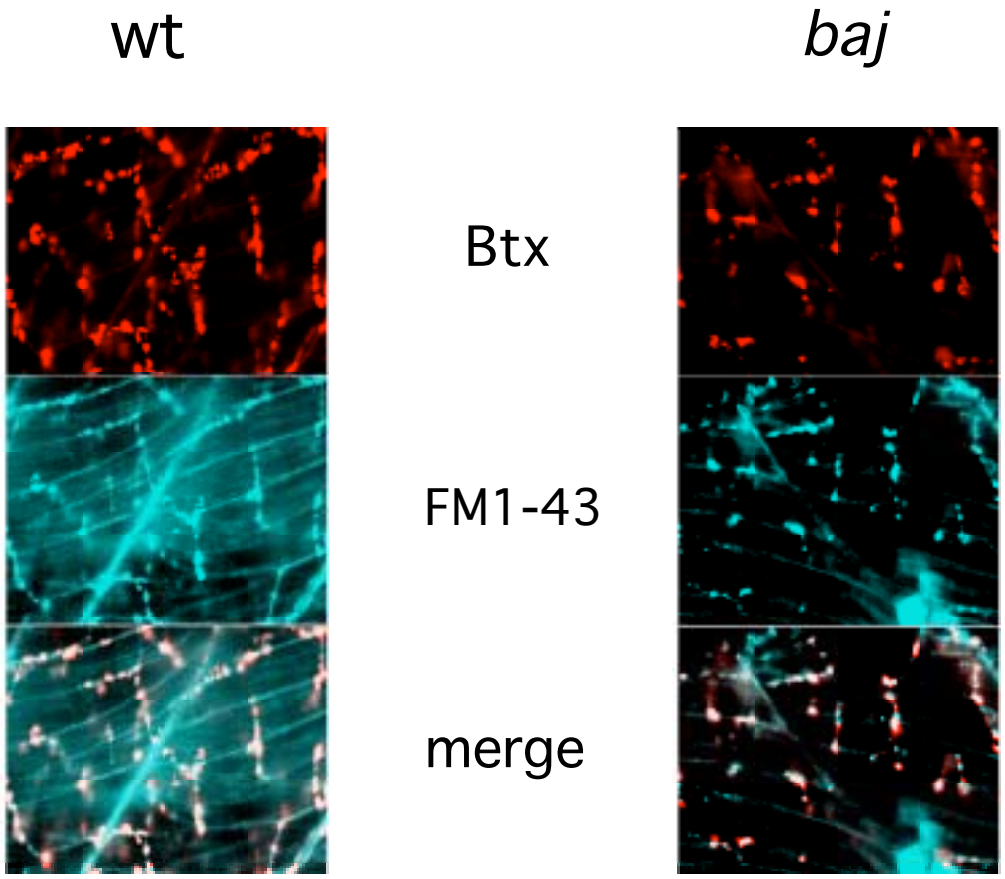

Figure 5. Double staining of AchR clusters and FM 1-43 labeling.

Whole mount staining of AchRs with Alexa Fluor 647-conjugated α-bungarotoxin (top) and synaptic vesicles with FM 1-43 dye (middle) in 72 hpf wild type (left) and *baj* (right).

Discussion

To uncover the mutation that underlies the motility phenotype in *baj*, a mutant fish with severely diminished touch response, we applied a set of quick screening tools in an attempt to find obvious defects in NMJ formation and neural muscular transmission. First, after close examination of the high-speed image of the escape response, we found that upon touch stimulation, *baj* homozygotes showed diminished initial tail bend and much weaker subsequent tail contractions compared to the wild type, albeit normal timing of the responses. Second, consistent with the phenotype, electrophysiology recordings of the spontaneous synaptic currents from the ventral fast muscle cells showed much decreased amplitude in *baj*, suggesting a defect in the neuromuscular transmission.

Both pre- and post-synaptic players at the neuromuscular junction could contribute to such attenuation in the spontaneous neurotransmission. Candidates include gene products involved in transmitter synthesis or filling of the presynaptic vesicles, and on the postsynaptic side, AchR and genes that modulate receptor function or localization. Two pieces of evidence argued against a post-synaptic origin for the defective synaptic transmission at *baj* NMJ. First, fluorescence conjugated α-bungarotoxin and FASII visualized normal postsynaptic AchRs clustering and acetylcholinesterase localizations at the synaptic sites in *baj* skeletal muscle. Although compromised AchR function at the synaptic sites or incomplete localization could potentially be responsible for the smaller synaptic currents, mutations in the genes encoding the various AchR subunits frequently interfere with the proper assembly and integration of AchRs onto the plasma membrane, thereby showing lack of toxin-labeling of the AchRs on the muscle surface and absence

of postsynaptic responses, such as the case in *nic* and *sop* (Westerfield et al, 1990, Ono et al, 2001). In some other cases, when mutations occurred in genes that control AchR clustering and localization, a decrease in the spontaneous synaptic currents was accompanied by diffused membrane distribution of the AchRs (Ono et al, 2002). However, no absence of AchR staining or change of AchR clustering pattern was found at *baj* NMJ.

Second, the spontaneous synaptic responses in *baj* showed normal current kinetics. Mutants with defective AchR gene usually present changes in the kinetics of synaptic responses. For instance, a point mutation in the α subunit of the muscle nAchRs underlies the slow decay kinetics of mEPCs in the mutant fish twister (Lefebvre et al, 2004). Therefore, this difference in magnitude alone in the absence of obvious defects in the current kinetics or postsynaptic organization argued against defects on the postsynaptic side of the neuromuscular transmission.

In the Ach metabolic pathway, there are four essential players for the synthesis, concentrated storage and release of the Ach molecule: 1) the sodium-dependent, high affinity Choline Transporter (ChT) that is responsible for the acute uptake of extracellular choline across the presynaptic plasma membrane (Jope and Jenden, 1979), 2) Choline acetyltransferase (ChAT), the enzyme that catalyzes the synthesis of Ach from choline and acetyl-CoA in the presynaptic terminal (Nachmansohn and Machado, 1943), 3) the vacuolar H^+-ATPase that functions as an ATP-dependent proton pumps and generates protonmotive forces to drive Ach transport across the synaptic vesicle membrane (Nelson 2003), 4) Vesicular Acetylcholine transporter (VAchT), the carrier for packaging Ach molecules into the presynaptic vesicles using the electrochemical gradient provided by

the Vacuolar proton ATP-ase (Parsons 2000). If any of these four key proteins shows impaired function, it would result in insufficient Ach filling of synaptic vesicles and as a result, postsynaptic responses at NMJ will show decreased amplitude, similar to what we found in *baj*. For example, in human, mutations in ChAT gene give rise to congenital myasthenic syndrome with episodic apnea (CMS-EA) (Ohno et al 2001). Patients with this motor disorder suffer from hypotonia and respiratory impairment at birth or in the neonatal period. Endplate studies from patients showed no AchR deficiency but slightly decreased amplitude in the miniature endplate potential (mEPP). Similarly, VAChT knock-down mice, in which the protein expression level were reduced to approximately 50% compared to the wild type, are myasthenic and showed decrease in amplitude and frequency of mEPP (Prado et al, 2006). Therefore, the aforementioned four genes became the top candidates for *baj* mutation.

In conclusion, our imaging and physiology results point to a presynaptic defect involving transmitter synthesis or release. Armed with this information, I proceeded to genetic means of identifying the culprit gene amongst the possible candidates. The results of these studies form the basis of the next chapter.

CHAPTER 3

IDENTIFICATION AND CONFIRMATION OF THE *BAJAN* GENE

Introduction

Two observations point to a presynaptic defect in the motoneurons as causal to the motility dysfunction in *bajan*. First, the spontaneous neuromuscular synaptic currents were greatly attenuated in *bajan* compared to wild type. Second, the postsynaptic receptor clusters, as determined by labeling with fluorescence-conjugated α-bungarotoxin, appeared normal in *bajan*. The most straightforward presynaptic determinant of synaptic strength is vesicular ACh content. The number of ACh molecules in a vesicle is a product of the synthesis of ACh and the rate of transport into the vesicle. The former process involves the provision of choline substrate by choline transporter (ChT) and the actual synthesis of ACh by choline acetyltransferase (ChAT). The latter involves the generation of electrochemical proton gradient by the vacuolar ATPase and the exchange between proton and Ach by the vesicular acetylcholine transporter (VAchT). Compromised function of any of these proteins would be predicted to reduce the amplitude of spontaneous synaptic currents without affecting the postsynaptic organization.

However, direct sequencing of these four top candidates could potentially be risky and extremely time-consuming due to several reasons. First, none of the four genes were

identified in the zebrafish genome and sequence information was available only on predicted transcripts based on protein sequence homology. Second, three out of four genes (except for VAchT) are large and comprised of multiple exons, which introduce additional technical difficulty. Third, although mutations in the four candidates would explain current results, the *baj* mutation could, in actuality, reside in a gene other than these candidates. Therefore, to further rule in or rule out a mutation in these candidate genes we employed a relatively unbiased genetic approach, positional cloning.

Generally, identification of a mutated gene by positional cloning involves the following basic steps: first, a low-resolution genome-wide scanning to assign a chromosomal location for the mutation; second, the intermediate-resolution mapping to position the gene between two flanking polymorphic markers; third, high-resolution mapping based on calculated recombination frequency in > 1000 individual mutants to continuously narrow down the region until it is within 1cM distance; fourth, construct a physical map with available information from the bacterial artificial chromosome (BAC) clone library; fifth, search for candidate transcripts and sequence them to locate the mutation (zon.tchlab.org).

Usually, the full procedure described above is implemented in the absence of obvious candidate genes. However, with the advantage of having candidate genes at the outset, we were able to use the first step Bulk Segregant Analysis (BSA) to determine the *baj* mutation. Bulk Segregant Analysis is the first step of the positional cloning approach (Michelmore et al, 1991; Talbot and Schier, 1999), which involves scanning the entire genome with polymorphic markers in order to place a mutation onto a specific linkage group in a genetic map. After assigning a chromosomal location to the *baj* mutation, I

could see whether the mutation mapped to the chromosome containing any of the predicted genes by using the zebrafish genome map that is currently being assembled by the Sanger Center.

The basic logic behind BSA or any subsequent steps of positional cloning is based on the meiotic recombination, one of the most basic phenomena in living organisms. Meiotic recombination, or cross-over, is a reciprocal recombination process that involves breakage and exchange of segments between two nonsister chromatids in prophase I of meiosis. It creates new sets of genes in the gametes that are different from either parent, therefore is an important step during revolution to gain genetic diversity. Generally, the closer the distance between two genes on one chromosome, the less likely it is for a cross-over to occur between them. Therefore, by comparing the frequency of recombination, multiple loci can be placed in relative position to each other, thus creating a genetic linkage map. The recombination frequency of 1% equals to 1 m.u. (map unit) or 1 cM (centimorgan), which translates roughly into 660 Kb physical distance in zebrafish genome.

In practice, a polymorphism is usually first identified and then tested in a large number of mutant individuals for its recombination frequency. The distance between the polymorphic marker and the mutation is directly proportional to the probability of a recombination event. The smaller the number of recombination events, the closer the marker is to the mutation site. By identifying multiple markers and comparing their recombination frequencies, one can keep searching in the correct direction until the recombination frequency becomes zero, which means that the marker is at or extremely

close to the mutation. If the next marker showed an increase in the recombination events, the mutation must lie between the last two markers tested.

The most frequently used markers in BSA are simple sequence length polymorphic (SSLP) markers, also named microsatellites. SSLP markers are relatively short DNA sequences consist of variable number of (CA)n repeats flanked by two primer sequences (Litt et al, 1989). The variable length of SSLPs in fish with different genetic backgrounds make them "agarose scorable", meaning that the length of SSLP markers can be reflected in the different sizes of the PCR amplified products shown on standard agarose gels. SSLPs appear frequently, span the whole zebrafish genome and their unique locations have been previously mapped onto specific linkage groups.

A set of 214 SSLPs (Mappairs, Clontech) has been selected from over 3000 markers on the MGH panel (http://zebrafish.mgh.harvard.edu) to scan the genome for linkage to *baj* mutation. The selected set contains roughly 8 to 9 markers per chromosome and provides enough coverage of the entire zebrafish genome (Postlethwait et al, 1998). A mutant and a sibling DNA pool was each made by extracting genomic DNAs from 20 individual embryos. It is crucial at this stage that all the embryos used for BSA are from the same family, since introducing a new set of allele can create false positive results. The appropriate primer pairs were used to amplify the 214 SSLP markers from the mutant and the sibling DNA pools. Amplified products were subsequently scored on three percent agarose gels and differential amplification patterns of a particular marker between mutant and sibling pools were recognized as possible positive linkage to the mutation.

Ideally, linkage is assumed when an additional band that is absent in the mutant pool appeared in the sibling pool. The logic behind the BSA analysis is that if the mutation and a particular marker co-reside on one chromosome, chances are that this marker will stay with the mutation during meiotic recombination event. Because individual fish that comprised the genomic DNA pools were independently sorted based on motility phenotype, it means that all the mutant embryos should carry the mutant strain allele for this specific marker while the sibling pools should show both the wild type strain allele and the mutant strain allele, hence the additional band. In some cases, however, when the positive marker is far away from the mutation (weak linkage), the additional band also shows up in the mutant pool but with much less intensities. Or, in other cases, false positive linkage was observed due to PCR amplification artifact. Therefore, retesting the candidate markers on each individual mutant and sibling embryo DNA is necessary to establish true linkage of the mutant allele to these markers or the chromosome it represents.

Methods

Generating mapping hybrids

Heterozygous fish for the *baj*-tf247 allele (SB366, DOB 5/03) were obtained from the Max Plank Institute in Tubingen Germany. Mapcross was performed by crossing the second generation of heterozygous *baj* (SB469, DOB 10/03), which were the offsprings from SB 366 incross, with Brian's wild type, a wild type strain purchased from a local pet

store. Heterozygous F1 fish from 3 different mapcrosses (SB545/546/547, DOB 4/04) were identified by multiple random incrosses. Wild type and mutant progeny (F2) from identified heterozygous F1 pairs were then collected for mapping experiments. Data of mapping experiments were acquired using embryos from a single pair of heterozygous F1 fish.

Genomic DNA extraction from F2 embryos and F1 adult fish

A single clutch of embryos was dechorionated and sorted based on phenotype at 72 hpf. Mutants and siblings were collected into separate eppendorf tubes and anesthetized with 5 minutes incubation on ice. 1ml of 100% methanol was added to the tube after removing the excess fluid. For quick embryo lysis, individual embryos were transferred with a glass Pasteur pipette into single wells in 96-well PCR plates (Applied Biosystems). Methanol evaporated when placing the plates in an air incubator at 70°C for 5 minutes. 25 μl of the embryo lysis buffer (~1.7mg/ml proteinase K in 1 X TE (10mM Tris, 1mM EDTA, PH 8.0)) were added into each well prior to overnight incubation with gentle shaking at 55C. Next morning, the plates were heated on a PCR block at 95°C for 10 minutes for proteinase K activity inactivation. Diluted DNA (1:20 in distilled water) samples were used for PCR amplification.

Genomic DNA of the adult F1 fish was obtained by tail clipping for analysis of the alleles carried. Fish was first anesthetized with 0.02% MS222 in system water for about 1 minute or until they showed sluggish, uncoordinated movements. Half of the tail fin was then excised with a surgical scissor and placed into a single well of a 96-well plate. 100μL of the adult fin lysis buffer (20mM NaCl, 10mM Tris, 10mM EDTA, 0.5%

SDS, 200μg/ml proteinase K) were added into each well, followed by 55°C overnight incubation and proteinase K inactivation in the next morning. Lysate was spun at 14,000 rpm to remove cell debris. To further improve the quality of DNA, the DNA in the supernatant was extracted using phenol/chloroform/isoamylalcohol (PCI, 25: 24:1, Invitrogen), precipitated and washed in ethanol and resuspended in distilled water.

Bulk Segregant Analysis

For low-resolution mapping, BSA was used to determine the chromosomal linkage. Embryos from a single pair of heterozygous F1 adults (SB 547 family #3) were collected for linkage analysis. Genomic DNA was extracted from 20 individual *baj* mutant and 20 sibling embryos at 72 hpf. Mutant and sibling DNA were then separately pooled by taking 12.5 μl from the 25 μl lysate of each individual embryos. Pooled mutant DNA and sibling DNA were then used as template in PCR amplification with 214 pairs of agarose scorable microsatellite markers (Mappairs, Clontech) to scan the genome for linkage.

The PCR reactions were done in 96-well plates. Each well held a 20 μl reaction containing genomic DNA template (8 μl of 1:20 diluted embryo lysate or 0.5 μl of adult fin DNA sample), 2 μl of 10X Taq buffer, 4 pmol of each primer, 1nmol of each dNTP and 0.5 U of Taq polymerase (Roche Applied Sciences). The following program was used on a GeneAmp PCR System 9700 (Applied Biosystems): 94°C for 2 min; 40 cycles of 94°C for 10 sec, 55°C for 30 sec, 72°C for 1 min; and final extension at 72°C for 5 minutes. Results of BSA were analyzed with gel electrophoresis. Approximately 15 μl of PCR products were loaded onto 3% TBE agarose gel (1:1 mixture of ultra pure agarose

from Invitrogen and metaphor agarose from Cambrex) with 0.8 μg/ml ethidium bromide. Mutant product and sibling product for each microsatellite marker were alternately loaded for easy comparison. The gel was run in 1X TBE at 150V for up to 2.5 hours. Pictures were taken under the UV light at around 30 minutes, 1.5 hour and at the end of the run. Results were analyzed by carefully examining any difference in product amplification patterns of each microsatellite markers between the mutant pool and sibling pool, which is suggestive of possible linkage. Positive markers were retested against the DNA samples from the same individuals used in the mutant and sibling pools. The segregation pattern of amplification products in individual mutants and siblings was used to determine the linkage of *baj* allele to the chromosome on which the positive markers locate.

RNA extraction, cDNA synthesis and sequencing

Total RNA extraction from 20 dechorionated 72 hpf embryos was performed using 800 μl Trizol Reagent (Gibco) following the instructions from Invitrogen. The RNA pellet from these 20 embryos was resuspended in 20 μl DEPC water (Ambion) and the concentration was determined using spectrophotometer. Approximately 500 ng to 1 μg of total RNA were used in a 20 μl cDNA synthesis reaction with the SuperScript III First-Strand Synthesis System for RT-PCR (Invitrogen).

To design primers for amplification of the zebrafish ChAT cDNA, a BLAST search was performed using published mouse ChAT protein sequence against the zebrafish genome with the tblastn program (www.ncbi.nlm.nih.gov/BLAST). A potential genomic region was found that coincide with the genomic sequence of zebrafish ChAT

predicted by the zebrafish genome-sequencing project database (www.ensembl.org). Using Biology workbench (http://seqtool.sdsc.edu/CGI/BW.cgi), the longest open reading frame was identified within the genomic sequence and the transcript was predicted and compared against published ChAT sequences in other species. Primers for amplifying zebrafish ChAT cDNA were then designed against regions of protein sequences well-conserved across species. Primers used in cDNA amplification and sequencing were: forward 5'-TGTACCTGACATGCATGGGTCACC-3' and reverse 5'-ATCTGAGCTGGTCTCCGCACATTC-3'.

ChAT cDNA was amplified in a 25 μl reaction containing 2.5 μl of 10X Buffer, 1 μl of MgSO4, 2.5 pmol of primers, 0.125 μmol of dNTP mix, 0.5 U of Platinum Taq High Fidelity polymerase (Invitrogen). The amplification protocol was: 94°C for 2 min, 25 cycles of 94°C for 10 sec, 61°C for 30 sec, 68°C for 2min and final extension at 68°C for 7 min. The products were analyzed on agarose gels and the band of expected size was excised for gel purification (QIAquick Gel Extraction Kit, Qiagen). The purified product was quantified with spectrophotometer and used for subsequent sequencing amplification.

To sequence the ChAT cDNA with an estimated size of 1.8Kb, 5 additional internal primers were used along with the forward and reverse primers to ensure overlapping sequences. Each sequencing PCR was performed in a 10-μl reaction containing 500ng of template, 2 μl of BigDye reaction mix (Applied Biosystems), and 5pmol of sequencing primer. The amplification program was: 25 cycles of 94°C for 10 sec, 50°C for 5 sec and 60°C for 4 min. The products were then purified (Qiangen DyeEx 2.0 Spin Kit, Qiagen), dried with speed vacuuming and resuspended in 12 μl Template

Suppression Reagent or Hi-Di Formamide (Applied Biosystems) before loading into an ABI Prism 310 Genetic Analyzer (Applied Biosystems).

In case of unsuccessful direct sequencing of the PCR product, the gel purified product was subcloned into the pCR4-TOPO vector (TOPO Cloning Kit for Sequencing, Invitrogen) and transformed into E. Coli (One Shot TOP-10 Chemically Competent E. Coli, Invitrogen). DNA was then extracted from the bacteria (QIAprep Spin Miniprep Kit, Qiagen) and used as template in the sequencing reactions.

RACE and cloning of full-length zebrafish ChAT

The very 5'- and 3'- end of the ensemble predicted ChAT transcript was not well conserved among different species. In order to amplify the 5' and 3' end of zebrafish ChAT, 5'- and 3'- rapid amplification of cDNA ends (RACE) were performed using Switching Mechanism At 5'-end of RNA Transcript (SMART, Clontech) kit. First strand 5'- RACE ready cDNA was synthesized from total RNA extracted from 1 day wild type embryos using the gene specific primer 5'-AGAGCATTTCCAGCGCAGTCGTCTGGGGGCTGG-3'. 5'RACE PCR was performed using the primer 5'-ATGTTGCGAGCCTCGGCCCACTGT-3' and the universal primer mix from the kit. An aliquot of the first step PCR product was purified (QIAquick PCR purification kit, Qiagen) and used as template in a nested PCR with the nested gene-specific primer 5'-TGGGGAGCTTCGGGAGAGC-3' and the nested universal primer from the kit. The nested PCR products were then gel purified and TOPO cloned for sequencing.

After acquiring the complete encoding sequence of zebrafish ChAT from the RACE results, the full length ChAT cDNA was amplified using primers 5'-TCTTCAACTTTGAGGATGCCAGTTTC-3' and 5'-TCCTGCGTCTTATGACTTGCTTCC-3' and subcloned into the pCR4-TOPO vector.

Genotyping by dCAPS

Derived cleaved amplified polymorphic sequence (dCAPS) analysis was used to genotype *baj*. A 216 bp region including the A to C mutation and one DdeI restriction site was amplified using primers 5'-GTTCAAACTCCTGTTTCTGATCATTGTCTT-3' and 5'-TGCTATCAGTGAACCTGTGAGCT-3'. The 25 μl PCR reaction was done using the following program: 94°C for 2 min, 35 cycles of 94°C for 10 sec, 57.3°C for 30 sec, 68°C for 30 sec and final extension at 68°C for 7 min. PCR products were digested with 5 U DdeI in a 25 μl reaction and results were analyzed with gel electrophoresis.

Morpholino phenocopy

Splice-site morpholino oligos were used to achieve *baj* phenocopy. The splice morpholino (5'-ATCATACACCTAACACAATGATCAG-3') was designed against the splice site where *baj* mutation occurred. Morpholino oligos were made into 3mM stock solution (~25ng/nl) in distilled water and stored at –20°C. Prior to injection, the morpholino stock solution was heated in the 65°C water bath for 5 minutes and mixed with Fast Green dye (Sigma) and distilled water to make a final working solution, 0.5 mM for the ATG morpholino and 2 mM for the splice one. Injection pipettes were pulled from 1.0 mm O.D. thin-wall borosilicate glass (World Precision Instruments Inc.,

Sarasota, FL) to create a long taper. The taper was then cut with a razor blade to obtain a 10-15 μm diameter tip. Morpholinos were pressure injected (~25 kPa, PLI-100 Medical Systems Corp.) into the yolk of one- to four-cell stage wild type embryos. The injection time varied to achieve a bolus of 100 μm diameter, equivalent to a 0.5 nl volume. At 48 hpf, injected embryos were analyzed and sorted based on their motility phenotype. The splice morpholino injected embryos that resembled *baj* phenotype were further analyzed with RT-PCR and sequencing.

Rescue of baj phenotype with mRNA injection

The full-length zebrafish ChAT cDNA was subcloned from pCR4-TOPO vector into pCS2+ vector (www.sitemaker.med.umich.edu). Approximately 8 μg of plasmid DNA were then linearized by NotI digestion over night. Digestion products were treated with proteinase K (400 μg/ml) in the presence of 0.5% sodium dodecyl sulphate (SDS) at 50°C for 30 minutes. The sample was then phenol/chloroform extracted, ethanol precipitated and resuspended in DEPC-treated water. *In vitro* transcription of the linearized sample was performed with mMessage mMachine *In vitro* Transcription Kit (Ambion) following the manufacturer's instructions. The harvested mRNA was resuspended in nuclease-free water and estimated by running an aliquot on denaturing gels. All the eggs born to a pair of *baj* heterozygous parents were injected with ~100 pg of wild type ChAT mRNA. At 48 hpf, embryos were assessed and counted based on their motility phenotype. The ratio of mutant embryos to total embryo number was compared with the Mendelian ratio. All embryos that displayed normal escape response were genotyped with dCAPS.

Immunohistochemistry

Staining of ChAT protein was carried out using whole-mount immunohistochemistry with 1:50 goat anti-ChAT affinity purified polyclonal antibody (Chemicon) and visualized with 1: 1000 secondary antibody (Alexa488-conjugated donkey anti-goat antibody from Jackson Labs) (details see Chapter 2 methods section). For double staining of AchR, α-bungarotoxin (10^{-7} μM) was added into secondary antibody incubation for 15 minutes prior to PBST wash and mounting.

Results

Generating map cross fish strain

One of the crucial prerequisite of successful mapping is the generation of a mapping hybrid strain. In any steps of the positional cloning process, in order to estimate the distance to the mutation based on calculated recombination frequency, identified markers have to be polymorphic between the mutant and the wild type alleles. Therefore, before the initiation of our mapping attempt, heterozygous Tu(mutant)/Tu fish were mated to different Brian's wild type, which is much more polymorphic than the Tu strain since it is not a lab inbred strain, to generate several mapcross families.

Baj allele was linked to chromosome 13

Bulk segregant analysis (BSA) was employed to assign the *baj* allele to a specific chromosome. In BSA, 214 simple sequence length polymorphism (SSLP) markers were amplified by PCR from genomic DNA pools from 20 mutants or siblings born to the same *baj* heterozygous parents. The amplified markers were then scored by gel electrophoresis and searched for differential amplification between mutant and sibling DNA pools. Products from marker Z17223 showed different gel patterns between mutant genomic DNA pool and sibling pool (Fig 1A), indicating linkage to chromosome 13. Since both bands amplified from the mutant and sibling pool but with different intensities, it might be a false positive or indication of a weak linkage. To confirm that the observed linkage was not a PCR induced false positive, Z17223 marker was retested on the individual mutant and sibling DNAs used to make up the BSA pool. Results

showed non-random segregation of the mutant allele (Tu) in the mutant group and sibling groups (Fig 1B), further supporting true linkage between the *baj* mutation and chromosome 13.

Sequencing VAChT and ChAT revealed single mutation in ChAT

After mapping the *baj* allele onto linkage group 13, a search for the predicted genomic locations of the proposed candidate genes was performed using zebrafish genome project database. Two potential candidates, vesicular acetylcholine transporter (VAchT) and choline acetyltransferase (ChAT), were predicted to be on chromosome 13. Sequencing the predicted VAchT cDNA in *baj* mutants did not show difference in the coding region comparing to wild type. However, in the process of sequencing zebrafish ChAT, reverse transcription polymerase chain reaction (RT-PCR) gel showed completely different patterns between mutants and wild type fish at 72 hpf. A single product was amplified from the wild type cDNA while three different products appeared in the mutant, none of which correspond to the wild type product in size (Fig 2). Cloning and sequencing the products revealed a single point mutation (A to C) at a splice acceptor site in ChAT gene, which completely disrupted the normal RNA splicing pattern in mutants. The mutation impeded the function of RNA spliceosomes and caused them to partially or entirely skip the exon following the mutation site or fail to splice out the two introns flanking this exon (Fig 2), thus creating three mutant transcripts.

Obtaining full-length cDNA encoding for zebrafish ChAT

Since the initial RT-PCR reaction only amplified the highly conserved region of ChAT, rapid amplification of cDNA ends (RACE) technique was performed in order to obtain the very 5'- and 3'- encoding sequence for zebrafish ChAT. The obtained sequence was then blasted against the zebrafish genome and was found in the vicinity of the known ChAT sequence. One translation starting site and one stop codon were predicted based on the longest open reading frame that encoded a protein sequence highly conserved across species. The correctness of the RACE-acquired sequence was verified by successfully re-amplifying ChAT with primers designed against sequences outside the predicted translation starting site and the stop codon. The full-length zebrafish ChAT cDNA was then cloned into pCR4-TOPO vectors.

Confirming the point mutation in genomic DNA

To avoid artifacts introduced during reverse transcription, the region encompassing the point mutation was amplified and sequenced from genomic DNA of mutant and wild type fish. The mutant genomic DNA pool showed a clear Cytosine (single blue peak) at the mutation site while the wild type showed a clear single green peak (Adenine) and the heterozygote showed an overlapping double peak (Fig 3).

Derived cleaved amplified polymorphic sequence (dCAPS) analysis was performed to confirm the single nucleotide transition as the mutation in each individual mutant fish, as well as to establish a means of genotyping the embryos (Neff et al, 2002). Using the online program dCAPS finder 2.0 (http://helix.wustl.edu/dcaps/dcaps.html), primers were designed to introduce additional enzyme restriction site in either wild type

or mutant product. PCR amplification of the 216 bp region encompassing the mutation and the additional restriction site was followed by DdeI enzymatic digestion and gel analysis. Since the forward primer introduced one mismatch to the sequence to create an additional DdeI restriction site in the wild type product, the wild type allele produced three bands at 119, 69 and 28bp while the mutant allele showed two bands at 147 and 69bp (Fig 4). In 300 individual mutant fish, dCAPS showed identical results, supporting the A to C switch to be the point mutation in *baj*.

Splice morpholino phenocopy

To provide additional evidence that the point mutation at the splice acceptor site in ChAT gene was responsible for the *baj* phenotype, a morpholino against the same intron-exon border sequence was designed (www.gene-tools.com). Injection of the ChAT spliced morpholino into wild type embryos created the exact phenocopy of *baj* mutants. The high-speed images of touch-elicited escape response from the splice morpholino injected fish showed similar incomplete initial bend and similarly weakened subsequent tail contractions (Fig 5C). RT-PCR analysis from the splice morpholino injected fish showed successful disruption of pre-mRNA splicing and absence of wild type product. Different from the mutant pattern, the splice morpholino only created one mis-spliced product, corresponding to the smallest-sized band in the mutant (Fig 6). Sequencing the product showed a complete match to the shortest mutant transcript.

Baj motility phenotype was rescued with wild type ChAT mRNA injection

To further prove that *baj* phenotype is due to the disruption of ChAT gene, wild type ChAT mRNA was injected into *baj* mutants for behavioral rescue. Full-length zebrafish ChAT cDNA was subcloned into an expression vector (pCS2+) and the wild type ChAT mRNA was transcribed from it. The mRNA was then microinjected into all the embryos born to *baj* heterozygote parents. Injected larvae were evaluated for touch response at 48 hpf by high-speed video. More than 90% (147/163) of the larvae showed normal touch response (Fig 5D) as compared to 75% based on Mendelian rule, suggesting successful behavioral rescue. The other 10% (16/163) of the larvae displayed less severe motility phenotype compared to mutant homozygotes. Genotyping all the individual larvae that showed normal escape response in the high-speed movies revealed the existence of mutant homozygotes among them (Fig 7), confirming successful behavioral rescue.

ChAT protein in baj was not detected with immunohistochemistry

The three mutant transcripts all have premature stop codons and encode truncated proteins of 80, 83 and 102 amino acids, comparing to the wild type ChAT with 637 amino acids (Fig 8A). Prediction based on the RT-PCR result would suggest that the mutated gene encoded severely truncated proteins that are predicted to be non-functional. Immunohistochemistry with polyclonal anti-ChAT antibody supported this prediction. In wild type fish, image showed clear labeling of spinal motoneuron cell bodies and their projecting axons, with nerve terminals overlapping α-bungarotoxin labeling of AchR

clusters. But no signal was detected in *baj* mutant under the same experimental and imaging conditions (Fig 8B).

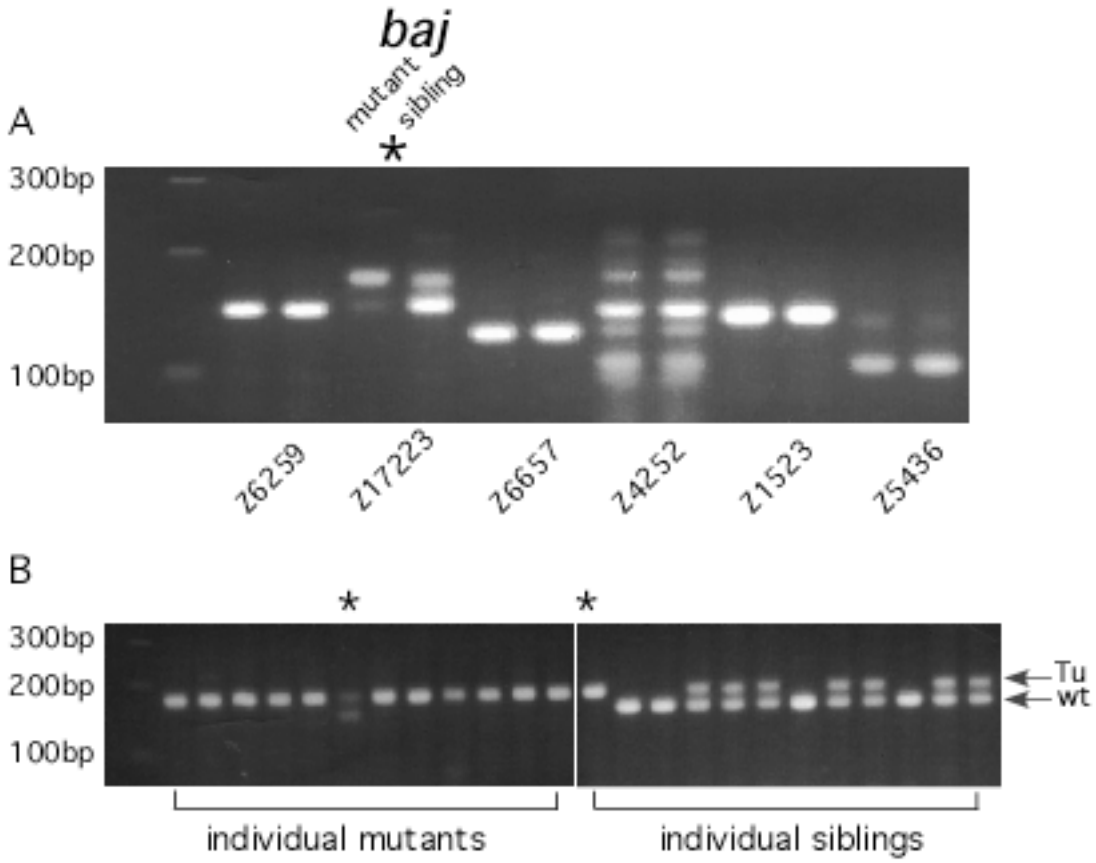

Figure 1. Bulk segregant analysis indicates linkage to chromosome 13

(A) Part of the Bulk segregant analysis gel pictures of 6 microsatellite markers (Z6259, Z17223, Z6657, Z4252, Z1523, Z5436). For each individual marker, the left lane is the PCR product amplified from the mutant DNA pool, and the right lane from the sibling pool. Differential amplification for marker Z17223 on LG 13 is indicated by an asterisk. A DNA mass ladder is shown in the first lane of the gel. (B) Amplification of the positive marker Z17223 on individual *baj* mutants and siblings (12 individuals for each). The mutant allele (Tu) is represented by the upper band and the wild type allele by the lower band (arrows). The asterisks mark the recombinant mutant and sibling individuals.

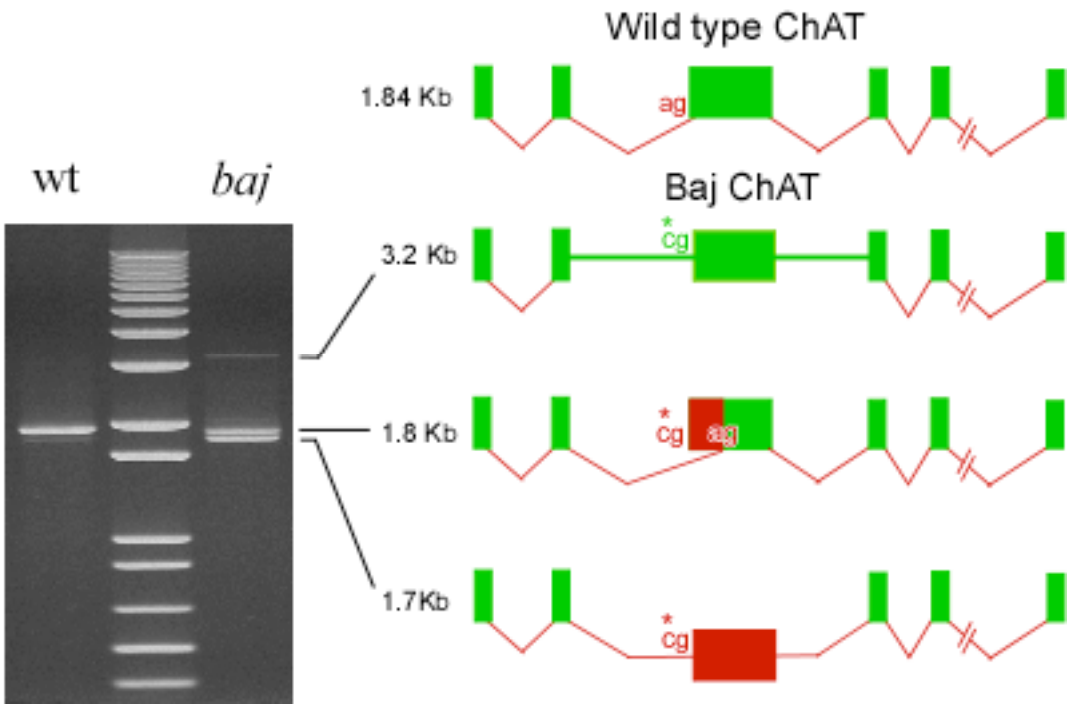

Figure 2. RT-PCR revealed disrupted pre-mRNA splicing pattern

In the left panel, RT-PCR gel picture of ChAT cDNA products amplified from 72 hpf wild type (left lane) and *baj* (right lane). The DNA mass ladder is shown in the middle. On the right is the diagram of ChAT premRNA splicing pattern and the resulted transcripts in wild type and *baj*, obtained based on sequencing results, and their correspondence to the PCR products. The asterisk indicates the A to C point mutation at a splice acceptor site. Green color represents the coding region and red represents the sequences that were spliced out.

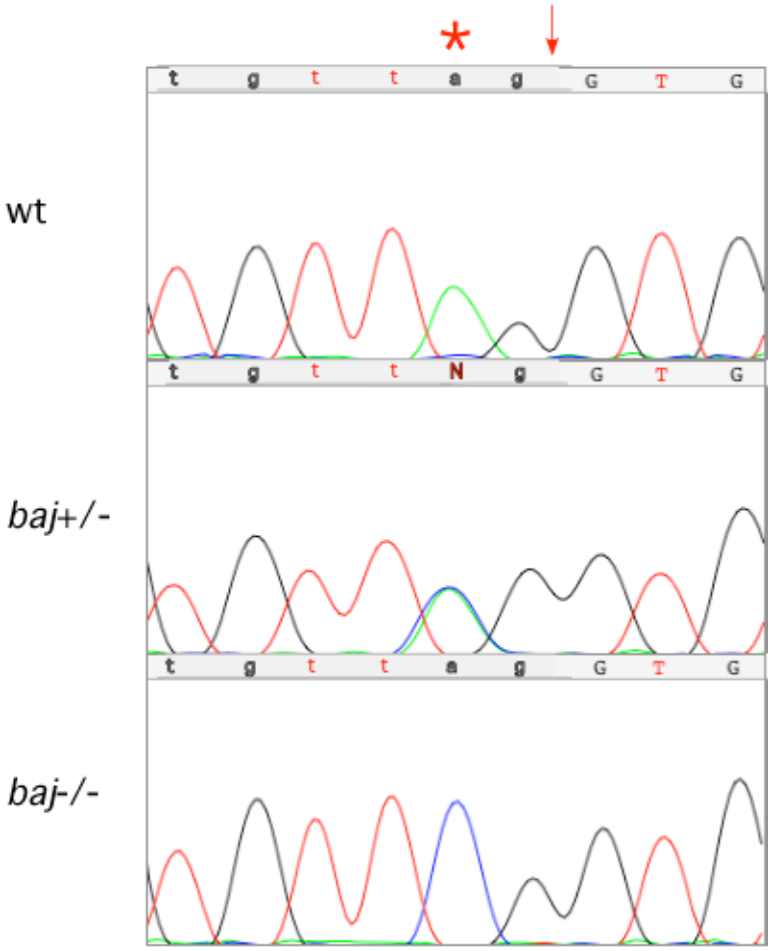

Figure 3. *baj* point mutation locates at a splice acceptor site in ChAT gene.

Sequence analysis of genomic DNA revealed an Adenine (green peak) to Cytosine (blue peak) transition at the splice acceptor site of intron 2, as indicated by the red asterisk. Overlapping double peaks at this position represent the presence of both wild type and mutant alleles in the *baj* heterozygous fish. The intron-exon border is represented by the red arrow.

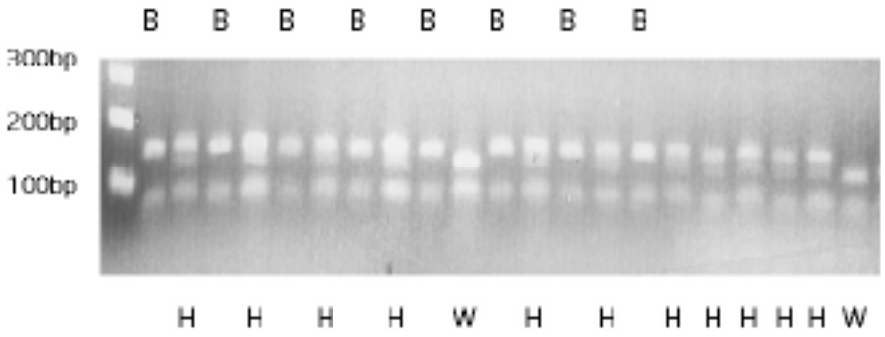

Figure 4. dCAPS analysis confirmed the presence of point mutation in individual *baj* mutants.

The dCAPS electrophoresis result was shown for 8 individual *baj* and 13 sibling individuals. All the individual larvae were identified at 72 hpf based on their motility phenotype and subsequently divided into the mutant group and the sibling group. PCR products from individual larvae were digested by DdeI and run on agarose gels. The wild type allele (W) showed double bands at 119 bp and 69 bp and the mutant allele (B) appeared at 147 bp and 69 bp. Triple bands represent sibling individuals that are heterozygous (H) to the *baj* mutation. The DNA mass ladder is shown in the left lane. dCAPS analysis was tested in 300 *baj* homozygous individuals and 200 siblings.

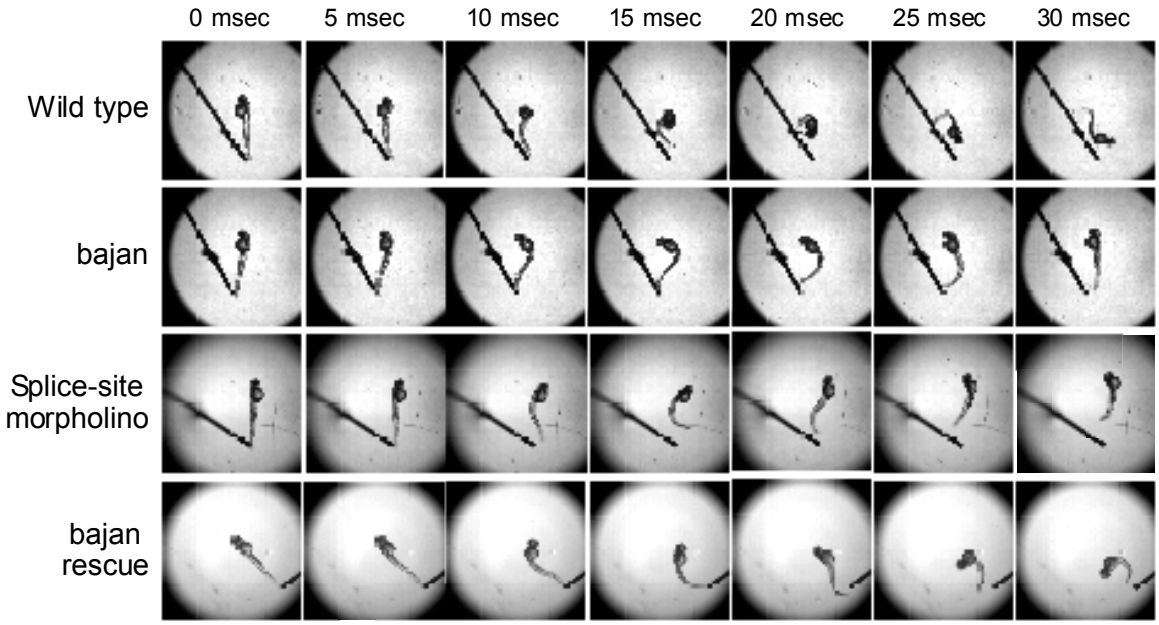

Figure 5. The effect of splice-site morpholino phenocopy and behavioral rescue of homozygous *baj* were assessed with high-speed imaging.

The escape responses of 48 hpf wild type, *baj* homozygote, splice-site morpholino-injected wild type fish and *baj* homozygotes injected with wild type ChAT mRNA (from top to bottom). Note the similarities in the diminished C-bend and subsequent tail movements between *baj* homozygote and the morphant fish. The *baj* mutant injected with full-length wild type ChAT mRNA showed normal escape response similar to that of wild type. Individual frames, captured at the rate of 1000 frames per second, were shown with 5 msec intervals.

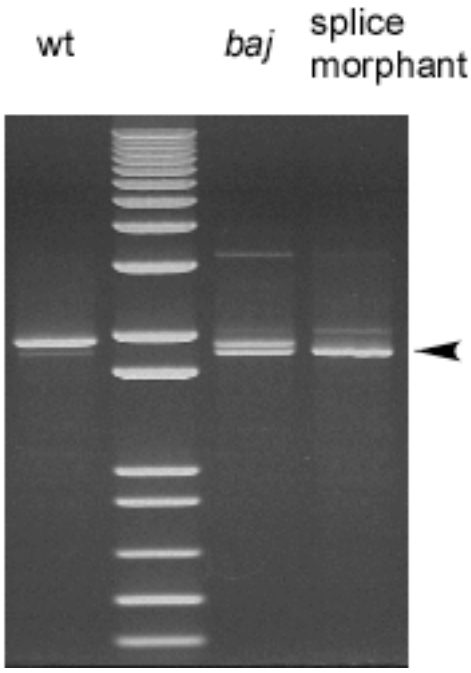

Figure 6. Splice morpholino phenocopy confirmed by RT-PCR analysis

RT-PCR analysis of ChAT cDNA from wild type (left lane), *baj* homozygotes (second to the right) and splice-site morpholino injected wild type fish (right lane) showed that the major product in the morphant fish corresponds in size to the 1.8Kb mutant transcript (arrowhead).

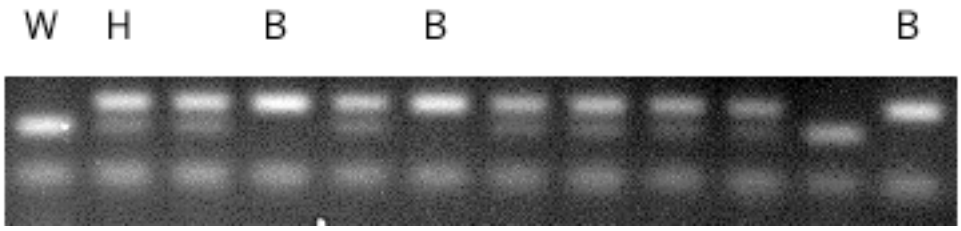

Figure 7. Behavioral rescue of *baj* homozygotes was confirmed by dCAPS analysis

48 hours after injecting wild type ChAT mRNA into all the offsprings born to *baj* heterozygous parents, larvae with normal escape response were genotyped by dCAPS analysis. The behaviorally rescued larvae showed a mixture of wild type (W), *baj* homozygotes (B) and heterozygote (H) in the dCAPS analysis.

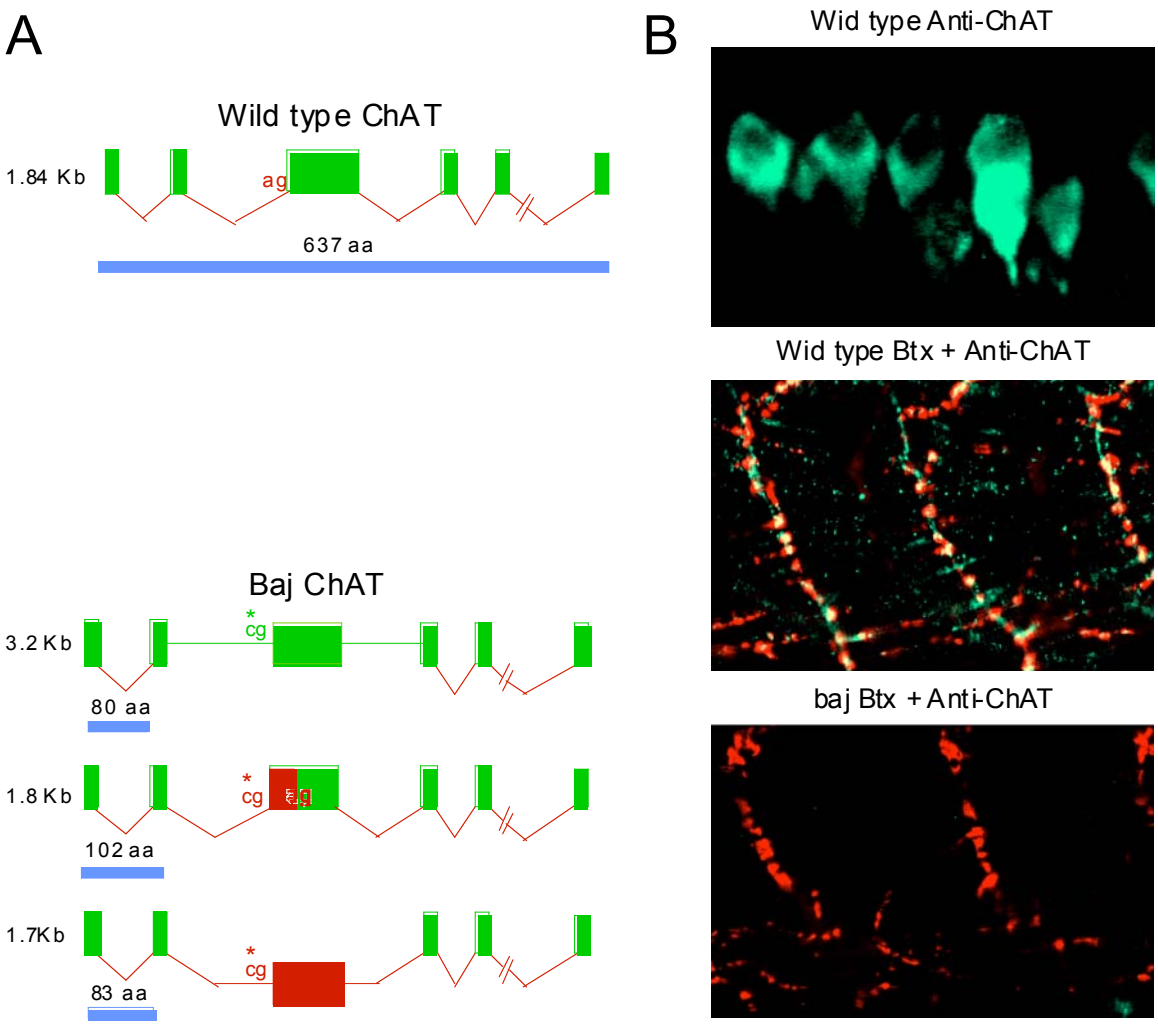

Figure 8. ChAT signal is not detected in *baj* with immunohistochemistry

(A) Diagram of ChAT transcripts and protein sizes in wild type and *baj*. Based on the RT-PCR and sequencing analysis results, the mutated ChAT gene in *baj* encode three severely truncated protein products of 80, 83 and 102 amino acids, compared to the wild type protein at 637 aa. (B) Immunohistochemistry images with anti-ChAT antibody and α-bungarotoxin staining in 72 hpf wild type and *baj*. In wild type, ChAT signal was detected in the spinal neuron somas (top) and their axons (middle). In *baj*, no ChAT signal was detected despite the clear labeling of neurites with α-bungarotoxin (bottom).

Figure 9. ChAT protein sequence alignment in different species.

Alignment of the ChAT amino acid sequences in human, pig, mouse, chicken and zebrafish. Identical residues are shown in green, conserved residues in yellow and others in white.

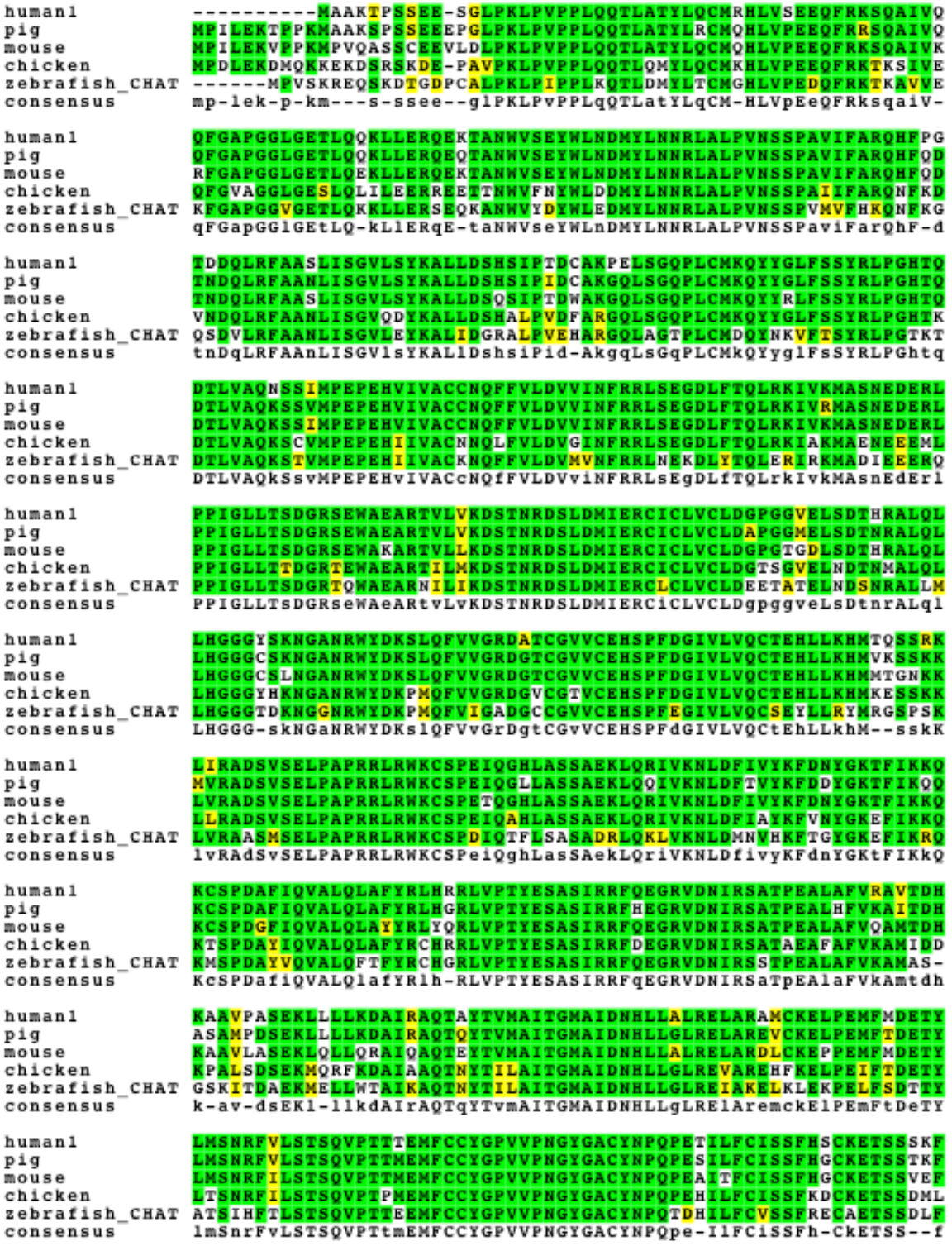
human1 ----------MAAKTPSSEE-SGLPKLPVPPLQQTLATYLQCMRHLVSEEQFRKSQAIVQ
pig MPILEKTPPKMAAKSPSSEEEPGLPKLPVPPLQQTLATYLRCMQHLVPEEQFRRSQAIVQ
mouse MPILEKVPPKMPVQASSCEEVLDLPKLPVPPLQQTLATYLQCMQHLVPEEQFRKSQAIVK
chicken MPDLEKDMQKKEKDSRSKDE-PAVPKLPVPPLQQTLQMYLQCMKHLVPEEQFRKTKSIVE
zebrafish_CHAT ------MPVSKREQSKDTGDPCALPKLPIPPLKQTLDMYLTCMGHLVPEDQFRKTKAVVE
consensus mp-lek-p-km---s-ssee--glPKLPvPPLqQTLatYLqCM-HLVpEeQFRksqaiV-
human1 QFGAPGGLGETLQQKLLERQEKTANWVSEYWLNDMYLNNRLALPVNSSPAVIFARQHFPG
pig QFGAPGGLGETLQQKLLERQEQTANWVSEYWLNDMYLNNRLALPVNSSPAVIFARQHFQD
mouse RFGAPGGLGETLQEKLLERQEKTANWVSEYWLNDMYLNNRLALPVNSSPAVIFARQHFQD
chicken QFGVAGGLGESLQLILEERREETTNWVFNYWLDDMYLNNRLALPVNSSPAIIFARQNFKD
zebrafish_CHAT KFGAPGGVGETLQKKLLERSEQKANWVYDYWLEDMYLNNRLALPVNSSPVMVFHKQNFKG
consensus qFGapGGlGEtLQ-kLlERqE-taNWVseYWLnDMYLNNRLALPVNSSPaviFarQhF-d
human1 TDDQLRFAASLISGVLSYKALLDSHSIPTDCAKPELSGQPLCMKQYYGLFSSYRLPGHTQ
pig TNDQLRFAANLISGVLSYKALLDSHSIPIDCAKGQLSGQPLCMKQYYGLFSSYRLPGHTQ
mouse TNDQLRFAASLISGVLSYKALLDSQSIPTDWAKGQLSGQPLCMKQYYRLFSSYRLPGHTQ
chicken VNDQLRFAANLISGVQDYKALLDSHALPVDFARGQLSGQPLCMKQYYGLFSSYRLPGHTK
zebrafish_CHAT QSDVLRFAANLISGVLEYKALIDGRALPVEHARGQLAGTPLCMDQYNKVFTSYRLPGTKT
consensus tnDqLRFAAnLISGVlsYKALlDshsiPid-AkgqLsGqPLCMkQYyglFsSYRLPGhtq
human1 DTLVAQNSSIMPEPEHVIVACCNQFFVLDVVINFRRLSEGDLFTQLRKIVKMASNEDERL
pig DTLVAQKSSVMPEPEHVIVACCNQFFVLDVVINFRRLSEGDLFTQLRKIVRMASNEDERL
mouse DTLVAQKSSIMPEPEHVIVACCNQFFVLDVVINFRRLSEGDLFTQLRKIVKMASNEDERL
chicken DTLVAQKSCVMPEPEHIIVACNNQLFVLDVGINFRRLSEGDLFTQLRKIAKMAENEEEML
zebrafish_CHAT DTLVAQKSTVMPEPEHIIVACKNQFFVLDVMVNFRRLNEKDLYTQLERIRKMADIEEERQ
consensus DTLVAQkSsvMPEPEHvIVACcNQfFVLDVviNFRRLsEgDLfTQLrkIvkMAsnEdErl
human1 PPIGLLTSDGRSEWAEARTVLVKDSTNRDSLDMIERCICLVCLDGPGGVELSDTHRALQL
pig PPIGLLTSDGRSEWAEARTVLVKDSTNRDSLDMIERCICLVCLDAPGGMELSDTNRALQL
mouse PPIGLLTSDGRSEWAKARTVLLKDSTNRDSLDMIERCICLVCLDGPGTGDLSDTHRALQL
chicken PPIGLLTTDGRTEWAEARTILMKDSTNRDSLDMIERCICLVCLDGTSGVELNDTNMALQL
zebrafish_CHAT PPIGLLTSDGRTQWAEARNILIKDSTNRDSLDMIERCLCLVCLDEETATELNDSNRALLM
consensus PPIGLLTsDGRseWAeARtvLvKDSTNRDSLDMIERCiCLVCLDgpggveLsDtnrALql
human1 LHGGGYSKNGANRWYDKSLQFVVGRDATCGVVCEHSPFDGIVLVQCTEHLLKHMTQSSRK
pig LHGGGCSKNGANRWYDKSLQFVVGRDGTCGVVCEHSPFDGIVLVQCTEHLLKHMVKSSKK
mouse LHGGGCSLNGANRWYDKSLQFVVGRDGTCGVVCEHSPFDGIVLVQCTEHLLKHMMTGNKK
chicken LHGGGYHKNGANRWYDKPMQFVVGRDGVCGTVCEHSPFDGIVLVQCTEHLLKHMKESSKK
zebrafish_CHAT LHGGGTDKNGGNRWYDKPMQFVIGADGCCGVVCEHSPFEGIVLVQCSEYLLRYMRGSPSK
consensus LHGGG-skNGaNRWYDKslQFVvGrDgtCGvVCEHSPFdGIVLVQCtEhLLkhM--sskK
human1 LIRADSVSELPAPRRLRWKCSPEIQGHLASSAEKLQRIVKNLDFIVYKFDNYGKTFIKKQ
pig MVRADSVSELPAPRRLRWKCSPEIQGLLASSAEKLQQIVKNLDFTVYKFDDYGKTFIKQQ
mouse LVRADSVSELPAPRRLRWKCSPETQGHLASSAEKLQRIVKNLDFIVYKFDNYGKTFIKKQ
chicken LLRADSVSELPAPRRLRWKCSPEIQAHLASSAEKLQRIVKNLDFIAYKFVNYGKEFIKKQ
zebrafish_CHAT LVRAASMSELPAPRRLRWKCSPDIQTFLSASADRLQKLVKNLDMNVHKFTGYGKEFIKRQ
consensus lvRAdSvSELPAPRRLRWKCSPeiQghLasSAekLQriVKNLDfivyKFdnYGKtFIKkQ
human1 KCSPDAFIQVALQLAFYRLHRRLVPTYESASIRRFQEGRVDNIRSATPEALAFVRAVTDH
pig KCSPDAFIQVALQLAFYRLHGRLVPTYESASIRRFHEGRVDNIRSATPEALHFVKAITDH
mouse KCSPDGFIQVALQLAYYRLYQRLVPTYESASIRRFQEGRVDNIRSATPEALAFVQAMTDH
chicken KTSPDAYIQVALQLAFYRCHRRLVPTYESASIRRFDEGRVDNIRSATAEAFAFVKAMIDD
zebrafish_CHAT KMSPDAYVQVALQFTFYRCHGRLVPTYESASIRRFQEGRVDNIRSSTPEALAFVKAMAS-
consensus KcSPDafiQVALQlafYRlh-RLVPTYESASIRRFqEGRVDNIRSaTpEAlaFVkAmtdh
human1 KAAVPASEKLLLLKDAIRAQTAYTVMAITGMAIDNHLLALRELARAMCKELPEMFMDETY
pig ASAMPDSEKLLLLKDAIRAQTQYTVMAITGMAIDNHLLGLRELAREVCKELPEMFTDETY
mouse KAAVLASEKLQLLQRAIQAQTEYTVMAITGMAIDNHLLALRELARDLCKEPPEMFMDETY
chicken KPALSDSEKMQRFKDAIAAQTNYTILAITGMAIDNHLLGLREVAREHFKELPEIFTDETY
zebrafish_CHAT GSKITDAEKMELLWTAIKAQTNYTILAITGMAIDNHLLGLREIAKELKLEKPELFSDTTY
consensus k-av-dsEKl-llkdAIrAQTqYTvmAITGMAIDNHLLgLRElAremckElPEmFtDeTY
human1 LMSNRFVLSTSQVPTTTEMFCCYGPVVPNGYGACYNPQPETILFCISSFHSCKETSSSKF
pig LMSNRFVLSTSQVPTTMEMFCCYGPVVPNGYGACYNPQPESILFCISSFHGCKETSSTKF
mouse LMSNRFILSTSQVPTTMEMFCCYGPVVPNGYGACYNPQPEAITFCISSFHGCKETSSVEF
chicken LTSNRFILSTSQVPTPMEMFCCYGPVVPNGYGACYNPQPEHILFCISSFKDCKETSSDML
zebrafish_CHAT ATSIHFTLSTSQVPTTEEMFCCYGPVVPNGYGACYNPQTDHILFCVSSFRECAETSSDLF
consensus lmSnrFvLSTSQVPTTtmEMFCCYGPVVPNGYGACYNPQpe-IlFCiSSFh-CkETSS--f
human1 AKAVEESLIDMRDLCSLLPPTESKPLATKEKATRPSQGHQP---
pig AKAVEESFIEMKGLCSLSQSGMGKPLATKEKVTRPSQVHQP---
mouse AEAVGASLVDMRDLCSSRQPAEGKPPTAKERARGPTKPSNLDYS
chicken AKAVEESLLEIRDLCNKCSSSTAKSLAKQEEATQLRSDRKL---
zebrafish_CHAT VKTLEGCLKEMQDLCRKCN-TEVKPADSTQRMEGNPKVMKNGSK
consensus akaveesliemrdLCs--q-tegKplatkekat-ps---q----

Discussion

Positional cloning has long been employed as an important method in the forward genetic studies to uncover the zebrafish mutations (Malicki et al, 2002). It usually starts with locating the mutation on a specific chromosome using bulk segregant analysis (BSA), followed by a systemic narrowing of the region by calculating recombination frequency of SSLP markers in a large number of individual mutants. Since I had four prospective candidates based on physiology and imaging results, I was able to use a shortcut strategy to determine the mutated gene responsible for the *bajan* phenotype. Results from BSA ruled out two candidates but were consistent with vesicular Acetylcholine Transporter (VAchT) or Choline acetyltransferase (ChAT) as underlying the *baj* phenotype. VAchT gene resides within the first intron of ChAT gene in both invertebrate and vertebrate systems, hence the term cholinergic gene locus (Eiden, 1998). VAchT is responsible for the transport of cytoplasmically synthesized Ach into synaptic vesicles and ChAT is the key enzyme for Ach synthesis. Mutation in either one of the two genes will cause insufficient filling of the synaptic vesicles, which would certainly explain the diminished touch response and the decreased amplitude of endplate currents observed in the physiology recordings. Therefore, we skipped the intermediate and high resolution mapping steps and immediately sequenced the two candidate genes on Chromosome 13 and found a single nucleotide change in the ChAT gene.

Unlike most of the previously identified mutations involving motility defects, the single nucleotide change found in *baj* was located on a splice acceptor site at the intron-exon border, rather than in the coding sequences, of the zebrafish ChAT gene. The A to C

switch altered the highly conserved spliceosome recognition sequence AG into CG, forcing the spliceosome complex to find the next available recognition site, thereby creating three incorrect mRNA transcripts in mutant fish. To confirm the single nucleotide transition as the *baj* mutation instead of a mere single nucleotide polymorphism (SNP), derived cleaved amplified polymorphic sequence (dCAPS) analysis was performed. In contrast to the more traditional methods for SNP detection like restriction fragment length polymorphism (RFLP), which require that the SNP itself introduce or remove an endonuclease recognition site, dCAPS utilizes mismatches in one of the two PCR primers flanking the SNP site to achieve the same restriction site alteration in either mutant or wild type sequences (Neff 02). Using web-designed primers (http://helix.wustl.edu/dcaps/dcaps.html) with minimal number of mismatches, a region encompassing the SNP was PCR amplified and appropriate enzyme was chosen for PCR product digestion and gel analysis. A difference in digestion product gel pattern between the mutant and wild type was used to genotype large numbers of mutant embryos. The consistent presence of adenine in each individual mutant fish tested confirmed that this single nucleotide change is the *baj* mutation.

To further support the link between the identified ChAT mutation and *baj* motility phenotype, we achieved behavioral phenocopy in wild type by knocking down the expression of ChAT gene. In reverse genetic approaches widely used in mouse or drosophila, target genes are first identified and their functions are studied by examining the effect caused by mutations or altered expression of the genes. The use of knockout technology, for example, allows targeted manipulation of genes with precise temporal and spatial controls. Thus, specific changes to any genomic sequences can be introduced

and subsequent effects can be evaluated in living animals (Hoffman and Merrill, 2007). Not equipped with the reliable techniques available in other model systems, inactivation of previously cloned genes in zebrafish have not been easy (Oates et al, 2000) but are possible through the use of morpholino injections (Nasevicius et al, 2000). Morpholino are synthetic antisense oligos specifically designed to block mRNA translation or modify pre-mRNA splicing through steric hinderance (Summerton et al, 1997). Morpholinos bind to mRNA with high affinity and specificity. In addition, owing to the chemically modified structure which distinguish them from nucleic acids, morpholinos are uncharged and usually non-toxic even when injected at high concentrations (Gene Tools). Excellent efficacy in eliminating gene functions was shown starting from early stages throughout the first 2 days of development (Scholpp and Brand, 2001). The blocking effects on mRNA translation or splicing can be assayed with immunoblotting or RT-PCR techniques, respectively. However, when attempting to mimic the effect of the point mutation on pre-mRNA splicing by blocking the same splice site with morpholino oligos, a different pattern of mRNA transcripts appeared in the RT-PCR gel analysis of the morphant fish. This discrepancy could be due to the differential steric hinderance achieved with a single nucleotide change or a 25 nucleotides long oligo.

As a complimentary approach to morpholino phenocopy in confirming that ChAT mutation is responsible for the mutant phenotype, transient expression of injected ChAT mRNA temporarily compensated for the loss of endogenous protein and rescued the behavioral phenotype. Owing to the instability of the injected mRNA, not every mutant embryo was rescued. However, a significant increase in the number of embryos showing

normal escape response (a decrease in the number of identifiable mutants) and results from the subsequent genotyping experiment indicated a successful rescue.

With successful confirmation of the mutation, I wondered to what extent ChAT function was impaired in *baj*. Based on the RT-PCR results, all three major transcripts in mutant fish encode severely truncated ChAT proteins with only one-eighth of the correct wild type ChAT protein sequence of 637 aa. Published crystal structure obtained from human and rat ChAT revealed in detail mechanisms of substrate binding and catalytic action (Cai et al, 2004; Govindasamy et al, 2004). Histidine 334 in rCHAT, the pivotal residue positioned in the center of the catalytic tunnel, provides the general base for interactions with either choline or acetyl-CoA depending on the direction of the reaction. This highly conserved key residue, together with Tyr95, Asp338, Arg458 and several other residues, formed the active site responsible for ChAT enzymatic activity. Since ChAT protein is highly conserved across species, especially within the vertebrate system (Fig 9), zebrafish ChAT would probably have very similar structure and share the same mechanisms. Based on the sequencing results, none of the residues involved in forming the enzymatic activity center exist in any of the truncated mutant proteins, suggesting that the mutation completely eliminated the production of functional ChAT protein in the mutant fish. Consistent with this prediction, immunohistochemistry experiment with anti-ChAT antibody failed to detect any fluorescence signal from ChAT protein in mutant fish.

Based on the above result, I considered *baj* as a ChAT null mutant.

CHAPTER 4

SYNAPSE MORPHOLOGY AND SYNAPTIC TRANSMISION AT *BAJAN* NMJ

Introduction

Based on the results from RT-PCR, we predicted that the mutated gene encoded a nonfunctional ChAT protein. Combined with the absence of ChAT signal in the immunohistochemistry experiments, the results suggested that *baj* carried a ChAT null mutation. Choline acetyltransferase (ChAT) is the key enzyme responsible for biosynthesis of acetylcholine, the first discovered neurotransmitter (Loewi, 1921). A member of the choline/carnitine acetyltransferase family, ChAT catalyzes the Ach synthesis reaction through the reversible transfer of an acetyl group between acetyl-CoA (AcCoA) and choline (Nachmansohn and Machado, 1943). Multiple ChAT mRNAs are transcribed but they all encode one protein with 68 kDa molecular mass, with the exception of a possible 82 kDa product in primates (Oda et al, 1995). The enzyme mostly exists in a soluble form but 10 to 20% of it presents as a membrane-bound type, of which the function remains unknown (Wu and Hersh 1994).

ChAT activity plays a crucial role in various physiological processes, including motor function, vegetative function in the autonomic nervous system and other integrative brain functions (Karczmar et al, 1993). Mutations or genetic manipulation of the ChAT gene have revealed inconsistent results. In human, decreased enzymatic

activity has been associated with several neurodegenerative diseases (Oda, 1999). Most definitely, mutations in ChAT gene give rise to congenital myasthenic syndrome with episodic apnea (CMS-EA) (Ohno et al 2001). Patients with this motor disorder suffer from hypotonia and respiratory impairment at birth or in the neonatal period. Sequencing analysis found multiple recessive mutations (including one frameshift null mutation) located in different domains of ChAT protein (Cai et al, 2004), causing impaired function or changes in the protein expression level. *In vitro* electrophysiology showed an abnormal decline of MEPP amplitude following a 5-minute 10 Hz stimulation but morphological studies of the muscle endplates found no AchR deficiency or postsynaptic structural abnormality (Byring et al, 2002).

In the ChAT knockout mutant mice, however, where target deletion of 2 exons from the murine ChAT gene completely inactivated the gene function, a more severe phenotype was observed. First, the homozygote mice die at birth. Second, based on intracellular recordings from muscle fibers in the neonatal mice, the neuromuscular transmission was completely abolished in the ChAT knockout. Third, histological studies indicated excessive intramuscular nerve branching, widened endplate band and decreased level of AchE in the synaptic cleft (Misgeld et al, 2002; Brandon et al, 2003).

Studying the effect of a ChAT null mutation in *baj* has some clear advantages over mammals. First, *baj* homozygotes are viable for about 5 days, providing a 3 to 4 day window to perform *in vivo* studies. Due to the rapid external development of zebrafish, electrophysiology recordings from a developing neuromuscular junction can be acquired during this time period. Second, compared to the absence of any synaptic currents at the mutant mice NMJ, initial electrophysiology recordings from the muscle in *baj* showed

diminished yet distinct responses. Owing to its reduced neuromuscular transmission, *baj* could potentially be a good model to study how decreased synaptic input alters the properties of transmitter release at the vertebrate NMJ. Third, unlike the case studies from human patients, electrophysiology and morphology experiments can be done *in vivo*.

The purpose of this chapter is to investigate the consequences of the *baj* mutation on synapse morphology and synaptic transmission and compare the findings with those shown in the ChAT knockout mice.

Methods

Labeling postsynaptic AchR clusters in dissociated skeletal muscle cells

AchRs were labeled with α-bungarotoxin in whole-mount zebrafish preparation before dissociation with collagenase. 72 hpf larvae were decapitated and double-side skinned to ensure good penetration for the toxin. The isolated tails were then immersed in a solution containing 100% Hanks and 0.1 μM α-bungarotoxin conjugated to Alexa Fluor 647 (Molecular Probes, Eugene OR) for a 15-minute incubation at RT. The tails were then washed in toxin-free 100% Hanks for 2 hours with frequent changes of solution to remove non-specific binding.

To obtain dissociated muscle cells, post-stained tails were treated with 0.5% collagenase (Invitrogen) in 100% Hank's for approximately 1.5 to 2 hours until the surface appeared fuzzy. The tails were then transferred to a 35mm petri dish with a

coverslip bottom with as little collagenase solution as possible followed by a gentle solution change with 100% Hanks. The digested tails were briefly triturated through a 200 μl pipette tip to harvest isolated skeletal muscle cells. Debris was removed from the dish and dissociated cells were allowed to settle to the bottom of the dish for about 20 minutes before imaging.

Fish preparation for the paired neuron-muscle recordings

Larval fish aged between 52 hpf and 120 hpf were anesthetized by placing them in 10% Hanks solution containing 0.08% tricaine methanosulphate (MS222; Wester Chemicals Inc., Scottsdale AZ) for 2 minutes. Embryos were subsequently decapitated and transferred into a Sylgard (Dow-corning, Midland MI)-coated recording chamber filled with bath recording solution. The tail was pinned down laterally onto the Sylgard lining by inserting two tungsten pins through the notochord at approximately tail segments 5 and 14. The skin between two pins on the topside was then removed. The larva was then treated with 2M formamide for 5 minutes to prevent muscle contraction, followed by an extensive wash with bath solution. Subsequent steps were performed on Axioskop FS upright microscope (Zeiss, Oberkochen, Germany) and viewed with 10X and 40X physiology achroplan objectives (Zeiss). To expose the spinal cord, dorsal muscle cells were removed by gentle suction using a ~15 μm O.D. glass pipette connected to a 1ml syringe. The superficial slow muscle layer on the ventral side was also removed to give access to the deeper fast muscle cells.

Paired recording of the CaP neuron and its target fast muscle cell

The CaP neurons were identified on the basis of position and size using differential interference contrast (DIC) optics. The pipettes used for motoneuron recordings were pulled from 1.5 mm O.D. Kwik-Fil borosilicate glass (World Precision Instruments Inc., Sarasota, FL) to a 2 to 3 μm outer diameter tip with a long taper for easier penetration of the spinal dura. Once filled with the neuronal pipette solution they ranged in resistance between 9 to 13 Mohm. Constant positive pressure (about 30mmHg) was applied to the neuronal pipette with a Dale 20 pneumatic transducer (Fluke Electronics, Carson City, NV) to keep the electrode tip clean during penetration of the dura and approaching of the CaP. Once whole-cell configuration was achieved, the neuron was held at –80 mV, close to the reported resting membrane potential (Buss et al, 2003). Whole-cell voltage clamp configuration of a target fast muscle cell was subsequently obtained using a muscle recording pipette. Neuronal action potentials were elicited by current injection into the soma under current clamp mode. Evoked endplate currents (EPCs) were recorded as muscle cells were held at –50 mV to inactivate sodium channels and minimize contraction. All recordings were done at room temperature.

High frequency stimulation

After the paired neuron-muscle configuration was established, a 20 second 100 Hz train was applied to the CaP neuron in the current clamp mode. Evoked responses from the muscle cell were recorded at –50 mV for the whole duration of stimulation. A 0.2 Hz stimulation immediately followed the train stimulation and postsynaptic responses were recorded to monitor the recovery of muscle EPCs. The recordings stopped when

post-stimulation EPCs recovered to the pre-stimulation level, or the increase of EPC amplitude reached a plateau. The continuous trace was digitized and analyzed with Clampfit (Molecular Devices, Sunnyvale, CA). The transmitter release was reflected in the amount of charge transferred, which is represented with the area between the continuous trace and the baseline. The amount of charge transfer for every second was measured and normalized to the total amount.

Results

Single postsynaptic AchR cluster in baj is enlarged

Staining of the postsynaptic AchRs with conjugated α-bungarotoxin showed no obvious defects in the receptor's clustering pattern (see Chapter 2). Staining with either FM1-43 or SV2 antibody indicated no obvious defects in nerve terminal distribution or number. In this chapter I examine in detail the effect of the defective ChAT gene on neuromuscular junction morphology, I labeled the postsynaptic AchR clusters in dissociated skeletal muscle cells with Alexa647-conjugated α-bungarotoxin and measured the number of clusters per each muscle cell and the area of each single AchR cluster. Different from the observation made in ChAT knockout mice (Misgeld 2002, Brandon 2003), the number of clusters per each muscle cell was not significantly different between wild type and mutant (Fig. 1A). The value corresponded to 5.49 ± 2.02 clusters per cell in mutants (n= 14) and 7.19 ± 1.33 clusters per cell in wild type (n=6) (Fig. 1B; $P > 0.05$). However, the area of single postsynaptic AchR cluster in mutant

muscle cells is significantly larger than that in wild type controls (Fig. 1A). The area of each cluster measured 2.45 ± 1.89 μm^2 in mutants (n=144) and 1.79 ± 1.13 μm^2 in wild type (n=102) (Fig 1B; $P < 0.005$). Similar to our finding, the enlargement of single postsynaptic AchR cluster area was previously described at the ChAT knockout mice NMJ (Brandon 2003, Misgeld 2002).

Bajan has smaller quantal size compared to wild type

Preliminary recordings have found a diminution of mEPC amplitude in *baj*. Similar differences were observed when comparing the overall recordings from *baj* and wild type muscle (Fig 2 and Table 1). The average amplitude of mEPCs in *baj* measured 206±66 pA (Fig 2A, n=14), which was significantly smaller than the average in wild type, 587±119 pA (n=10) ($P<0.0001$). The frequency versus amplitude distribution for the mEPC averages from each recording revealed two non-overlapping unimodal distributions for *baj* and wild type muscle (Fig 2B), suggestive of a smaller quantal size.

mEPC kinetics and frequency are comparable between baj and wild type

In contrast, the two key parameters of the current kinetics, rise time and decay time constant, showed no significant difference in overall values between wild type and *baj*. In *baj* homozygotes, the average rise time of mEPCs was 0.18±0.03 ms and the average decay time constant was 0.54±0.09ms, almost identical to the wild type value at 0.18±0.03 ms and 0.54±0.09 ms (Fig 2C, $P=0.99$). The frequency of mEPCs was also compared for possible differences between wild type and *baj*. While the values varied greatly in individual cells, mEPC frequency in *baj* averaged at 11.0 ±11.3 events per

minute, not significantly different from the wild type average at 10.8±7.4 events per minute. The original data from each individual cells are shown in table 1.

Reduced amplitude of the evoked postsynaptic responses in baj

To record the evoked synaptic responses, I used a paired neuron-muscle paradigm (Fig 3) developed in our lab (Wen and Brehm, 2005). Compared to wild type, the evoked postsynaptic currents (EPCs) in the mutants also showed much decrease in the current amplitude, as was found in the spontaneous responses. The difference in amplitude is shown in the sample traces of EPCs (Fig 4) from wild type and *baj*. When comparing all the data from wild type and *baj*, the average amplitude of *baj* EPCs corresponded to 1.16±0.53 nA (n=9), much smaller than the wild type value at 3.19±2.20 nA (n=11) (Fig 5A, $P<0.01$). The difference can also be seen in the frequency distribution of the averaged EPC amplitude from multiple muscle cells (Fig. 5B). Despite of some minor overlap between the wild type and the mutant distribution, they still formed two obviously distinct groups.

As for the current kinetics parameters, no significant difference was found between wild type and mutants. The average rise time of *baj* EPCs measured 0.297±0.044 ms, compared to that of wild type at 0.269±0.036 ms (Fig 5C, $P=0.14$). The average decay time constant for *baj* and wild type measured 0.612±0.095 ms and 0.639±0.070 ms, respectively (Fig 5C, $P=0.47$). The original EPC data for each individual muscle cells are shown in table 2.

Bajan has comparable quantal content as WT

It has been observed in several organisms that decreased postsynaptic activity could induce a compensatory increase of the presynaptic transmitter release (Davis and Goodman, 1998; Turrigiano and Nelson, 2004). In order to examine whether the decrease in quantal size in *baj* elicited a change in the presynaptic vesicle release, I estimated and compared the quantal content of the *baj* and wild type NMJ and found no significant difference between them. The quantal content was calculated by the direct method, dividing the mean EPC amplitude by the mean mEPC amplitude. The quantal content in *baj* averaged at 5.64±2.54 (n=9), comparable to the wild type value at 5.43±3.75 (n=11) ($P>0.05$).

Frequency-dependent synaptic response in Baj is comparable to WT

To study how the weakened neuromuscular synapse in *baj* would perform in response to high frequency stimulation, I recorded synaptic currents evoked by stimulating the motoneuron at 100 Hz for 20 seconds. In wild type the evoked responses consistently showed three phases: in the first 1 to 2 seconds, EPCs followed neuronal action potential faithfully, but the amplitude decline rapidly during the initial few stimuli (Fig 6A, time point 1). In the next 2 seconds or so, a burst of activity, including synchronous response mixed with non-synchronous response, occurred in between two consecutive neuronal action potentials (Fig 6A, time point 2). From around 5 seconds on, more and more synaptic failure showed up and finally more than 90% of the neuronal action potentials failed to elicit any detectable postsynaptic current (Fig 6A, time point 3).

Baj homozygous mutant fish showed the same time course as wild type under the 100hz stimulation paradigm (Fig 6B). The transmitter release could be indirectly reflected in the amount of charge transferred during synaptic currents. We therefore measured the charge transfer and plotted the averaged normalized charge transfer over time, providing a measure for cumulative transmitter release. Based on the cumulative plot, at 5 seconds after 100hz stimulation, 75% of total charge transfer has been accomplished in wild type fish (n=8), while 77% is finished in *baj* (n=11) (Fig 7).

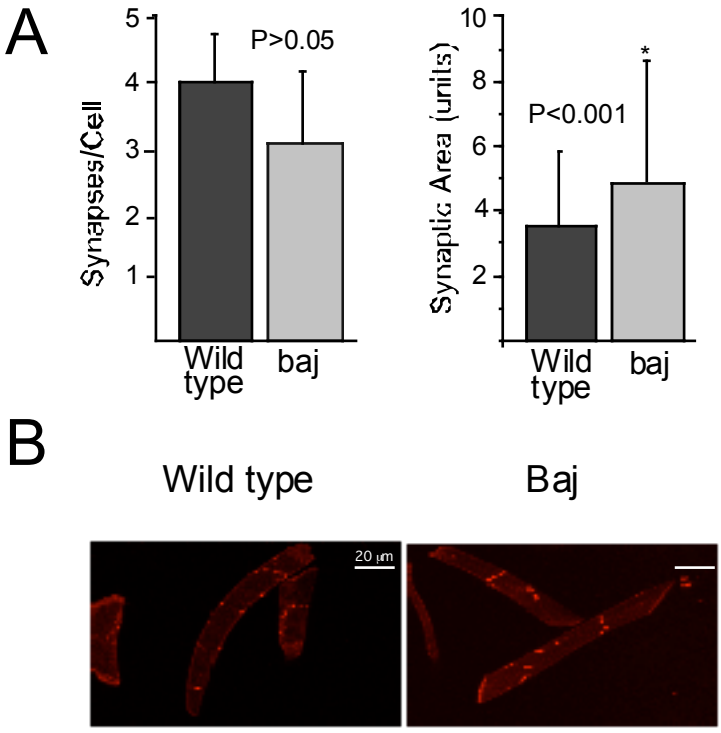

Figure 1. Enlarged single AchR clusters at *baj* NMJ.

(A) Quantification analysis showed enlarged single synaptic area but similar number of synapse on each muscle cell in *baj* (grey) compared to wild type (black). (B) Representative image from the staining of postsynaptic AchRs with Alexa Fluor 647-conjugated α-bungarotoxin in the dissociated skeletal muscle cells from 72 hpf wild type (left) and *baj* (right).

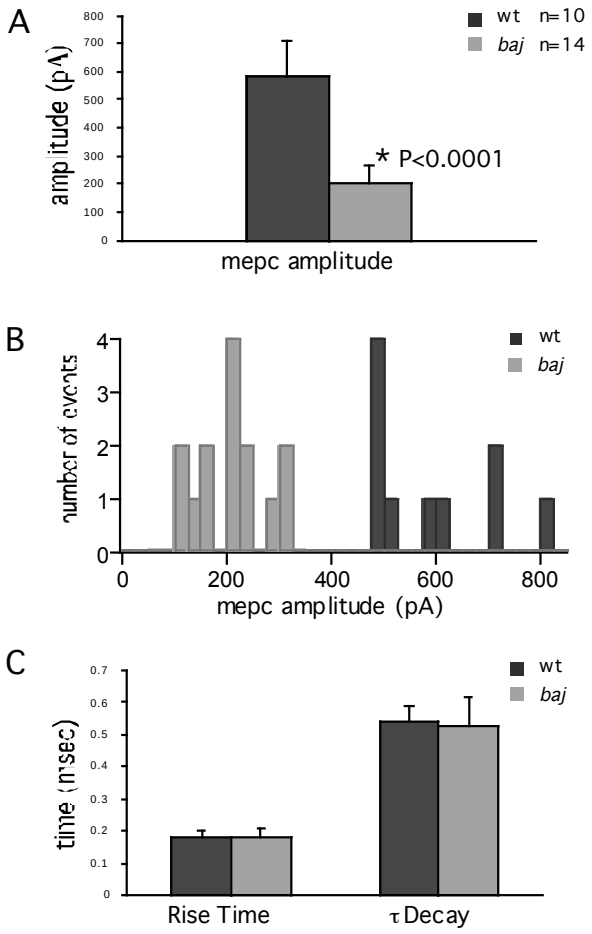

Figure 2. Whole-cell voltage clamp recordings of spontaneous synaptic currents from 72 hpf wild type and *baj* larvae.

(A) Mean amplitude of mEPCs in wild type (n=10) and *baj* (n=14). (B) Amplitude distribution of mEPCs in wild type and *baj*. (C) 10 to 90% Rise time and decay time constant of mEPCs in wild type and *baj*.

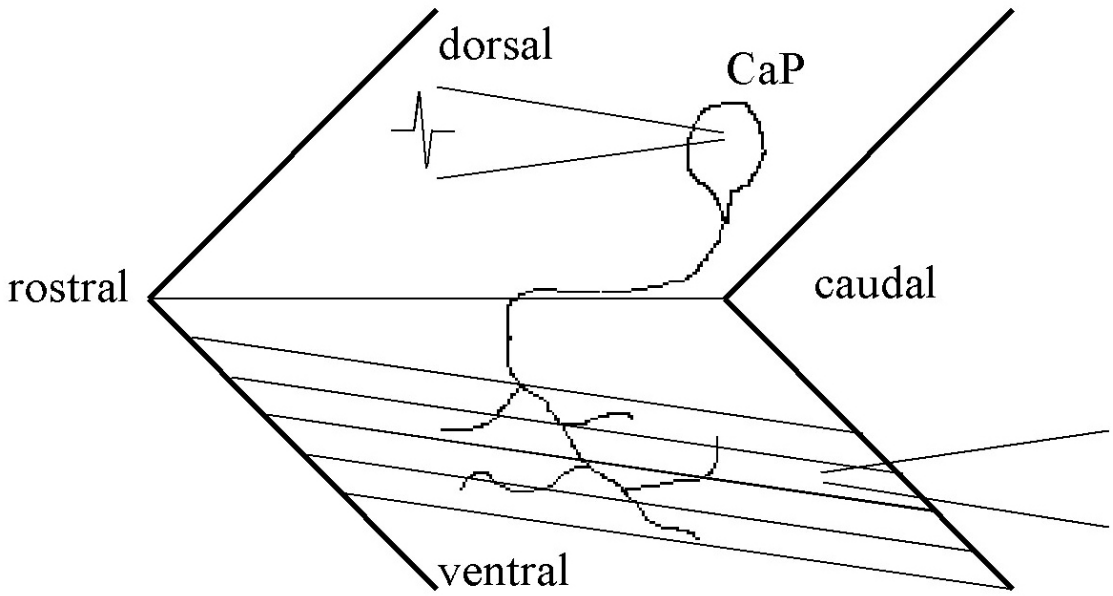

Figure 3. Diagram of paired neuron-muscle recording

In the diagram of the paired neuron-muscle recording, caudal primary motoneuron (CaP) and its ventrally projected axon are shown together with its target fast skeletal muscle cells (running oblique to the tail axis). Two recording electrodes are shown, one on the target muscle and the other one on the CaP soma. Synaptic responses can be elicited by injecting currents through the neuron pipette on the motoneuron cell body.

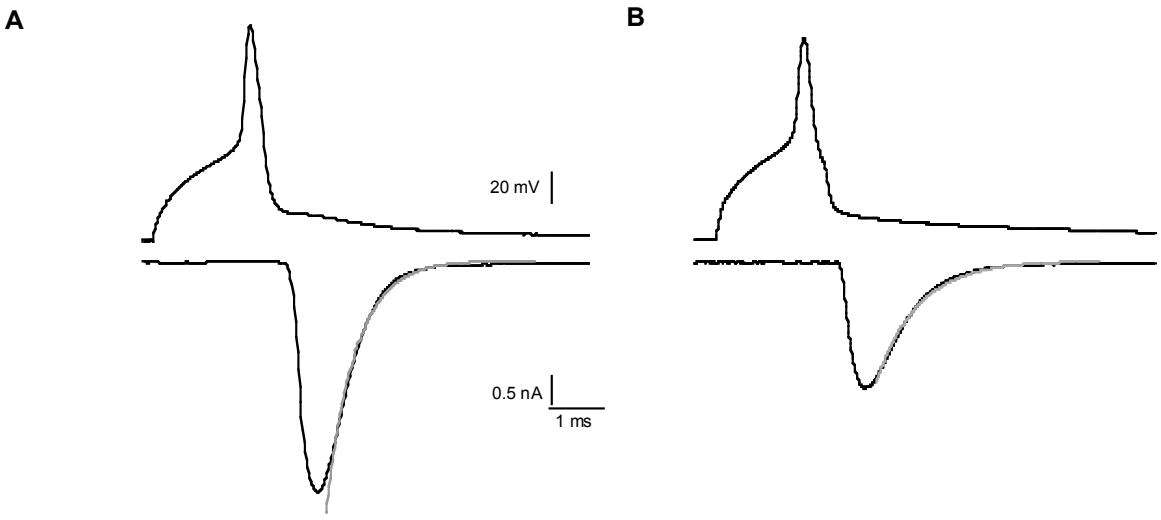

Figure 4. Representative traces of paired neuron-muscle recordings for the evoked postsynaptic responses

Data presented were obtained from a single recording in 72 hpf wild type (A) and *baj* (B) larvae. Sample traces of neuronal action potentials (top trace) in current clamp mode and individual EPCs (bottom traces) recorded in fast skeletal muscle with membrane potential held at –50 mV. The decay phase of EPCs are fitted with a single exponential function (grey line).

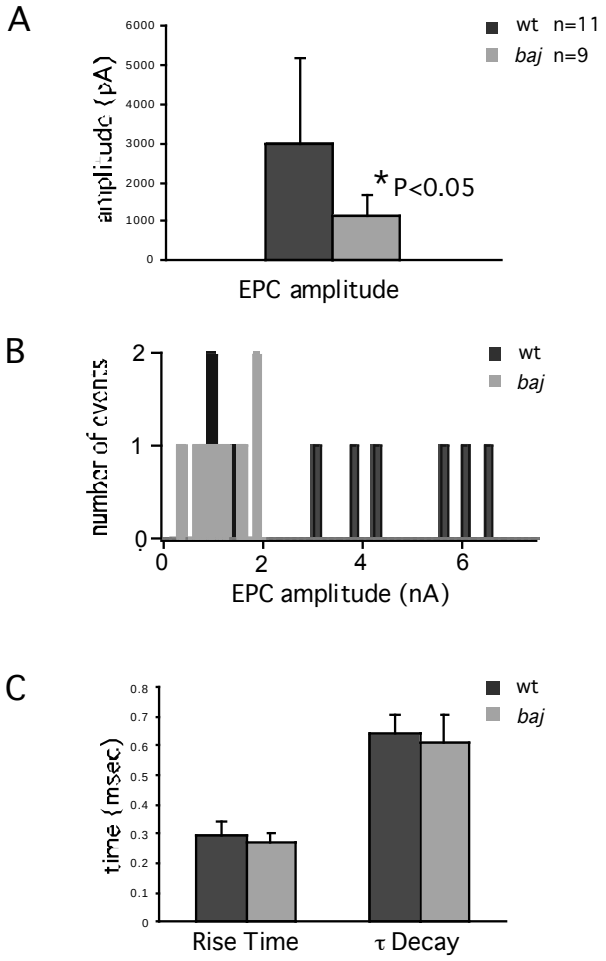

Figure 5. Whole-cell voltage clamp recordings of evoked synaptic currents from 72 hpf wild type and *baj* larvae.

(A) Mean amplitude of EPCs in wild type (n=11) and *baj* (n=9). (B) Amplitude distribution of EPCs in wild type and *baj*. (C) 10 to 90% rise time and decay time constant of EPCs in wild type and *baj*.

Figure 6. Representative Traces of the evoked synaptic responses during 100 Hz stimulation

Traces presented are recorded from 72 hpf wild type (A) and *baj* (B). The first 10 seconds of the evoked responses are shown in a compressed time scale (top). Traces from three different time points were selected to represent three different stages during the repetitive high-frequency stimulation (bottom): (1) EPCs followed the neuronal action potentials faithfully; (2) a mixture of synchronous and asynchronous release appeared; (3) synaptic failures appeared.

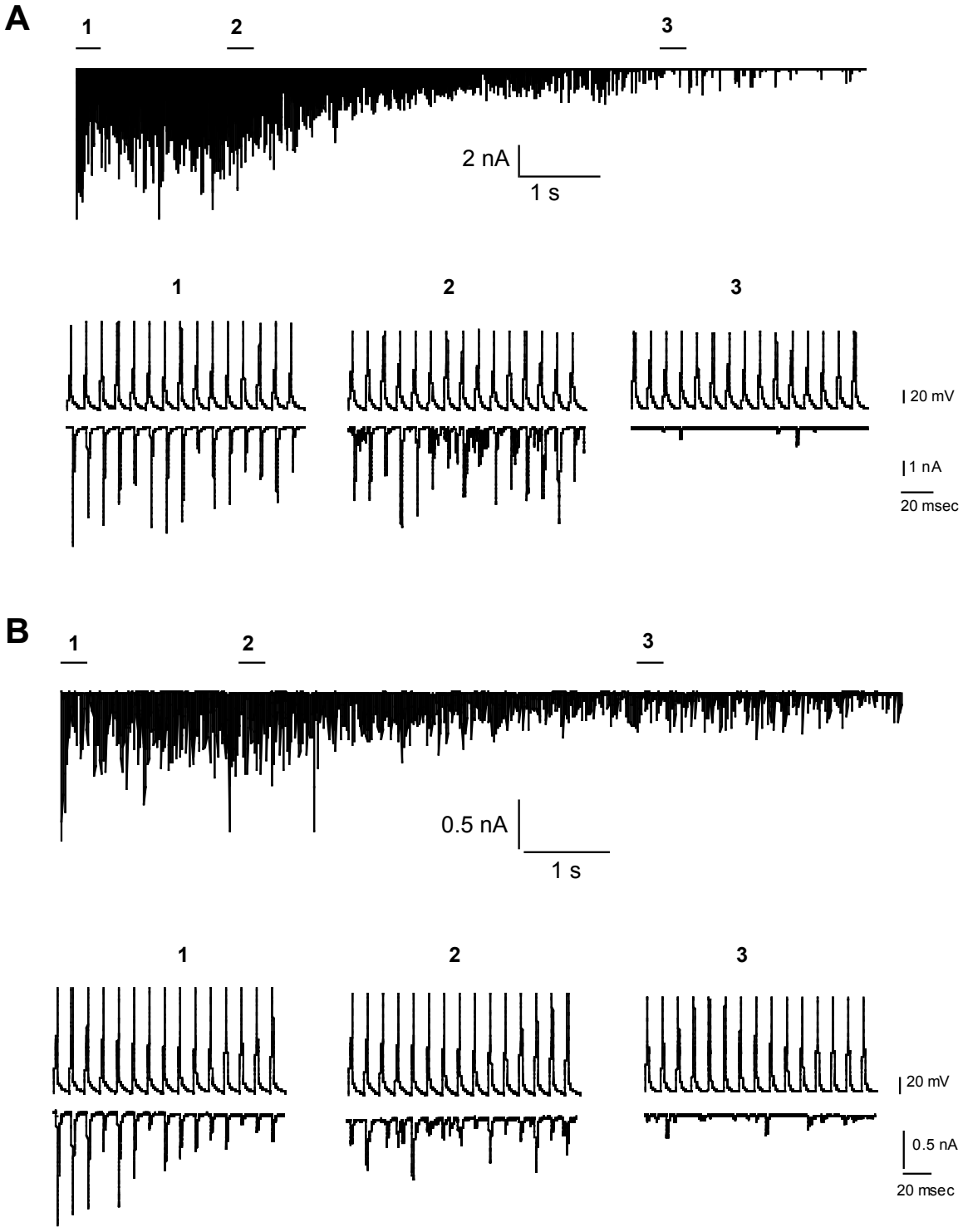
A
1
2
3
2 nA
1 s
1
2
3
20 mV
1 nA
20 msec
B
1
2
3
0.5 nA
1 s
1
2
3
20 mV
0.5 nA
20 msec

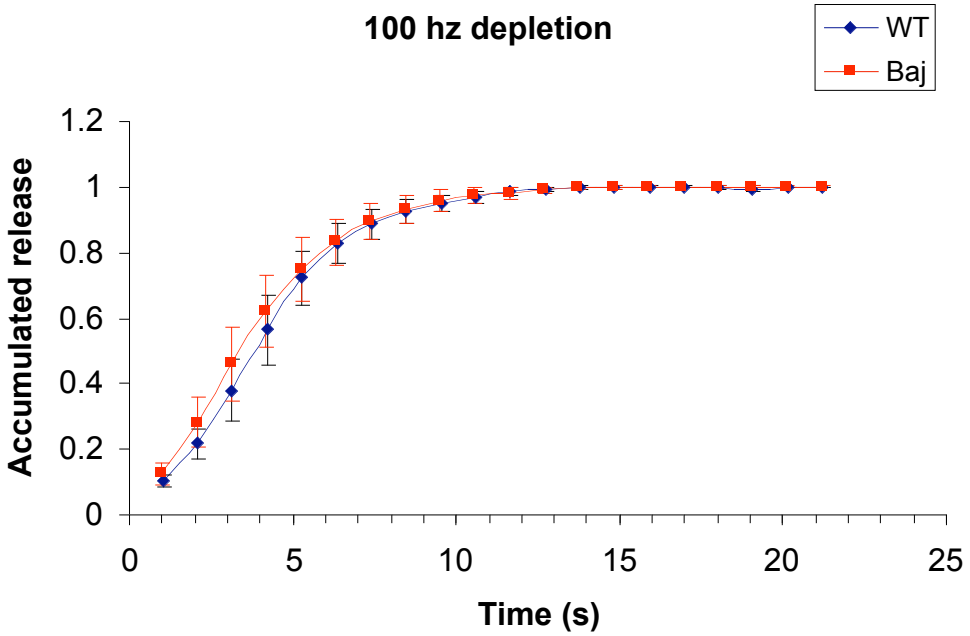

Figure 7. Cumulative transmitter release during 100 Hz stimulation

Cumulative plot of transmitter release in wild type (blue, n=8) and *baj* (red, n=11) during 20 seconds 100 Hz stimulation.

Table 1. Comparison of mEPCs in 72 hpf wild type and *bajan*

Cell code	Minutes recorded	Averaged event number	Events per minute	10 to 90% Rise time (ms)	Decay time constant (ms)	Amplitude (pA)
wild type						
010506a	2.3	10	4.35	0.13	0.51	-489.74
010606a	5	41	8.20	0.20	0.55	-613.22
010606b	1.3	31	23.85	0.19	0.60	-477.65
010606c	4	27	6.75	0.22	0.56	-711.18
010606d	3	16	5.33	0.18	0.55	-486.43
081706a	7	33	4.71	0.18	0.53	-811.26
081706b	3	36	12.00	0.19	0.62	-480.07
081706c	10	54	5.40	0.18	0.55	-700.92
081706d	2	45	22.50	0.15	0.43	-586.78
081706e	4	60	15.00	0.17	0.49	-511.50
n=10						
Average			10.81	0.18	0.54	-586.88
SD			7.36	0.03	0.05	119.28
baj						
080606-1a	7	7	1.00	0.20	0.65	-222.30
080606-1b	4	18	4.50	0.18	0.42	-201.85
080906a	6	33	5.50	0.17	0.54	-308.21
080906-1b	5	39	7.80	0.20	0.54	-232.41
080906-1c	3	8	2.67	0.23	0.67	-160.88
081306-1a	2.5	26	10.00	0.22	0.60	-280.26
081306-1b	2	16	8.00	0.20	0.63	-245.42
081306-1c	2	29	14.50	0.15	0.51	-155.54
081406-1a	4	24	6.00	0.18	0.50	-109.46
081406-1b	5	50	10.00	0.18	0.51	-303.75
081406-1c	4	12	3.00	0.20	0.62	-125.87
081406-1d	2	15	7.50	0.18	0.52	-120.18
081506-1a	5	189	37.80	0.14	0.43	-210.40
081506-1b	1	35	35.00	0.13	0.37	-214.37
n=14						
Average			10.98	0.18	0.54	-206.49
SD			11.34	0.03	0.09	65.53

Table 2. Comparison of EPCs in 72 hpf wild type and *baj*

Cell code	10-90% Rise time (ms)	Decay time constant (ms)	Average amplitude (pA)
wild type			
040409-3a	0.28	0.71	-4280.00
040416-1	0.35	0.74	-1528.56
040421-1	0.31	0.67	-960.98
040429-2a	0.30	0.61	-6489.14
040511-1	0.31	0.58	-777.75
040511-2	0.29	0.62	-6072.58
040810-1	0.34	0.71	-3134.48
040811-2	0.29	0.63	-986.12
040818-3	0.37	0.68	-5628.81
040819-3	0.25	0.54	-1405.17
040820-1	0.28	0.66	-3819.63
n=11			
Average	0.31	0.65	-3189.38
SD	0.03	0.06	2198.17
baj			
060407-1	0.24	0.53	-1123.13
060502-1	0.25	0.71	-895.69
060504-1	0.28	0.72	-1844.50
060505-1	0.34	0.63	-1593.91
060519-1	0.31	0.75	-1852.50
060523-2	0.26	0.59	-339.14
060602-1	0.25	0.56	-980.70
060608-1	0.26	0.56	-1225.70
060705-1	0.24	0.47	-621.56
n=9			
Average	0.27	0.61	-1164.09
SD	0.04	0.09	525.31

Discussion

Results from RT-PCR, sequencing and immunohistochemistry experiments suggested that *baj* carry a null mutation of the zebrafish ChAT gene.

However, fluorescence imaging of the synaptic markers in *baj* did not reveal the morphological defects found in the ChAT knockout mice. In contrast to the extensive nerve branching and enlarged endplate area in the homozygous mutant mice, *baj* showed normal postsynaptic AchR clustering and presynaptic nerve branching in the whole-mount preparation. What could account for the discrepancy between *baj* and ChAT knockout mice? One possibility is that these different findings might reflect an intrinsic drawback of fluorescence imaging in whole-mount zebrafish preparation, the relatively poor resolution on the third dimension. Unlike mice, zebrafish muscle cells are poly-innervated, which means that multiple synaptic sites coexist on one muscle fiber and these sites are contacted by different motoneuron axons (Westerfield et al, 1986). Therefore, in the whole-mount preparation, multiple synapses on different layers of muscle cells overlap on top of each other, making it difficult to detect the subtle changes in the synaptic area or nerve terminal branching patterns. To eliminate this possibility, I re-examined the postsynaptic organization by fluorescence labeling of the AchR clusters in dissociated muscle cells.

Fluorescence imaging in dissociated muscle cells revealed an increase in the single postsynaptic AchR cluster area in *baj*, as was previously described in the ChAT knockout mice. However, when compared to the changes found in the mouse model, the difference is quite subtle between *baj* and wild type. In *baj*, the area of single AchR

cluster increased only by 40% compared to wild type. In the homozygous mutant mice, there was a 50% to 100% increase (Misgeld et al, 2002). What could be the explanation for the less severe morphological abnormalities observed in *baj* mutants?

One important difference between *baj* and ChAT knockout mice phenotypes lies in the results from the electrophysiological recordings in the muscle. In the ChAT knockout mice, intracellular sharp-electrode recordings from myotubes showed complete absence of spontaneous endplate potentials (mEPPs) and nerve-evoked endplate potentials (EPPs) while cholinergic agonist carbachol elicited normal postsynaptic responses (Misgeld 02, Brandon 03). In contrast, we found significantly diminished yet clearly distinct spontaneous and evoked postsynaptic responses in *baj* mutants with whole-cell recordings from the fast skeletal muscle cells. Could the different level of residual neuromuscular transmission account for the discrepancies observed in the synapse morphology of *baj* and ChAT knockout mice?

In mouse myotube cultures, activation of postsynaptic AchRs was shown to induce dispersion of the AchR clusters previously induced by agrin (Lin 05). In addition to the *in vitro* findings, eliminating the Ach biosynthesis in agrin mutants by creating a double knockout mice deficient in agrin and ChAT maintained the AchR clusters which would be otherwise dispersed (Lin 05). Based on the above results, Ach- and agrin-mediated signaling modules were proposed (Misgeld 02) and shown (Lin 05) to play opposing roles in regulating the average area of individual AchR clusters. Acetylcholine was shown to act as the negative signal in regulating neuromuscular synapse formation during development. Agrin, the nerve-derived factor important for postsynaptic differentiation, play an opposing role to Ach (Sanes and Lichtman 01). In the absence of

Ach molecule, nascent AchR clusters were not "trimmed" as efficiently, thus leading to the enlarged area of individual AchR clusters in ChAT deficient mutants. Therefore, the low level of cholinergic activation in *baj* might be sufficient to partially reverse the effect caused by the deficient ChAT gene, resulting in the subtle alterations observed.

Based on the results from the paired neuron-muscle recording, I compared the quantal content at wild type and *baj* NMJ and found no significant difference between them. It is a puzzling observation since the activity-dependent regulation of presynaptic vesicle release has been well characterized at Drosophila neuromuscular transmission. Experiments done at the Drosophila NMJ exploited genetic tools to manipulate synaptic activity through alteration of the innervation pattern (Davis and Bezprozvanny, 2001) or postsynaptic excitability. Methods for altering postsynaptic excitability include introducing mutation (Petersen et al, 1997), modification of protein kinase A activity (Davis et al, 1998) and in other cases, expressing a Kir2.1 potassium channel to hyperpolarize the muscle cell (Paradis et al, 2001). Regardless of the method used, results showed that when there is a decrease in the synaptic activity, compensation occurred through an increase either in the quantal size or in the presynaptic release probability (Davis and Goodman, 1998; Petersen et al, 1997).

The absence of homeostatic regulation in zebrafish might be due to the difference between vertebrate and invertebrate systems. There has not been such convincing evidence found at the vertebrate NMJ as from the Drosophila, except for the findings in the neuregulin knockout mice with a significant reduction in the postsynaptic AchR density (Sandrock 97). Since the proposed retrograde signal and the postsynaptic determinant that is responsible for sensing the change and generating the retrograde

signal are still unknown, the inconsistent results could be attributed to the different properties of glutamatergic and cholinergic synapses. Alternatively, it might be due to the different origins of perturbations. So far all the evidence for homeostasis is based on postsynaptic perturbations while the altered activity in *baj* occurred presynaptically. A presynaptic compensation for a presynaptic defect has never been shown.

Another property of the synaptic function that could be affected by the decreased quantal size in *baj* is the frequency dependency of synaptic response. *Baj* is capable of following low frequency nerve stimulation (< 20 Hz), at least for a short period of time (data not shown). But, during the escape response or burst swimming of the fish, the motoneurons are required to fire action potentials at 50 Hz or higher (Buss and Drapeau, 2001). Such an intense neuronal activity poses a challenge to the impaired synaptic transmission at *baj* NMJ. Therefore, I examined how the neuromuscular synapse in *baj* would perform upon high-frequency nerve-stimulation.

In the cumulative normalized plot of transmitter release, represented by the charge transfer of the evoked synaptic responses, no significant difference was found between wild type and *baj* in the time course of presynaptic release in response to a 20 second 100 Hz stimulation. It is consistent with the previous findings at the rat or snake NMJ that partially filled (Elmqvist and Quastel, 1965; Searl et al, 1991) or empty vesicles (Parsons et al, 1999) undergo exocytosis at a normal rate, suggesting that the vesicle recycling process is independent from the vesicle filling.

Another interesting finding came from the mEPC amplitude distribution histogram where no overlap was present between the two unimodal distributions of wild type and *baj* mEPC, which suggested that no vesicle in the presynaptic terminal of *baj*

NMJ is completely filled with Ach. It raised the question as to why without stimulation (or with rest), the vesicles are not filled completely. It has been shown previously that the process of synaptic vesicle filling is rapid compared to the rate of vesicle recycling as suggested by the lack of change in mEPC amplitude during repetitive high-frequency stimulation (Zhou et al, 2000). Therefore, the vesicle filling should not be the rate-limiting process, unless other molecules that mediate the synaptic transmission in the absence of Ach, were transported into the vesicle at a much slower rate.

In summary, the synapse development and transmitter release is relatively intact compared to the defects found in ChAT knockout mice. Therefore, I propose that the residual neuromuscular transmission is sufficient to sustain synapse formation and synaptic function. The mechanism underlying the residual transmitter release at NMJ albeit a loss-of-function ChAT gene will be discussed in the next chapter.

CHAPTER 5

MECHANISMS FOR RESIDUAL NEUROMUSCULAR TRANSMISSION IN *BAJAN*

Introduction

Considering the previous findings from physiology recordings, it seems paradoxical that the neuromuscular transmission can be retained without the synthesis of the proper neurotransmitter, acetylcholine. However, there are several potential explanations for the residual synaptic transmission at the mutant neuromuscular junctions.

First, other molecules might serve as the alternative neurotransmitter in *baj*. Since there is no significant difference found in the current kinetics of synaptic responses, the hypothetical alternative neurotransmitter most likely possesses similar chemical or structural characteristics. Serum choline was observed in single channel recordings to activate AchRs with a low open probability (Zhou et al, 1999). It was also shown *in vitro* that choline was transported by vesicular acetylcholine transporter (VAchT) with a lower affinity (Bravo et al, 2004), suggesting that choline is present in synaptic vesicles. Combined with its large resource in the zebrafish embryo, choline could potentially be the alternative neurotransmitter in *baj* when Ach is absent.

Second, more than one copy of ChAT gene could be present in the zebrafish genome. A duplication event occurred in the teleost genomes after the divergence from the mammals, resulting in the presence of two or more homologues of the mammalian counterparts in the zebrafish genome (Postlethwait et al, 1999). Since the two homologues might have divided the functions of the original genes, the predicted ChAT gene that carries the point mutation might not be the only gene encoding the ChAT protein.

Third, the mutated gene still might retain certain ability to be correctly spliced and transcribe very little amount of normal ChAT mRNA. Results from several previous experiments did not reveal the presence of wild type ChAT transcript in *baj* mutants. In the RT-PCR experiment, none of the product bands detected in the mutants corresponded to the wild type band (Fig 2 in Chapter 3) after a 30-cycle PCR amplification. In addition to the gel result, when the amplification products were excised, gel purified and cloned for individual sequencing, not one wild type transcript was found in over 50 clones that were sequenced. Also in the immunohistochemistry experiment with anti-ChAT antibody, no signal was detected in the mutants (Fig 8 in Chapter 3). However, negative results in the experiments above cannot completely exclude the possibility that very little amount of ChAT mRNA and protein exist in the mutants. The lack of fluorescence signal in the immunohistochemistry result could be a direct outcome of its low sensitivity. As for the more sensitive RT-PCR reaction, preferential amplification of the major products in *baj* cDNA could have masked the presence of trace amount of the wild type transcript. Methods for differential amplification of the wild type transcript are needed.

Fourth, in zebrafish and xenopus, maternal loading of mRNAs represents a significant portion of the embryonic RNA (Crippa, 1969; Wehman et al, 2006) and plays an important role in early embryonic development before the activation of zygotic genome (Davidson et al, 1968; Hake and Richter, 1997). The maternal mRNAs were synthesized and deposited during oogenesis and remained in the oocyte in an inactive state. This inactive state was achieved by translational repression mechanisms such as poly(A) tail deadenylation (Richter et al, 1999) and miRNA regulation (Giraldez et al, 2006) until the activation signals relieve the repression (Johnstone and Lasko, 2001). The activation of maternal mRNA could happen at oocyte maturation, fertilization or anytime during the early embryonic development (Hake and Richter, 1997).

Maternal loading of mRNA or protein has been shown to account for the different phenotypes observed among different animal model systems. The anaphase-promoting complex 2 (APC2) null mutants in several model systems showed a variable level of severity, from the early embryonic lethality in mouse to late larval lethality in Drosophila to adult sterility in C. elegans (Wehman et al, 2006). This observed disparity was suggested to be the result of maternal protein present in Drosophila and C. elegans, in fulfilling their needs for rapid embryonic divisions during early development (O'Farrell et al, 1989). Similarly, the differing degrees of severity observed between *baj* and CHAT knockout mice could also be attributable to the maternal rescue in zebrafish.

The purpose of this chapter is to examine the potential mechanisms that account for the residual neuromuscular transmission at *baj* NMJ.

Methods

mEPCs recording with Fasciculin II incubation

To test whether acetylcholine or choline is responsible for the observed neurotransmission at *baj* NMJ, whole-cell recordings in muscle cells were performed to compare the effect of Fasciculin II on mEPCs current kinetics. 72 hpf wild type and mutant larvae were prepared for muscle recordings as previously described (Chapter 2). 330 μM of Fasciculin II was applied to bath solution in addition to the 1.5 μM TTX and pretreated for 30 minutes before recording started. The rise time, decay time constant and amplitude of mEPCs with and without treatment of FASII were compared between wild type and *baj*.

Semi-quantitative RT-PCR analysis for wild type ChAT transcript in 1 to 4 day wild type and baj mutant

Total RNA extraction from 24 hpf to 96 hpf embryos was performed using 800 μl Trizol Reagent (Gibco) following the instructions from Invitrogen. A variable number of embryos were used to minimize the difference between the amounts of total RNA harvested from different age embryos. For example, I used 60 embryos at 24 hpf and 30 embryos at 48 hpf and 20 embryos for 72 hpf and 96 hpf. The RNA pellet was resuspended in 20 μl DEPC water (Ambion) and the concentration was determined using spectrophotometer. Approximately 500 ng of total RNA were used in a 20 μl cDNA synthesis reaction with the SuperScript III First-Strand Synthesis System for RT-PCR (Invitrogen).

ChAT cDNA and beta-actin cDNA were amplified in a 25 μl reaction containing 2.5 μl of 10X Buffer, 1 μl of MgSO4, 2.5 pmol of primers, 0.125 μmol of dNTP mix, 0.5 U of Platinum Taq High Fidelity polymerase (Invitrogen). The primers used to amplify ChAT transcripts were: forward 5'-TGGCTTGAAGACATGTATTTGAAAC-3' and reverse 5'-AGCACGTCCATCAATTAGAGC-3'. The primers used to amplify beta-actin transcript were: forward 5'-GTCGTTGACAACGGCTCC-3' and reverse 5'-TCCCATGCCAACCATCACTC-3'.

In order to minimize the inaccurate quantification of the PCR templates caused by multiple products, the extension time in the PCR protocol was limited to 30 seconds for preferential amplification of the shorter wild type product (Fig. 2). To avoid saturation of PCR amplification, PCR reactions were performed with different number of cycles at an increment of 5 cycles, and the results were compared with gel analysis to identify a cycle number that could clearly show the increase of ChAT product in 24 hpf to 96 hpf wild type cDNAs. The amplification protocol for ChAT was: 94°C for 2 min, 40 cycles of 94°C for 10 sec, 55.1°C for 30 sec, 68°C for 30 sec and final extension at 68°C for 5 min. The PCR protocol for β-actin amplification was: 94°C for 2 min, 25 cycles of 94°C for 10 sec, 57.5°C for 30 sec, 68°C for 30 sec and final extension at 68°C for 5 min.

To achieve semi-quantification of the ChAT product in *baj*, β-actin was used as internal controls. β-actin was amplified from 24 hpf to 96 hpf wild type and mutant cDNAs with a non-saturating cycle number. Products were analyzed on agarose gels and the amount of template used in each reaction was modified until all bands showed same level of intensity.

Morpholino knockdown against the translation initiation site

ATG morpholino is the 25 nt oligo that direct against the translational starting site of zebrafish ChAT (5'-GAAACTGGCATCCTCAAAGTTGAAG-3'). The 300 nmole dry powder was made into 3mM stock solution (25.5ng/nl) in distilled water and stored at –20°C. Method for injection was described in Chapter 3. The injection time varied to achieve a bolus of 100 μm diameter, equivalent to a 0.5 nl volume (~2.1ng).

Results

Fasciculin II induced prolonged decay and increased current amplitude of mEPC in both wild type and baj

To distinguish whether acetylcholine or choline is mediating synaptic transmission, I inhibited the acetylcholinesterase with Fasciculin II (FAS II). Fasciculin II, a potent cholinesterase inhibitor originally extracted from snake venom, undermines cholinesterase activity mainly by sterically blocking the ligand binding site (Bourne et al, 1995). The role of cholinesterase at the synaptic cleft is to clear away the Ach released from presynaptic terminals through hydrolysis. Therefore, inhibiting the cholinesterase function is expected to result in slower decay kinetics and slightly larger amplitude of postsynaptic responses in muscle, due to lingering Ach molecules rebinding to AchRs. Inhibition of cholinesterase should not have an effect on *baj*'s synaptic currents if Ach is not the transmitter in mutants.

For this purpose, mEPCs were recorded in 72 hpf embryos in the presence of 330 μM Fasciculin II toxin. The amplitude and kinetics of mEPCs were compared between FASII treated fish and untreated controls in both wild type and mutants. In wild type fish treated with FASII, mEPCs showed much prolonged decay time constant and increased current amplitude (Fig 1 A&C). The decay time constant τ averaged at 0.54 ± 0.08 ms without FASII and 0.99 ± 0.44 ms with FASII treatment ($P < 0.001$). The average mEPC amplitude measured at 594 ± 209 pA without FASII versus 702 ± 250 pA with FASII treatment ($P < 0.0001$). In *baj* mutants, similar increases in both decay time constant and current amplitude were observed with FASII treatment (Fig 1 B&D). The decay time constant τ measured 0.52 ± 0.11 ms without FAS versus 0.88 ± 0.42 ms with FAS treatment ($P < 0.001$). And the mEPC amplitude averaged at 240 ± 129 pA without FAS versus 367 ± 172 pA with FAS ($P < 0.001$). The results of this experiment support Ach as the neurotransmitter that mediates the synaptic responses in *baj*.

No duplication of ChAT gene was found in the zebrafish genome

To test the possibility that multiple copies of ChAT gene might be present in the zebrafish genome, I took an extremely well conserved portion of the protein sequence surrounding the enzymatic activity center (Histidine334) and blasted it against the whole zebrafish genome, and the result came out with the same predicted ChAT gene where the point mutation resided. This result argues against a potential duplicated ChAT gene being responsible for the Ach synthesis in *baj* mutants.

Small amount of ChAT transcripts were detected in baj with a modified RT-PCR protocol

To detect the presence of wild type ChAT transcript in *baj*, primers used in RT-PCR reaction were specially designed to improve the amplification of the wild type ChAT transcript in *baj* cDNA. Since the three mutant transcripts covered the whole sequence of the wild type ChAT mRNA, there are no unique primers that anneal only to the wild type transcript. To solve this problem, primers were designed to target a region that is 168 bp long in the wild type transcript but also present in the longest *baj* transcript that includes the wild type coding sequence plus a unspliced intron of approximately 1.2 Kb (Fig 2). These special primers not only eliminated the amplification from two other major mutant transcripts, thereby facilitated the amplification of the wild type transcript, but also enabled the easy distinction between the wild type and mutant products on gel electrophoresis analysis. The extension time in the PCR protocol was also limited to 30 seconds for preferential amplification of the shorter wild type product.

RT-PCR analysis was done in 24 hpf to 96 hpf wild type and mutant embryos. A single product of 168 bp was amplified from 24 hpf to 96 hpf wild type cDNAs (Fig. 3A, top lanes 2 to 5). In *baj*, a very faint band at the correct size was amplified from the mutant cDNAs at all 4 ages (Fig. 3A, top lanes 6 to 9), revealing the presence of wild type ChAT mRNA transcript in *baj* mutants throughout the first few days of embryo development.

To estimate the relative amount of wild type ChAT mRNA present in the mutants, a more quantitative measurement such as real-time PCR is needed. However, quantification of the templates with real-time PCR requires the amplification of a single product in the reaction, which is not possible in this case. Therefore I resorted to a semi-

quantified PCR amplification to estimate the level of wild type transcript in the mutants. Semi-quantification of the reaction was achieved by careful controls in multiple steps throughout the RT-PCR procedure. First, total RNA extractions were performed from a variable number of embryos at different ages to minimize the difference in the amount of harvested RNA. Second, the reverse transcription started from an equal amount of total RNA for embryos of all ages. Third, I modified PCR protocol to favor the amplification of the short wild type product. Fourth, I tested the PCR reaction with different amplification cycles to find a non-saturating phase. Fifth, I used β-actin as a semi-quantitative internal control for equal amount of cDNA template and equal loading for gel electrophoresis (Fig. 3A, bottom lanes). Combining all the measures above, based on the difference in PCR amplification cycle numbers, the amount of wild type ChAT mRNA transcript in *baj* mutants at its peak (48 hpf), was estimated to be approximately 1/256 of that in the wild type. The detected wild type ChAT mRNA transcript offered a potential origin for the residual Ach that mediates the defective neuromuscular transmission in *baj*.

The amount of wild type ChAT transcripts in baj decays after 48 hpf

The amount of β-actin product amplified from day 1 to day 4 wild type and *baj* fish was compared to ensure equal amount of cDNA template and equal loading in all lanes (Fig 3B, bottom lanes). With an even amount of β-actin products amplified from wild type and *baj* cDNA, I compared the changes in the amount of wild type ChAT transcripts over time between day 1 to day 4 wild type and *baj* fish. The amount of ChAT transcripts in wild type showed a steady increase between 24 hpf and 96 hpf (Fig 3B top

lane 2 to 5). But in *baj* the ChAT product peaked at 48 hpf and subsequently showed a clear decrease at 72 hpf and 96 hpf. (Fig 3B top lane 6 to 9).

Postsynaptic responses at baj NMJ decrease during development

In agreement with the results from the semi-quantitative RT-PCR analysis, I observed that their phenotype appeared to be more severe over time while analyzing the high-speed movies of the mutant motility phenotype taken at different ages. From 72 hpf when the phenotype was mostly robust to 120 hpf when some mutant larvae started to die, the already diminished initial C-bend of the escape response kept decreasing in strength and eventually became almost indiscernible.

To establish whether decreased synaptic drive is responsible for the behavioral change, spontaneous postsynaptic responses from the muscle were recorded from 48 hpf to 96 hpf. The change of amplitude and frequency of mEPCs over this 3-day period were compared between wild type and mutants. In wild type embryos, the mEPC amplitude did not change significantly between 48 hpf and 96 hpf (Fig 4A). The average mEPC amplitude measured 480 ± 124 pA for 48 hpf, 587 ± 119 pA for 72 hpf and 478 ± 95.6 pA for 96 hpf ($P > 0.05$). In *baj* homozygotes, however, while the amplitude of mEPCs was consistently smaller than wild type over the 3-day period, mEPC amplitude at 96 hpf showed a significant decrease compared to those at 48 hpf or 72 hpf ($P < 0.0001$) (Fig 4A). The mEPC amplitude in *baj* averaged 53.2±22.3 pA at 96 hpf, 156.0±58.4 pA at 48 hpf and 205 ± 61.9 pA at 72 hpf.

Similar decrease was found in the mEPC frequency in mutants. The mEPC frequency in wild type muscle showed a clear increase over time (Fig. 4B), indicating the

maturation of NMJ during early development (Nguyen et al, 1999). The mEPC frequency measured 2.34 ± 1.54 at 48 hpf, 10.8 ± 7.36 events/min at 72 hpf and 20.5 ± 16 events/min at 96 hpf. A different pattern was observed in *baj* where the mEPC frequency decreased at 96 hpf (Fig. 4B). The mEPC frequency measured 2.84 ± 2.81 events/min at 48 hpf, 11 ± 7.36 events/min at 72 hpf and 7.52 ± 10 events/min at 96 hpf. The reduction in spontaneous synaptic response amplitude and frequency in *baj* is consistent with the maternal deposit of ChAT that wears off over time.

ATG-morpholino result supported the presence of maternal ChAT

Next I attempted to identify the source of ChAT mRNA present in the mutant. One way to distinguish if the transcripts are of zygotic or maternal origin is to conduct RT-PCR analysis before the zygotic gene expression turns on at the mid-blastula transition (~2.5 hpf or around 512-cell stage) (Kane DA 93, Mathavan 05). I attempted to amplify the ChAT transcripts from the wild type cDNAs harvested at one-cell stage and 16-cell stage. A correct-size product was amplified from the control cDNA at 512-cell stage but no product appeared for 1-cell and 16-cell stage (data not shown).

Since methods for direct detection of the maternal ChAT failed, I resorted to indirect evidence to determine if maternal ChAT mRNA is responsible for sustaining the low level Ach production. I attempted to knockdown all ChAT mRNA expression by morpholino injection aiming to block the translation initiation and compared the results with the splice-site morpholino. Since all maternal loading of mRNAs are pre-spliced, the splice-site morpholino will only affect the zygotic transcript. With ATG-morpholino (morpholino oligos designed against the translation initiation site), however, translation

of both maternal and zygotic ChAT mRNA will be blocked. A difference in the phenotype between splice-site morphant and ATG-morphant will be consistent with the presence of maternal ChAT mRNA in mutants.

The ATG-morpholino was injected into wild type embryos and the behavioral phenotype of the morphant fish were assessed after 48 hpf. Unlike the splice-site morpholino injected embryos, the survival rate of ATG-morphant was below par and the survivors bore various anatomical defects. To avoid the possibility that the observed phenotype results from the unspecific effect of morpholino oligo injection, I carefully titrated the dosage of ATG morpholino but had a perplexing observation. There seems to be a threshold for the phenotypes. That is, while less than threshold amount of the ATG morpholino oligos produced no phenotype in any of the embryos injected, a slight increase to the threshold would kill half of the injected embryos and induce extensive morphological defects in the rest of the fish. The unusual phenomenon could be due to the crucial roles Ach plays in survival during development (Oliff and Gallardo, 1999; Atluri et al, 2001).

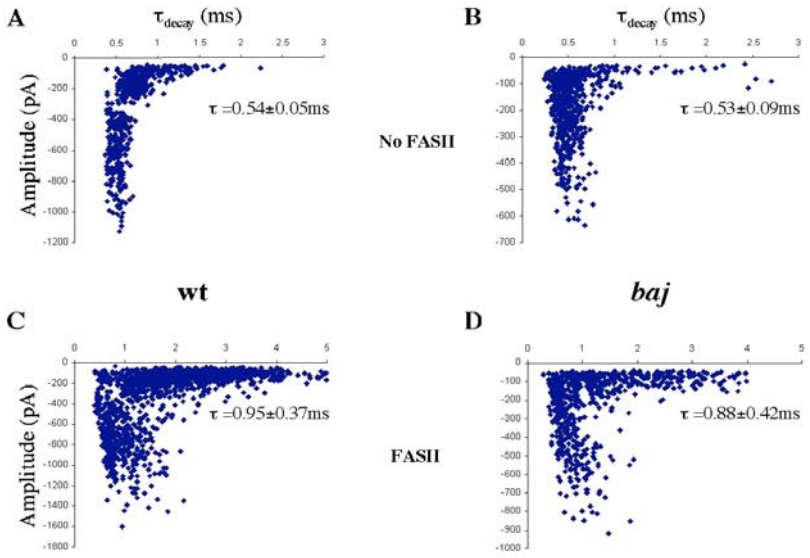

Figure 1. Fasciculin II prolonged mEPC decay in both wild type and *baj*.

Acetylcholinesterase inhibitor Fasciculin II elicited similar effect on the amplitude and decay time constant of mEPCs in 72 hpf wild type (A and C) and *baj* (B and D). Scatter plots of decay time constant τ versus current amplitude in wild type with (C) or without (A) FAS II treatment and *baj* with (D) or without (B) FAS II treatment are shown.

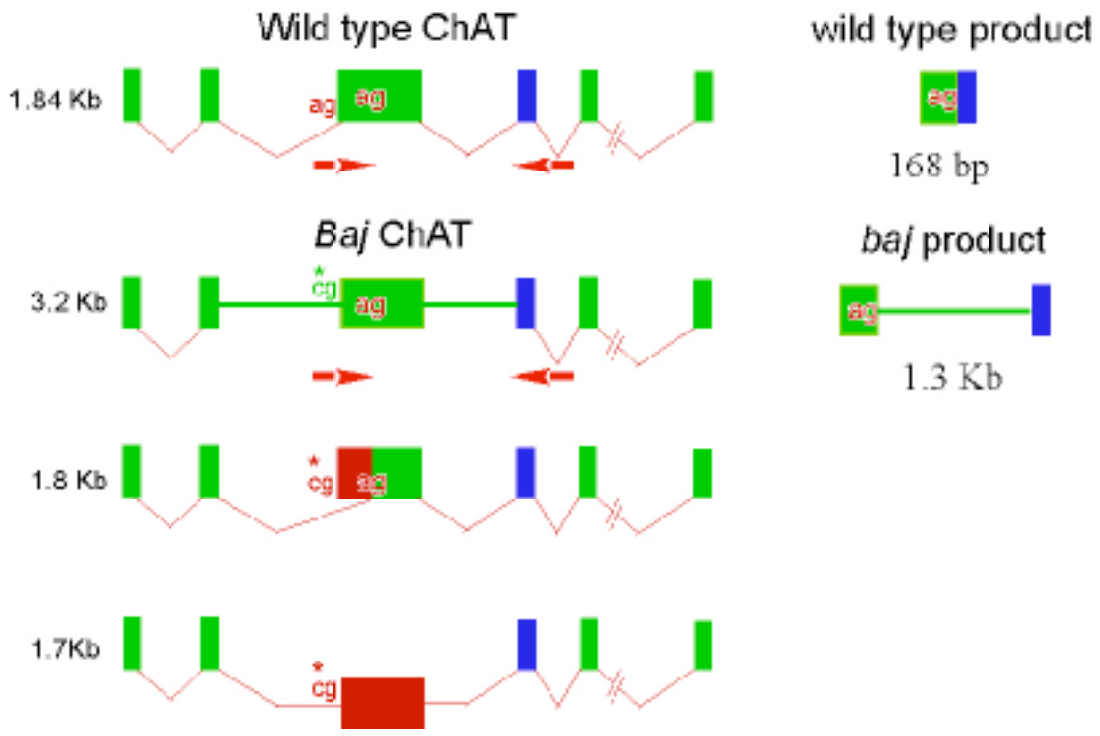

Figure 2. Diagram of the primer design for detecting ChAT mRNA in *baj*

In order to detect correct ChAT mRNA in *baj*, primers were designed to maximize the size difference between the wild type product and mutant product for easy distinguishment on gel electrophoresis. The forward primer was selected within the first 41 bp of exon 3 (from the beginning of exon 3 till the cryptic splice site ag), which is only present in the 3.2 Kb mutant transcript, to ensure single mutant product. The reverse primer was designed against the sequence across exon 4 (blue) and exon 5 to avoid amplification of the genomic DNA. Primers were denoted with red arrows. The amplified wild type product is 168 bp. The mutant product is 1.3 Kb due to retention of a intron in the 3.2 Kb mutant transcript.

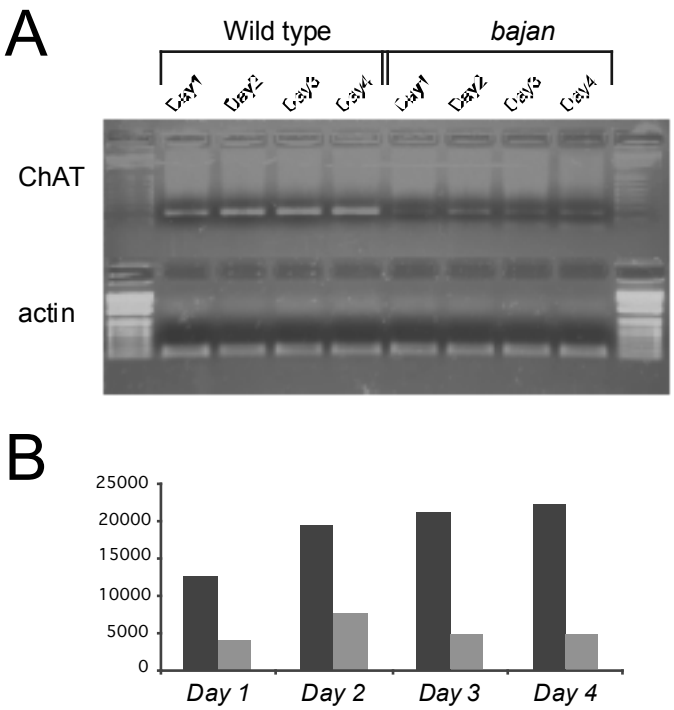

Figure 3. Semi-quantitative RT-PCR analysis detected wild type ChAT mRNA in *baj*.

(A) Electrophoresis result for wild type ChAT mRNA amplification in 1 to 4 day wild type and *baj*. Wild type ChAT can be detected in *baj* mutants at all ages with the amount peaked at 48 hpf. Amplification of β-actin was performed in the same reaction mix to ensure equal amount of template and equal loading across different lanes. (B) Digitized gel band intensity plot for the ChAT products in 1 to 4 day wild type (black) and *baj* (grey).

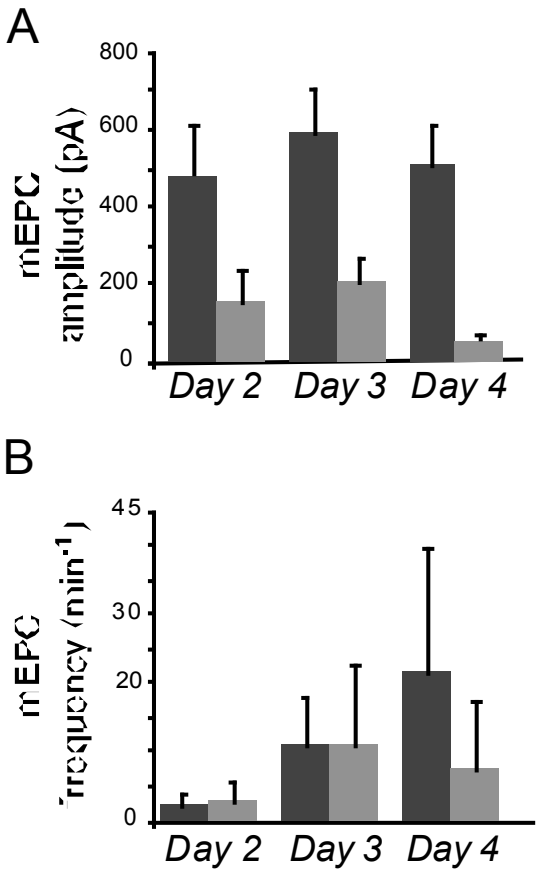

Figure 4. mEPC amplitude and frequency in *baj* decrease during development

The amplitude (A) and frequency (B) of mEPCs showed significant decrease in day 4 *baj* mutants (grey) compared to wild type (black).

Discussion

If indeed the low levels of neuromuscular transmission sustained the synapse formation at *baj* NMJ, what is mediating the cholinergic activities if no Ach is synthesized in the mutants? Choline was an obvious candidate since it has been shown *in vitro* to activate AchRs and could be transported by VAchT into the synaptic vesicles (Zhou et al, 1999, Bravo et al, 04). The lower affinity of the transporter to choline (Bravo et al, 2004) could potentially explain the incompletely filled vesicles in *baj*. To distinguish whether choline or Ach is acting as the neurotransmitter at mutant NMJ, I compared the effect of cholinesterase inhibitor on spontaneous synaptic currents in wildtype and *baj*. Results showed similar degree of slowing down in decay kinetics with FASII treatment in both wildtype and *baj* (Fig 1), indicating that Ach is still the neurotransmitter at *baj* NMJ.

The cholinesterase experiment proved the existence of Ach at the mutant NMJ, but what could be the source of Ach in a ChAT null mutant? One possibility is that maternal infusion of ChAT might be the source for the residual transcripts and enzymatic activity. Based on the high-speed movies, it appeared that from 72 hpf to 96 hpf, the mutants' ability to mount an escape response upon touch stimuli greatly reduced. Consistent with the change in behavior, the amplitude and frequency of mEPCs dropped significantly at 96 hpf (Fig 4). Since maternal infusions of mRNAs and proteins wear off over time, this unusual decrease in the spontaneous synaptic activity during development is consistent with the hypothesis that maternal origin of ChAT is responsible for synthesizing Ach in the mutants.

However, my attempts to directly amplify the maternal ChAT transcripts in early development (one-cell and 16-cell stage) failed. Also, in the semi-quantified RT-PCR experiment, instead of a steady decrease over time, the ChAT transcripts in *baj* started with little amount at 24 hpf, peaked at 48 hpf and maintained a lower level at 72 and 96 hpf. These results argued against maternal ChAT mRNA as the source for residual Ach in *baj*.

Alternatively, maternal loading of ChAT protein might sustain the Ach production in the mutants. Although the immunohistochemistry experiment did not reveal the presence of any ChAT protein, the negative results could be due to the low sensitivity of the immunohistochemistry method and a more sensitive western blot experiment was attempted using the same polyclonal antibody. Unfortunately, although the antibody recognized and bond ChAT protein in the immunohistochemistry, it did not work under the western blot conditions.

A third possibility is that the mutated zygotic ChAT gene could encode a very small amount of ChAT protein. Although the point mutation severely reduced the preciseness and efficiency of ChAT pre-mRNA splicing in *baj*, it is possible that a small amount of wild type ChAT transcript is still correctly spliced from the mutated gene. Based on the results of my experiments, it was not possible to determine whether the residual ChAT mRNA was from zygotic origin.

Yet another possibility remains to be tested is that other members of the acetyltransferase family might catalyze the Ach synthesis reaction with less efficiency. ChAT belongs to a big family of acetyltransferases, all of which are capable of catalyzing reactions between acetyl-CoA and another substrate (Jogl 2004; Ramsay and Naismith,

2003). One of the family members, carnitine acetyltransferase (CrAT) plays crucial roles in the transport of fatty acid across the mitochondrial membrane for β-oxidation (Bieber 1988, Evans 2003). It was shown *in vitro* that CrAT could catalyze the acetylcholine synthesis reaction with approximately 100 times less affinity for choline (Goodman and Harbison, 1981). Pharmacological approaches with specific ChAT and CrAT inhibitors could be used to dissect out the separate Ach synthesis activities of the two enzymes, as was previously shown in the rat retina (Sastry et al, 1994). However, the lack of choline acetylating activity by the brain lysates of ChAT knockout mice does not support this hypothesis (Misgeld et al, 2002).

In conclusion, the results of my experiments favor the hypothesis that residual Ach maintains the synapse formation and the low level of neurotransmission observed in *baj* mutants.

CHAPTER 6

CONCLUSIONS

1. A point mutation in choline acetyltransferase (ChAT) gene underlies *baj* motility phenotype.

Baj homozygotes display greatly diminished touch-mediated escape response. Consistent with its behavioral phenotype, both spontaneous miniature endplate current and evoked endplate current from fast skeletal muscle cells showed a decrease in amplitude but normal current kinetics in *baj* homozygotes, indicating aberrant neuromuscular transmission. Mapping and sequencing results revealed a mutation at a splice acceptor site in the gene encoding ChAT, the synthesis enzyme for Ach. The point mutation disrupted the normal pre-mRNA splicing pattern and instead of one wild type transcript, created three transcripts, all of which encode severely truncated ChAT proteins predicted to have no enzymatic function. In agreement with the prediction, labeling with anti-ChAT antibody was absent in the *baj* mutants. Successful phenocopy in the wild type fish with splice-site morphlino injection and behavioral rescue in homozygous *baj* with the wild type ChAT mRNA further supported that the mutation in ChAT gene is responsible for *baj* motility phenotype.

2. Residual Ach sustains synapse formation and synaptic transmission in *baj*.

Fluorescence imaging of the major pre- and post-synaptic markers in whole-mount zebrafish preparation did not reveal obvious morphological defects in the pre- or post-synaptic organization. Fluorescence imaging of AchR clusters in dissociated skeletal muscle cells showed enlarged area of single AchR clusters but normal number of synapses per cell. Electrophysiological recordings showed a reduced yet distinct level of neuromuscular transmission and a normal time course of presynaptic vesicle release. The above observations are consistent with but much less severe than what was seen in ChAT knockout mice (Misgeld et al, 2002, Brandon et al, 2003), suggesting that the low level of cholinergic activation in *baj* is sufficient to partially reverse the effect caused by the deficient ChAT gene. The comparable effects of Fasciculin II on the current kinetics in wild type and bajan confirmed the presence of residual acetylcholine at mutant NMJ.

3. Maternal origin of ChAT might be the source for Ach production in *baj*

The observation that *bajan*'s motility phenotype deteriorates over time suggested the involvement of maternal loading of ChAT. Consistent with the observation, electrophysiological recordings found a decrease of mEPCs frequency and amplitude over time in the mutant fish, supporting the existence of pre-fertilization deposit of maternal ChAT mRNA or protein. However, attempts to directly detect the presence of maternal ChAT mRNA have failed. Also, RT-PCR analysis of ChAT transcript in day 1

to day 4 wild type and mutants showed that the amount of ChAT transcript in *baj* displayed a peak at day 2 instead of a steady decrease over time, arguing against the maternal ChAT mRNA being responsible for the residual Ach production in *baj*.

BIBLIOGRAPHY

Amatruda JF, Zon LI (1999). Dissecting hematopoiesis and disease using the zebrafish. Devel Biol 216 (1): 1-15.

Amsterdam A, Lin S, Moss LG, Hopkins N (1996). Requirements for green fluorescent protein detection in transgenic zebrafish embryos. Gene173(1 Spec No):99-103.

Ando H, Furuta T, Tsien RY, Okamoto H (2001). Photo-mediated gene activation using caged RNA/DNA in zebrafish embryos. Nature Genet 28 (4): 317-325.

Arnaout R, Ferrer T, Huisken J, Spitzer K, Stainier DYR, Tristani-Firouzi M, Chi NC (2007). Zebrafish model for human long QT syndrome. Proc Natl Acad Sci 104 (27): 11316-11321.

Atluri P, Fleck MW, Shen Q, Mah SJ, Stadfelt D, Barnes W, Goderie SK, Temple S, Schneider AS (2001). Functional nicotinic acetylcholine receptor expression in stem and progenitor cells of the early embryonic mouse cerebral cortex. Dev Biol. 240(1):143-56.

Baier H, Klostermann S, Trowe T, Karlstrom RO, Nüsslein-Volhard C, Bonhoeffer F (1996). Genetic dissection of the retinotectal projection. Development 123:415-25.

Baker K, Warren KS, Yellen G, Fishman MC (1997). Defective "pacemaker" current (I-h) in a zebrafish mutant with a slow heart rate. Proc Natl Acad Sci 94 (9): 4554-4559.

Bajjalieh SM, Peterson K, Shinghal R, Scheller RH (1992). SV2, a brain synaptic vesicle protein homologous to bacterial transporters. Science 257(5074):1271-3.

Behra M, Cousin X, Bertrand C, Vonesch JL, Biellmann D, Chatonnet A, Strahle U (2002). Acetylcholinesterase is required for neuronal and muscular development in the zebrafish embryo. Nature Nedurosci 5 (2): 111-118.

Betz WJ and Bewick GS (1992). Optical analysis of synaptic vesicle recycling at the frog neuromascular junction. Science 255 (5041): 200-203.

Bieber LL (1988). Carnitine. Annu Rev Biochem 57:261-83.

Bingham PM, Levis R, Rubin GM (1981). Cloning of DNA sequences from the white locus of D. melanogaster by a novel and general method. Cell 25(3):693-704.

Blusztajn JK and Wurtman RJ (1983). Choline and Chjolinergic neurons. Science 221 (4611): 614-620.

Bolker JA (1995). Model system in developmental biology. Bioessays 17 (5): 451-455.

Bourne Y, Taylor P, Marchot P (1995). Acetylcholinesterase inhibition by fasciculin: crystal structure of the complex. Cell 83(3): 503-512

Brandon EP, Lin W, D'Amour KA, Pizzo DP, Dominguez B, Sugiura Y, Thode S, Ko CP, Thal LJ, Gage FH, Lee KF (2003). Aberrant patterning of neuromuscular synapses in choline acetyltransferase-deficient mice. J Neurosci 23(2): 539-549

Bravo DT, Kolmakova NG, Parsons SM (2004). Choline is transported by vesicular acetylcholine transporter. J Neurochem 91: 766-768

Brockerhoff SE, Hurley JB, Janssenbienhold U, Neuhauss SCF, Driever W, Dowling JE, (1995). A behavioral screen for isolating zebrafish mutants with visual-system defects. Proc Natl Acad Sci 92 (23): 10545-10549.

Briggs JP (2002). The zebrafish: a new model organism for integrative physiology. Am J Physiol Regul Integr Comp Physiol 282(1):R3-9.

Brownlie A, Donovan A, Pratt SJ, Paw BH, Oates AC, Brugnara C, Witkowska HE, Sassa S, Zon LI (1998). Positional cloning of the zebrafish sauternes gene: a model for congenital sideroblastic anaemia. Nature Genet 20 (3): 244-250.

Buss RR, Drapeau P (2001). Synaptic drive to motoneurons during fictive swimming in the developing zebrafish. J Neurophysiol 86(1):197-210.

Buss RR, Bourque CW, Drapeau P (2003). Membrane properties related to the firing behavior of zebrafish motoneurons. J Neurophysiol 89(2):657-64.

Cai Y, Cronin CN, Engel AG, Ohno K, Hersh LB, Rodgers DW (2004). Choline acetyltransferase structure reveals distribution of mutations that cause motor disorders. EMBO J 23: 2047-2058.

Crippa M, Gross PR (1969). Maternal and embryonic contributions to the functional messenger RNA of early development. Proc Natl Acad Sci USA 62(1): 120-127.

Cui, W.W., Low, S.E., Hirata, H., Saint-Amant, L., Geisler, R., Hume, R.I., and Kuwada, J.Y. (2005). The zebrafish shocked gene encodes a glycine transporter and is essential for the function of early neural circuits in the CNS. J. Neurosci. 25(28):6610-6620.

Davis GW, DiAntonio A, Petersen SA, Goodman CS (1998). Postsynaptic PKA controls quantal size and reveals a retrograde signal that regulates presynaptic transmitter release in Drosophila. Neuron 20: 305-315.

Davis GW, Bezprozvanny I (2001). Maintaining the stability of neural function: a homeostatic hypothesis. Annu Rev Physiol 63:847-69.

Davidson EH, Crippa M, Mirsky AE (1968). Evidence for the appearance of novel gene products during amphibian blastulation. Proc Natl Acad Sci 60(1):152-9.

del Castillo and Katz B (1955). On the localization of acetylcholine receptors. J. Physiol- 128 (1): 157-181.

Downes GB and Granato M (2004). Acetylcholinesterase function is dispensable for sensory neurite growth but is critical for neuromuscular synapse stability Devel Biol 270 (1): 232-245.

Dreyer F. Peper K, Akert K, Sandri C, Moor H (1973). Ultrastructure of active zone in frog neuromuscular junction. Brain Res 62 (2): 373-380.

Driever W, Solnica-Krezel L, Schier AF, Neuhauss SC, Malicki J, Stemple DL, Stainier DY, Zwartkruis F, Abdelilah S, Rangini Z, Belak J, Boggs C (1996). A genetic screen for mutations affecting embryogenesis in zebrafish. Development. Dec;123:37-46.

Driever W, Fishman MC (1996). The zebrafish: Heritable disorders in transparent embryos J Clin Invest 97 (8): 1788-1794.

Drummond F. Putt W, Fox M, Edwards YH (1997). Cloning and chromosome assignment of the human CDX2 gene Annals Hum Genet 61: 393-400 Part 5 .

Eaton RC and Didomenico R. (1986). Role of the teleost escape response during development. Transactions of the American Fisheries Society 115 (1): 128–142.

Eiden LE (1998). The cholinergic gene locus. J Neurochem 70: 2227-2240.

Elmqvist D, Quastel DMJ (1965). Presynaptic action of hemicholinium at neuromuscular junction. J. Physiol 177 (3): 463

Evans AM, Fornasini G. (2003). Pharmacokinetics of L-carnitine. Clin Pharmacokinet 42(11):941-67.

Fatt P, Katz B (1953). The electrical properties of crusteacean muscle fibers. J Physiol 120 (1-2): 171

Fishman MC, Stainier DYR, Breitbart RE, Westerfield M (1997). Zebrafish: Genetic and embryological methods in a transparent vertebrate embryo. METHODS CELL BIOL 52: 67-82.

Flanagan-Steet H, Fox MA, Meyer D, Sanes JR (2005). Neuromuscular synapses can form *in vivo* by incorporation of initially aneural postsynaptic specializations. Development 132(20):4471-81.

Giraldez AJ, Mishima Y, Rihel J, Grocock RJ, Van Dongen S, Inoue K, Enright AJ, Schier AF (2006). Zebrafish MiR-430 promotes deadenylation and clearance of maternal mRNAs. Science 312 (5770): 75-79.

Gleason MR, Armisen R, Verdecia MA, Sirotkin H, Brehm P, Mandel G (2004). A mutation in serca underlies motility dysfunction in accordion zebrafish. Develop Biol 276 (2): 441-451.

Goodman DR, Harbison RD (1981). Characterization of enzymatic acetylcholine synthesis by mouse brain, rat sperm, and purified carnitine acetyltransferase. Biochem Pharmacol 30(12):1521-8.

Govindasamy L, Pedersen B, Lian W, Kukar T, Gu Y, Jin S, Agbandje-McKenna M, Wu D, McKenna R (2004). Structural insights and functional implications of choline acetyltransferase. J Struct Biol 148(2): 226-235.

Granato, M., van Eeden, F.J., Schach, U., Trowe, T., Brand, M., Furutani-Seiki, M., Haffter, P., Hammerschmidt, M., Heisenberg, C.P., Jiang, Y.J., Kane, D.A., Kelsh, R.N., Mullins, M.C., Odenthal, J., and Nüsslein-Volhard C (1996). Genes controlling and mediating locomotion behavior of the zebrafish embryo and larva. Development 123:399-413.

Guo S, Brush J, Teraoka H, Goddard A, Wilson SW, Mullins MC, Rosenthal A (1999). Development of noradrenergic neurons in the zebrafish hindbrain requires BMP, FGF8, and the homeodomain protein soulless/Phox2a. Neuron 24(3):555-66.

Haffter P, Granato M, Brand M, Mullins MC, Hammerschmidt M, Kane DA, Odenthal J, van Eeden FJ, Jiang YJ, Heisenberg CP, Kelsh RN, Furutani-Seiki M, Vogelsang E, Beuchle D, Schach U, Fabian C, Nüsslein-Volhard C (1996). The identification of genes with unique and essential functions in the development of the zebrafish, Danio rerio. Development 123:1-36.

Hake LE, Richter JD (1997). Translational regulation of maternal mRNA. Biochim Biophys Acta 1332(1):M31-8.

Heasman J, Wessely O, Langland R, Craig EJ, Kessler DS (2002). Vegetal localization of maternal mRNAs is disrupted by VegT depletion. Develop Biol 240 (2): 377-386.

Higashijima S, Okamoto H, Ueno N, Hotta Y, Eguchi G (1997). High-frequency generation of transgenic zebrafish which reliably express GFP in whole muscles or the whole body by using promoters of zebrafish origin. Dev Biol 192(2):289-99.

Higashijima S, Masino MA, Mandel G, Fetcho JR (2004). Engrailed-1 expression marks a primitive class of inhibitory spinal interneuron. J Neurosci 24(25):5827-39.

Hirata H, Saint-Amant L, Downes GB, Cui WW, Zhou W, Granato M, Kuwada JY (2005). Zebrafish bandoneon mutants display behavioral defects due to a mutation in the glycine receptor beta-subunit. Proc Natl Acad Sci 102(23):8345-50.

Hoffman JA, Merrill BJ. (2007). New and renewed perspectives on embryonic stem cell pluripotency. Front Biosci 12:3321-32.

Ibanez-Tallon I, Wen H, Miwa JM, Xing J, Tekinay AB, Ono F, Brehm P, Heintz N (2004). Tethering naturally occurring peptide toxins for cell-autonomous modulation of ion channels and receptors *in vivo* Neuron 43 (3): 305-311.

Janz R, Sudhof TC (1999). SV2C is a synaptic vesicle protein with an unusually restricted localization: Anatomy of a synaptic vesicle protein family Neurosci 94 (4): 1279-1290 .

Jogl G, Hsiao YS, Tong L (2004). Structure and function of carnitine acyltransferases. Ann N Y Acad Sci 1033:17-29.

Johnstone O, Lasko P (2001). Translational regulation and RNA localization in Drosophila oocytes and embryos. Annu Rev Genet 35:365-406.

Jope RS, Jenden DJ (1979). Cholin and phospholipid metabolism and the synthesis of acetylcholine in rat brain. J Neurosci Res 4 (1): 69-82.

Karczmar AG (1993). Brief presentation of the story and present status of studies of the vertebrate cholinergic system. Neuropsychopharmac 9: 181-199.

Karlsson E, Mbugua PM, Rodriguez-Ithurralde D (1984). Fasciculins, anticholinesterase toxins from the venom of the green mamba Dendroaspis angusticeps. J Physiol (Paris) 79(4):232-40.

Katz B, Miledi R (1995). Release of acetylcholine from a nerve terminal by electric pulses of variable strength and duration. Nature 207(5001):1097-8.

Kimmel CB, Kane DA, Walker C, Warga RM, Rothman MB (1989). A mutation that changes cell movement and cell fate in the zebrafish embryo. Nature 337 (6205): 358-362 .

Kimmel CB, Ballard WW, Kimmel SR, Ullmann B, Schilling TF (1995). Stages of embryonic development of the zebrafish. Dev Dyn 203(3), 253-310.

Knapik EW, Goodman A, Ekker M, Chevrette M, Delgado J, Neuhauss S, Shimoda N, Driever W, Fishman MC, Jacob HJ (1998). A microsatellite genetic linkage map for zebrafish (Danio rerio). Nat Genet 18(4): 338-343.

Lefebvre JL, Ono F, Puglielli C, Seidner G, Franzini-Armstrong C, Brehm P, Granato M (2004). Increased neuromuscular activity causes axonal defects and muscular degeneration. Development 131(11):2605-18.

Linney E, Hardison NL, Lonze BE, Lyons S, DiNapoli L (1999). Transgene expression in zebrafish: A comparison of retroviral-vector and DNA-injection approaches Devel Biol 213 (1): 207-216.

Litt M, Buder A, Vissing H, van Tuinen P, Ledbetter DH (1989). An anonymous single-copy clone, p55-B1, from chromosome 17 identifies a TaqI RFLP [HGM9 no. D17S86] Nucleic Acids Res 17(6):2371.

Liu GS, Tsien RW (1995). Synaptic transmission at single visualized hippocampal bouttons. Neuropharmacol 34 (11): 1407-1421.

Loewi O (1921). Uber humorale ubertragbarkeit der hirzenwickung. Plfugers Arch 189: 239-242.

Long Q, Meng A, Wang H, Jessen JR, Farrell MJ, Lin S. (1997). GATA-1 expression pattern can be recapitulated in living transgenic zebrafish using GFP reporter gene. Development 124(20):4105-11.

Lorent K, Liu KS, Fetcho JR, Granato M (2001). The zebrafish space cadet gene controls axonal pathfinding of neurons that modulate fast turning movements. Development 128 (11): 2131-2142.

Luna VM, Brehm P (2006). An electrically coupled network of skeletal muscle in zebrafish distributes synaptic current. J Gen Physiol 128(1):89-102.

Malicki J, Neuhauss SC, Schier AF, Solnica-Krezel L, Stemple DL, Stainier DY, Abdelilah S, Zwartkruis F, Rangini Z, Driever W (1996). Mutations affecting development of the zebrafish retina. Development 123:263-73.

Malicki JJ, Pujic Z, Thisse C, Thisse B, Wei X (2002). Forward and reverse genetic approaches to the analysis of eye development in zebrafish. Vision Res 42(4):527-33.

McCallum CM, Comai L, Greene EA, Henikoff S (2000). Targeted screening for induced mutations. Nature Biotech 18 (4): 455-457.

Michelmore RW, Paran I, Kesseli RV. (1991). Identification of markers linked to disease-resistance genes by bulked segregant analysis: a rapid method to detect markers in specific genomic regions by using segregating populations. Proc Natl Acad Sci 88(21):9828-32.

Misgeld T, Burgess RW, Lewis RM, Cunningham JM, Lichtman JW, Sanes JR (2002). Roles of neurotransmitter in synapse formation: development of neuromuscular junctions lacking choline acetyltransferase. Neuron 36(4):635-48.

Mizuno T, Shinya M, Takeda H. (1999). Cell and tissue transplantation in zebrafish embryos. Methods Mol Biol. 1999;127:15-28.

Nachmansohn D, Machado AL (1943). The formation of acetylcholine. A new enzyme choline acetylase. J Neurophysiol 6: 397-403.

Nasevicius A, Ekker SC (2000). Effective targeted gene 'knockdown' in zebrafish. Nat Genet 26(2):216-20.

Neff MM, Turk E, Kalishman M (2002). Web-based primer design for single nucleotide polymorphism analysis. Trends Genet 18(12): 613-615.

Nelson N (2003). A journey from mammals to yeast with vacuolar H+-ATPase (V-ATPase). J Bioenerg Biomembr 35(4):281-9.

Oates AC, Bruce AE, Ho RK (2000). Too much interference: injection of double-stranded RNA has nonspecific effects in the zebrafish embryo. Dev Biol 224(1):20-8.

Oda Y, Imai S, Nakanishi I, Ichikawa T, Deguchi T (1995). Immunohistochemical study on choline acetyltransferase in the spinal cord of patients with amyotrophic lateral sclerosis. Pathol Int 45: 933-939.

Oda Y (1999). Choline acetyltransferase: the structure, distribution and pathologic changes in the central nervous system. Pathol Inl 49: 921-937.

O'Farrell PH, Edgar BA, Lakich D, Lehner CF (1989). Directing cell division during development. Science 246(4930):635-40.

Oliff HS, Gallardo KA (1999). The effect of nicotine on developing brain catecholamine systems. Front Biosci 4:D883-97.

Ohno K, Tsujino A, Brengman JM, Harper CM, Bajzer Z, Udd B, Beyring R, Robb S, Kirkham FJ, Engel AG (2001). Choline acetyltransferase mutations cause myasthenic syndrome associated with episodic apnea in humans. Proc Natl Acad Sci 98: 2017-2022.

Ono F, Higashijima S, Shcherbatko A, Fetcho JR, Brehm P (2001). Paralytic zebrafish lacking acetylcholine receptors fail to localize rapsyn clusters to the synapse. J Neurosci 21(15):5439-48.

Ono F, Shcherbatko A, Higashijima S, Mandel G, Brehm P (2002). The zebrafish motility mutant twitch once reveals new roles for rapsyn in synaptic function. J Neurosci 22(15):6491-8.

Ono F, Mandel G, Brehm P (2004). Acetylcholine receptors direct rapsyn clusters to the neuromuscular synapse in zebrafish. J Neurosci 24(24):5475-81.

Parsons MJ, Campos I, Hirst EM, Stemple DL (2002). Removal of dystroglycan causes severe muscular dystrophy in zebrafish embryos.Development 129(14):3505-12.

Parsons SM (2000). Transport mechanisms in acetylcholine and monoamine storage. FASEB J 14(15):2423-34.

Petersen SA, Fetter RD, Noordermeer JN, Goodman CS, DiAntonio A (1997). Genetic analysis of glutamate receptors in Drosophila reveals a retrograde signal regulating presynaptic transmitter release. Neuron 19: 1237-1248.

Peterson RT, Link BA, Dowling JE, Schreiber SL (2000). Small molecule developmental screens reveal the logic and timing of vertebrate development. Proc Natl Acad Sci 97(24):12965-9.

Picciotto MR (1999). Knock-out mouse models used to study neurobiological systems. Crit Rev Neurobiol 13(2):103-49.

Postlethwait JH, Yan YL, Gates MA, Horne S, Amores A, Brownlie A, Donovan A, Egan ES, Force A, Gong Z, Goutel C, Fritz A, Kelsh R, Knapik E, Liao E, Paw B, Ransom D, Singer A, Thomson M, Abduljabbar TS, Yelick P, Beier D, Joly JS, Larhammar D, Rosa F, Westerfield M, Zon LI, Johnson SL, Talbot WS (1998). Vertebrate genome evolution and the zebrafish gene map. Nat Genet 18(4):345-9. Erratum in: Nat Genet 19(3):303.

Postlethwait J, Amores A, Force A, Yan YL (1999). The zebrafish genome. Methods Cell Biol 60:149-63.

Prado VF, Martins-Silva C, de Castro BM, Lima RF, Barros DM, Amaral E, Ramsey AJ, Sotnikova TD, Ramirez MR, Kim HG, Rossato JI, Koenen J, Quan H, Cota VR, Moraes MF, Gomez MV, Guatimosim C, Wetsel WC, Kushmerick C, Pereira GS, Gainetdinov RR, Izquierdo I, Caron MG, Prado MA (2006). Mice deficient for the vesicular acetylcholine transporter are myasthenic and have deficits in object and social recognition. Neuron 51(5):601-12.

Ramsay RR, Naismith JH (2003). A snapshot of carnitine acetyltransferase. Trends Biochem Sci 28(7):343-6.

Ribera AB, Nüsslein-Volhard C (1998). Zebrafish touch-insensitive mutants reveal an essential role for the developmental regulation of sodium current. J Neurosci 18(22):9181-91.

Richter JD (1999). Cytoplasmic polyadenylation in development and beyond. Microbiol Mol Biol Rev 63(2):446-56.

Ruff RL (2003). Neurophysiology of the neuromuscular junction: overview. Ann N Y Acad Sci 998:1-10.

Salpeter MM, Marchaterre M, Harris R (1988). Distribution of extrajunctional acetylcholine receptors on a vertebrate muscle: evaluated by using a scanning electron microscope autoradiographic procedure. J Cell Biol 106(6):2087-93.

Sandrock A, Dryer S, Rosen K, Gozani S, Kramer R (1997.) Maintenance of acetylcholine receptor number by neuregulins at the neuromuscular junction *in vivo*. Science 276: 599-604.

Sastry BV, Janson VE (1994). Retinal cholinergic system: characterization of rat retinal acetyltransferases using specific inhibitors of choline- and carnitine-acetyltransferases. J Ocul Pharmacol 10(1):203-15.

Scholpp S, Brand M (2001). Morpholino-induced knockdown of zebrafish engrailed genes eng2 and eng3 reveals redundant and unique functions in midbrain--hindbrain boundary development. Genesis 30(3):129-33.

Searl T, Prior C, Marshall IG (1991). Acetylcholine recycling and release at rat motor nerve terminals studied using (-)-vesamicol and troxpyrrolium. J Physiol 444:99-116.

Schredelseker J, Di Biase V, Obermair GJ, Felder ET, Flucher BE, Franzini-Armstrong C, Grabner M (2005). The beta 1a subunit is essential for the assembly of dihydropyridine-receptor arrays in skeletal muscle. Proc Natl Acad Sci 102(47):17219-24.

Streisinger G, Walker C, Dower N, Knauber D, Singer F (1981). Production of clones of homozygous diploid zebra fish (Brachydanio rerio). Nature 291(5813):293-6.

Stuart GW, Vielkind JR, McMurray JV, Westerfield M (1990). Stable lines of transgenic zebrafish exhibit reproducible patterns of transgene expression. Development 109(3):577-84.

Summerton J, Stein D, Huang SB, Matthews P, Weller D, Partridge M (1997). Morpholino and phosphorothioate antisense oligomers compared in cell-free and in-cell systems. Antisense Nucleic Acid Drug Dev 7(2):63-70.

Svoboda KR, Linares AE, Ribera AB (2001). Activity regulates programmed cell death of zebrafish Rohon-Beard neurons. Development 128(18):3511-20.

Talbot WS, Schier A (1999). In The Zebrafish: Genetics and Genomics, H.W. Detrich, III, M. Westerfield, and L.I. Zon, eds., San Diego, CA: Academic Press, Methods Cell Biol 60:259-286.

Trevarrow B, Marks DL, Kimmel CB. (1990). Organization of hindbrain segments in the zebrafish embryo. Neuron 4(5):669-79.

Turrigiano GG, Nelson SB (2004). Homeostatic plasticity in the developing nervous system. Nat Rev Neurosci 5(2):97-107.

Warkman AS, Krieg PA (2007). Xenopus as a model system for vertebrate heart development. Semin Cell Dev Biol 18(1):46-53.

Warren KS, Fishman MC (1998)"Physiological genomics": mutant screens in zebrafish. Am J Physiol. 275(1 Pt 2):H1-7.

Wehman AM, Staub W, Baier H (2007). The anaphase-promoting complex is required in both dividing and quiescent cells during zebrafish development. Dev Biol 303(1):144-56.

Wen H, Brehm P (2005). Paired motor neuron-muscle recordings in zebrafish test the receptor blockade model for shaping synaptic current. J Neurosci 25(35): 8104-8111.

Westerfield M, McMurray JV, Eisen JS (1986). Identified motoneurons and their innervation of axial muscles in the zebrafish. J Neurosci 6(8):2267-77.

Westerfield M, Liu DW, Kimmel CB, Walker C (1990). Pathfinding and synapse formation in a zebrafish mutant lacking functional acetylcholine receptors. Neuron 4(6):867-74.

Westerfield (1994). The Zebrafish Book: A Guide for the Laboratory Use of Zebrafish (Danio Rerio*)

Wienholds E, van Eeden F, Kosters M, Mudde J, Plasterk RH, Cuppen E (2003). Efficient target-selected mutagenesis in zebrafish. Genome Res 13(12):2700-7.

Wu D, Hersh LB (1994). Choline acetyltransferase: celebrating its fiftieth year. J Neurochem 62: 1653-1663.

Zhang J, Lefebvre JL, Zhao S, Granato M (2004). Zebrafish unplugged reveals a role for muscle-specific kinase homologs in axonal pathway choice. Nat Neurosci 7(12):1303-9.

Zhou M, Engel AG, Auerback A (1999) Serum choline activates mutant acetylcholine receptors that cause slow channel congenital myasthenic syndromes. Proc Natl Acad Sci 96(18): 10466-10471.

Zhou Q, Petersen CC, Nicoll RA (2000). Effects of reduced vesicular filling on synaptic transmission in rat hippocampal neurones. J Physiol 525 Pt 1:195-206.

REFERENCE MATERIAL

List of Abbreviations

baj	*bajan*
AchR	acetylcholine receptor
BAC	bacterial artificial chromosome
BSA	bulk segregant analysis
cDNA	complimentary DNA
ChAT	choline acetyltransferase
cM	centimorgan, unit of genetic distance
CrAT	carnitine acetyltransferase
dCAPS	derived cleaved amplified polymorphic sequence
DHP	dihydropyridine receptor
GFP	green fluorescence protein
hpf	hours postfertilization
LG	linkage group (chromosome)
mEPC	miniature endplate current
NMJ	neuromuscular junction
PCR	polymerase chain reaction
RACE	rapid amplification of cDNA ends
RT-PCR	reverse transcriptase polymerase chain reaction
SNP	single nucleotide polymorphism

SSLP	simple sequence length polymorphism
Tu	Tubingen wild type strain of zebrafish
WT	wild type strain of zebrafish